Use of green methods for the synthesis of aluminosilicates for the valorization of glycerol via dehydration

Iván Darío Mora Vergara

Tesis presentada como requisito para acceder al título de: Doctor en Ingeniería Química

Director:

Víctor Gabriel Baldovino Medrano

Doctor en Ingeniería Química

Codirector:

José Antonio Henao Martínez

Doctor en Química

Universidad Industrial de Santander

Facultad de Ingenierías Fisicoquímicas

Escuela de Ingeniería Química

Doctorado en Ingeniería Química

Bucaramanga

2023

Agradecimientos

A Colciencias por su apoyo económico en el marco del Programa de Doctorados Nacionales Convocatoria 617.

A los miembros del Centro de Investigaciones en Catálisis de la Universidad Industrial de Santander (CICAT-UIS).

A Mauricio y Edwing por su amistad y apoyo a lo largo de este camino.

Agradezco a mis directores, el profesor Víctor Gabriel Baldovino y el profesor José Antonio Henao Martínez, por su respaldo y por brindarme palabras de estímulo en momentos cruciales.

Al Laboratoire Catalyse et Spectrochimie (ENSICAEN – Université de CAEN – CNRS) y a la Dr. Francoise Maugé y por su colaboración durante la realización de mi pasantía doctoral.

A Belkys Johana, mi compañera de vida, por el apoyo inquebrantable y su cariño sincero que ha sido como un refugio en el que siempre encuentro consuelo y fortaleza.

A mi familia, cuya presencia ha sido un pilar constante de apoyo y comprensión. A mis hermanos que han sido un soporte y ejemplo a lo largo de este camino.

A mi padre por todo lo que han hecho por mí a lo largo de los años. Por su dedicación, sacrificio y amor incondicional han dado forma a la persona que soy hoy.

A mi querida madre, que, aunque ya no estés físicamente a mi lado, su amor, sabiduría y bondad siguen vivos en cada rincón de mi corazón. Tus enseñanzas perduran como un faro de luz que ilumina mi camino y me guía en cada paso que doy.

Dedicatoria

A la memoria de mi madre, cuyo amor y apoyo incondicional fueron mi faro constante en este viaje académico. A pesar de tu partida, siento tu presencia en cada página escrita, en cada desafío superado y en cada logro alcanzado. Tu espíritu perseverante y tu devoción por el conocimiento siguen inspirándome a buscar la excelencia en todo lo que hago. Siempre vives en mi corazón y en cada logro que obtengo.

Contents

Page.

List of Tables

Page.

List of Figures

Page.

List of Appendix

Page.

Resumen

Título: Uso de métodos verdes para la síntesis de aluminosilicatos para la valorización de glicerol vía deshidratación[*].

Autor: Iván Darío Mora Vergara[**]

Palabras Clave: zeolita, sol-gel, mecanoquímica, glicerol, deshidratación.

Descripción:

Esta investigación se centró en estudiar métodos de síntesis ambientalmente sostenibles para la zeolita ZSM-5 sin usar estructurantes orgánicos ni solventes. Se profundizó en factores cruciales como la composición del gel de síntesis y el tiempo de cristalización. La síntesis Sol-Gel se analizó en una primera parte, utilizando cristales de zeolita ZSM-5 como sitios de nucleación. Se analizaron los diferentes tipos de precursores de silicio, el impacto de las influencias de las semillas y el papel de la alcalinidad en la producción de ZSM-5 sin un agente director de estructura orgánico (OSDA). En la segunda parte, se investigó la síntesis de ZSM-5 sin solventes, analizando cómo el tamaño de las partículas del precursor de silicio afecta las características morfológicas, texturales y cristalográficas de los materiales. Los materiales sintetizados en las dos primeras partes de la reacción de deshidratación del glicerol se evaluaron en el tercer segmento. Esta evaluación consideró las relaciones aluminio-silicio, la acidez y las propiedades texturales de los materiales.

[*] Tesis doctoral

[**] Facultad de Ingenierías Fisicoquímicas. Escuela de Ingeniería Química. Doctorado en Ingeniería Química. Director: Prof. Víctor Baldovino Medrano. Codirector: Prof. José Antonio Henao Martínez.

Abstract

Title: Use of green methods for the synthesis of aluminosilicates for the valorization of glycerol via dehydration[*].

Author: Iván Darío Mora Vergara[**]

Keywords: zeolite, sol-gel, mechanochemistry, glycerol, dehydration.

Description: This research focused on studying environmentally sustainable synthesis methods for ZSM-5 zeolite without using organic structurants or solvents. Crucial factors such as the composition of the synthesis gel and the crystallization time were deepened. The Sol-Gel synthesis was analyzed in the first part, using ZSM-5 zeolite crystals as nucleation sites. The different types of silicon precursors, the impact of seed influences, and the role of alkalinity in the production of ZSM-5 without an organic structure-directing agent (OSDA) were analyzed. In the second part, the synthesis of ZSM-5 without solvents was investigated, analyzing how the silicon precursor particles' size affects the materials' morphological, textural, and crystallographic characteristics. The materials synthesized in the first two parts of the glycerol dehydration reaction were evaluated in the third segment. This evaluation considered the aluminum-silicon ratios, the acidity, and the textural properties of the materials.

[*] Ph.D. thesis

[**] Facultad de Ingenierías Fisicoquímicas. Escuela de Ingeniería Química. Doctorado en Ingeniería Química. Director: Prof. Víctor Baldovino Medrano. Codirector: Prof. José Antonio Henao Martínez.

General introduction

Conventionally, zeolites are synthesized by the so-called hydrothermal method from silicate or aluminosilicate gels in an alkaline medium at temperatures between 60 and 200°C. The method involves using structure-directing organic agents whose removal is done by combustion at high temperatures; this generates polluting gases such as NOx and greenhouse gases such as CO_2 (Asgar Pour & Sebakhy, 2022) (Ma et al., 2020). In addition, the hydrothermal method implies a duration between 1-20 days, operating at temperatures between 80 and 200°C, which makes it a process with a high energy cost (Asgar Pour & Sebakhy, 2022)(Cundy & Cox, 2005). In view of the above, new synthesis methods have been presented in the literature that favor: (1) the reduction or elimination of the use of toxic organic structuring agents; (2) the use of structuring agents of low toxicity and low cost; (3) the minimization or elimination of the use of solvents during the synthesis; (4) the optimization in the use of the energy required for the thermal treatment of the solid precursors of the finished materials (H. Pan et al., 2010)(F. Pan et al., 2017). Given the theme of the present investigation (see: Problem Statement), some of the recent advances aimed at finding methods for the synthesis of zeolites that contemplate points 1, 2, 3 and 4 mentioned above will be reviewed below (Asgar Pour & Sebakhy, 2022)(Majano et al., 2014).

Zones et al, used in the synthesis of SSZ-25 zeolites a series of amines such as piperidine, cyclopentyl amine, and isobutylamine, among others, as co-structuring agents of low toxicity, which in addition to having the pore filling function contributed to the modulation of the basicity of the system (Goel et al., 2015). The presence of these amines in the synthesis reduced the structuring agent and the crystallization time of the zeolite. Lee et al. designed structuring agents

containing acetal groups to synthesize ZSM-5 zeolites that can be removed from the zeolite pores, before the calcination step, through hydrochloric acid extraction processes (Lee et al., 2003). Removing the structuring agent through this methodology did not generate degradation of the zeolite structure. Jin et al., reported other research involving structuring agent recovery and developed a strategy for extracting the structuring agent P123 using ultrasound. Optimizing the extraction process allowed the recovery of 75 % of the P123 used for the synthesis (Nada & Larsen, 2017). The material subjected to extraction presented a uniform porous structure and a high surface area compared to the calcined material. The strategy proposed by Jin et al., also implies the possibility of reducing contamination due to the elimination of the structuring agent by calcination and even the possibility of reusing it (Nada & Larsen, 2017).

Machado et al., synthesized MFI or MOR-type zeolites without using structuring agents starting from the same synthesis gel. The control of the final structure of the material was done by varying the temperature and crystallization time. One of the notable results of this work was that the Si/Al molar ratio of the final zeolite was different from the molar ratio of the synthesis gel. This difference increased when a higher silicon content was used. The authors also found an upper limit for **Si** incorporation into the structure of MFI-type zeolites (Machado et al., 1999). Bellucci et al, also reported the synthesis of ZSM-5 type zeolites without the use of structuring agents, finding that the most critical parameters for the direction of the zeolite structure are the SiO_2/Al_2O_3 ratio and the OH^-/SiO_2 ratio; the synthesis was carried out in an alkaline medium with the help of NaOH and KOH (Bellussi et al., 1988).

Another strategy for synthesizing zeolites free of organic structuring agents involves adding zeolite seeds while preparing the synthesis gel. Xie et al, used this technique to synthesize ZSM-5 zeolites with SiO_2/Al_2O_3 ratios between 30 and 70 using NaY-type zeolites as seed

(Katryniok, et. al., 2009). The results showed that the synthesis without the seed leads mainly to forming a tetragonal form of silicon dioxide (creative); when the seed/SiO_2 mass ratio was 0.05, the ZSM-5 zeolite fully crystallized 48h. The reason why so much research is carried out on the synthesis of zeolites is because of the versatility that they can offer when used in catalytic processes. One of these processes is the dehydration of glycerol, particularly the glycerol produced in the synthesis of biodiesel. Biodiesel is produced from vegetable oils and animal fats and is composed of alkyl esters produced from the transesterification of triglycerides (TG) or the esterification of free fatty acids (FFA) with short-chain alcohols and in the presence of acid catalysts. The process for obtaining biodiesel involves the formation of 10% glycerol, therefore large volumes of this by-product are generated (Katryniok et al., 2009) (Talebian-Kiakalaieh et al., 2014). There is a limited market for the use of glycerol as a raw material in the pharmaceutical and cosmetic industry. These industries are not able to absorb the volume of glycerol currently produced (Pan, et. al., 2017; Wu, et. al., 2019).

Different processes have been investigated to valorize glycerol, being the dehydration towards acrolein using acid catalysts one of the most promising routes (Katryniok et al., 2009). Aluminosilicate type materials have been used as catalysts for this purpose and yields towards acrolein between 75-85% have been obtained. However, these undergo rapid deactivation due to coke deposition on their surface. This problem can be mitigated by adjusting the acid-base and textural properties of the catalysts (Talebian-Kiakalaieh et al., 2014)

The investigations reported previously show the different possibilities for the development of processes based on the principles of green chemistry, which allow the obtaining of zeolitic materials with a low environmental impact. In short, and firstly, the recovery of glycerol through the dehydration reaction using solid acids as catalysts provides the opportunity to take advantage

of a low-cost by-product that can be found in abundance. In particular, the use of aluminosilicates as catalysts in the glycerol dehydration reaction is promising due to the versatility with which the properties of these materials can be adjusted to match the needs of the processes in which they are used. However, industrialization of the process is not yet possible, one of the main problems being the rapid deactivation of the catalysts due to coke formation. This can be reduced by tuning the acid properties of the aluminosilicate (type, strength, and concentration of acid sites) and adjusting its textural characteristics (pore size and structure). On the other hand, the processes for obtaining these aluminosilicates can be proposed to reduce the environmental impact that their synthesis implies, as shown in the section "Green routes for zeolite synthesis".

To evaluate the catalyst behavior of synthetized materials, selected ZSM-5 type zeolites was studied in the gas phase glycerol dehydration reaction using a fixed bed reactor that operated continuously. The analyzed materials were prepared using two methods: 1) the sol-gel method without organic structuring agent (OSDA), using as silicon precursors (Ludox, Fumed Silica 1 and Tetraethyl orthosilicate (TEOS); 2) The solvent-free method and OSDA using three silicon sources with different particle sizes (Fumed Silica 1, Fumed Silica 2 and silica gel). Additionally, the change in the silicon-aluminum ratio with materials prepared with the TEOS precursor and the synthesis method one was evaluated. As result, it was found that the main product for all the materials is acrolein, that the materials prepared by the Sol-Gel method had a catalytic performance like commercial zeolite, and materials prepared by the solvent-free method presented a lower conversion.

1. Scope of the Thesis

This research focused on the synthesis of ZSM-5 zeolite using synthesis processes for materials with low environmental impact: organic structuring agent-free synthesis, mechanochemical and solvent-free synthesis. The influence of some key variables in the synthesis of the materials will be determined, such as: the composition of the synthesis gel and the crystallization time. In this research, different routes for the synthesis of aluminosilicates with various acidic and textural properties were studied.

In the first part, the synthesis of ZSM-5 zeolite was studied through the Sol-Gel route using ZSM-5 zeolite crystals as seed and acting as a structuring agent. The effects of silicon precursor type, seed type, and alkalinity on the production of organic structure directing agent (OSDA)-free zeolite ZSM-5. Three silicon precursors were selected: one of the molecular types, tetraethyl orthosilicate (TEOS), and two bulk silicas; colloidal silica, Ludox, and fumed silica. As for the effect of seed type, three commercial zeolites, namely Na-ZSM-5, Na-mordenite, and Na-Y, were used as seeds. The syntheses were carried out by varying the $NaOH/SiO_2$ ratio in three values: 0.32, 0.42, and 0.58.

It was found that with TEOS, the margin for zeolite production is wider than with the other precursors; under the lowest alkalinity conditions, zeolite ZSM-5 could be obtained even without the help of seed zeolite, which was not possible with the other two precursors of, in which the presence of zeolite ZSM-5 was necessary. It was also shown that the seed zeolites can exert a directing effect on the structure of the synthesis mixture around it but that the composition of the said mixture was what determined the majority phase to be formed. Regarding the use of zeolite

Y as seed, in this work, it was observed that it did not have a relevant or beneficial effect for obtaining zeolite ZSM-5, given that the results without the presence of seed were the same or even better.

In the second part of this work, the synthesis of ZSM-5 zeolite without the use of solvent and structuring agent was studied. Some critical aspects of the solvent-free synthesis of ZSM-5 zeolite were studied. Aspects such as the influence of the particle size variation of the silicon source on the morphological, textural, and crystallographic properties of zeolite ZSM-5 were analyzed. In the first part of the work, the synthesis of ZSM-5 zeolite was explored with the help of an organic structuring agent (OSDA), finding that the size of the silicon particles only generated morphological changes when silica gel was used. It was also found that the crystals obtained using OSDA are much larger than those obtained using seeds and have larger surface areas. It was found that a high concentration of **Na** favors the appearance of phases such as mordenite (MOR) and larger silica gel particles. Finally, a comparison was made by varying the crystallization time between mechanochemical and sol-gel synthesis to study the differences and common aspects. In the third part of this work, some of the materials synthesized in part I and II, were tested in the dehydration reaction of glycerol to acrolein. The reaction was carried out in the gas phase and continuously, the effect of the aluminum silicon ratio, the acidity of the materials and their textual properties were analyzed.

In the last part of this work, the catalytic behavior was studied for various ZSM-5 type zeolites in the gas phase glycerol dehydration reaction using a fixed bed reactor that operated continuously. The analyzed materials were prepared using two methods: 1) the sol-gel method without organic structuring agent (OSDA). Using three different silicon precursors (Ludox, Fumed Silica 1, and Tetraethyl orthosilicate (TEOS); 2) The solvent-free method and OSDA using three

silicon sources with different particle sizes (Fumed Silica 1, Fumed Silica 2 and silica gel). Additionally, it was evaluated the change in the silicon-aluminum ratio with materials prepared with the TEOS precursor and the synthesis method one was evaluated.

Among the findings, it was found that the materials prepared by the sol-gel route, free of OSDA, presented an activity and yield comparable to that of commercial zeolite. It was also determined that, regardless of the silicon precursor used and the synthesis method, acrolein was the main product.

2. Effects of the type of silicon precursor, type of seed, and alkalinity over the production of ZSM-5 zeolite

2.1 Abstract

This chapter studied the effects of silicon precursor type, seed type, and alkalinity on the production of organic structure directing agent (OSDA)-free zeolite ZSM-5. Three silicon precursors were selected: one of the molecular types, tetraethyl orthosilicate (TEOS), and two bulk silicas; colloidal silica, Ludox, and fumed silica. As for the effect of seed type, three commercial zeolites, namely Na-ZSM-5, Na-mordenite, and Na-Y, were used as seeds. The syntheses were carried out by varying the $NaOH/SiO_2$ ratio in three values: 0.32, 0.42, and 0.58.

It was found that with TEOS, the margin for zeolite production is wider than with the other precursors; under the lowest alkalinity conditions, zeolite ZSM-5 could be obtained even without

the help of seed zeolite, which was not possible with the other two precursors of, in which the presence of zeolite ZSM-5 was necessary. It was also shown that the seed zeolites can exert a directing effect on the structure of the synthesis mixture around it but that the composition of the said mixture was what determined the majority phase to be formed. Regarding the use of zeolite Y as seed, in this work, it was observed that it did not have a relevant or beneficial effect for obtaining zeolite ZSM-5, given that the results without the presence of seed were the same or even better.

The NaOH concentration plays a crucial role in ZSM-5 zeolite formation. With the lowest concentration ($NaOH/SiO_2$=0.32), the presence of ZSM-5 seed was always necessary to obtain crystalline ZSM-5 zeolite with a high surface area, regardless of silicon precursor. With the intermediate concentration ($NaOH/SiO_2$=0.42), it is possible to obtain zeolite ZSM-5 with the precursor TEOS and Fumed silica in the seedless system and with zeolite Y; however, the formation of the mordenite phase is also promoted. Finally, with the highest alkalinity ($NaOH/SiO_2$=0.58), the production of zeolite ZSM-5 is not favored, while the formation of the mordenite phase is promoted.

Keywords. ZSM-5 zeolite, Seed, Silicon Precursor, sodium hydroxide.

2.2 Introduction

Zeolites are microporous and crystalline materials used as adsorbents, ion exchangers, and catalysts (Cundy & Cox, 2003; Cundy & Cox, 2005). About 232 types of zeolites are known, between natural and synthetic, and ZSM-5 zeolite is one of the best known within the second group (FCC catalysts, 2020). Its synthesis is carried out conventionally through the hydrothermal method

and with the help of Organic Structure Directing Agents (OSDA) such as tetrapropylammonium cations (TPA^+) (Cundy & Cox, 2005). Its porous structure with three-dimensional channels (straight and sinusoidal channels), thermal stability (up to 900°C), and acidity (490 NH_3 μmol/g) (Rieg et al., 2021; Caldeira, et. al, 2016; Pérez-Page et al., 2016; Hoff, et. al., 2016), make ZSM-5 zeolite used in applications such as cracking, isomerization, aromatization, and alkylation (FCC catalysts, 2020; Yue et al., 2018). Thanks to its application possibilities, its synthesis is the subject of many investigations to modify its physicochemical properties and improve the way it is obtained. One of the main focuses of research is to avoid using OSDA like in conventional synthesis; its elimination through calcination increases the cost of production due to higher power consumption and generates pollution in water and air (Yue et al., 2018; Iyoki, et. al., 2014; Ren, et. al., 2012; M. O. Corp, 1991).

It has been analyzed how the proper establishment of the initial molar ratios of the synthesis gel (SiO_2/Al_2O_3, $NaOH/SiO_2$, H_2O/SiO_2) can lead to producing zeolite ZSM-5 without the use of OSDA or seeds (Dai, et. al., 1986; Shiralkar & Clearfield, 1986; Lowe, et. al., 1994; Aiello, etl. Al., 1987). Shiralkar et al. (1989), highlight the importance of the Na^+ ion to balance the charge generated in the structure of the zeolite being able to obtain. The authors also state that the composition range in which the ZSM-5 zeolite is prepared without quartz or mordenite is narrower than when using OSDA. Schweiger et al. (1989), reported an optimal range in the initial composition of the synthesis mixture to obtain zeolite ZSM-5 without OSDA, showing that this range was narrower than when using the organic template. They also found that the zeolite obtained by the OSDA-free method had a lower concentration of internal silanol groups.

Dai et al. (Dai, et. al., 1986; Dai, et. al., 1989), in addition to investigating the optimal conditions for obtaining zeolite ZSM-5, the authors found that these are subject to the type of

silicon precursor. They found that using colloidal silica with 20 nm particles, it was possible to obtain ZSM-5 zeolite with a high degree of purity, but if the particle size increased to 35 nm under the same synthesis conditions, mordenite was formed. This phenomenon was attributed to the difference in the dissolution rate of the silicon particles in the synthesis medium. Tissleri and his group (Tissler, et. al., 1989), also studied three different sources of silicon in obtaining zeolite ZSM-5 (waterglass, hydrogel silica and pyrogenic silica), they found that the composition range in which zeolite ZSM-5 can be obtained without impurities, changes depending on the precursor. With fumed silica this margin was greater (Si/Al=12-200 and OH^-/SiO_2=0.15-0.6) than with Silica hydrogel (Si/Al=12-60 and OH^-/SiO_2=0.2-0.3), in the case of waterglass, they could not obtain zeolite ZSM-5 without impurities. They also reported that using seed the synthesis time is reduced and that the ZSM-5 zeolite obtained without OSDA had a more homogeneous distribution of aluminum than its counterpart. Kalipcilar et al. (2001), also report experiments varying the type of silicon precursor; they found that when using silicic acid, the material they obtained was a mixture of quartz and zeolite ZSM-5, and the use of colloidal silica with particles of size ≈ 12 nm (Ludox HS40) led to the formation of zeolite ZSM-5 with small amounts of quartz. In contrast, the use of colloidal silica containing methanol as a stabilizer (Merck Art. no: 12475) led to the obtaining of zeolite ZSM-5 with higher crystallinity than with the use of Ludox HS40. The ethanol in one colloidal silica acts as a structure-directing agent. In addition to the differences in crystallinity, the use of the two types of colloidal silica also leads to changes in the size of the crystals formed, although their shape was similar (Kalipcilar et al., 2001).

As discussed above, the choice of the initial synthesis conditions and the silicon source affect the purity and morphological characteristics of the ZSM-5 zeolite without using OSDA or seed; however, the synthesis margin is limited. Using zeolite crystals as seeds helps to expand the

alternatives when obtaining ZSM-5 zeolite without using OSDAs, and numerous investigations have focused on establishing the role of these seeds in the synthesis. Cundy et al (2003). Posit that the seed provides a surface area on which a new product can grow; since this area does not have to self-generate through primary nucleation, the induction period decreases. Additionally, it postulates that seed crystals' surface presents recognition elements that can give a kinetic advantage to one phase over others, reducing the formation and impurities. Itabashi et al., (2012) state that the critical factor in seed-assisted synthesis is the similarity between the composite building unit of the seed and those of the zeolite that can be obtained with the synthesis gel without adding seed. It shows that obtaining zeolite ZSM-5 can be achieved by adding zeolite ZSM-5 seeds in a synthesis gel that, without it, would give rise to mordenite zeolite, with which it shares the *mor* CBU. Yu et al., consider that the seed crystals generate new crystallization nuclei, on whose surface are terminal T-OH groups that facilitate the recognition of the composite units formed in the gel and provide a surface area in which said units can be tied and stacked to form a new zeolite layer. Using ZSM-5 or ZSM-11 seeds, they can get pure ZSM-5 zeolite with high crystallinity; however, using zeolite Y (no common SBU with target ZSM-5 zeolite), they get low crystallinity material composed of the mordenite and ZSM-5 phases. In relation to the use of seeds that do not have common compositional units with the objective zeolite, the work reported by Goel et al., shows that it is possible to obtain zeolite ZSM-5 using zeolite Y as seed, in this process they state that there is an interzeolite transformation; however, obtaining ZSM-5 zeolite is viable only when there is ZSM-5 seed or when OSDA is present. The work of Pan et al. (2010), states how with the use of zeolite Y as seed it is possible to obtain zeolite ZSM-5. The effect of the seed is emphasized when comparing the synthesis without its presence (formation of keatite) with the synthesis in which it is present (zeolite ZSM-5 with high relative crystallinity). The research carried out by Qin

et al. (2019) reports obtaining zeolite ZSM-5 directly from zeolite Y without the help of OSDA or seeds. The authors state that for this phenomenon to occur, it is necessary that the composition of the synthesis mixture (molar ratios ($NaOH/SiO_2$, SiO_2/Al_2O_3, H_2O/SiO_2), be favorable for the synthesis of zeolite ZSM-5 without OSDA and postulate that it is only possible to obtain through the seed-assisted method structures with common CBUs does not apply to all zeolite syntheses. Dos Santos et al. (2020), show through SEM images how the seed zeolite Y crystals are transformed to obtain zeolite ZSM-5; as the solution from the synthesis medium is incorporated the crystals suffer a partial dissolution as species of aluminosilicates. Under the conditions reported in his work, the authors obtain ZSM-5 zeolite in 5 days, what without seed takes ten.

2.3 Experimental section

2.3.1 Materials

Silicon precursors: tetraethyl orthosilicate (Sigma-Aldrich, ≥99.0% (GC)), LUDOX® HS-40 (Sigma-Aldrich, colloidal silica, 40 wt % suspension in H_2O), fumed Silica (Sigma-Aldrich, SiO_2 (7-12 nm)). Seed zeolites: ZSM-5 (CBV2314-Zeolyst International), mordenite (CBV10A-Zeolyst International), Y (CBV100-Zeolyst International). Mineralizing agent: sodium hydroxide (NaOH, > 99%, Merck).

2.3.2 Materials synthesis

2.3.2.1 Experimental design. The silicon precursor (TEOS, Ludox, fumed silica), the $NaOH/SiO_2$ molar ratio (0.32, 0.42, 0,58), the type of seed (ZSM-5, MOR, Y, syntheses without a seed were also performed under the same conditions for comparison purposes), and the hydrothermal time (24 and 48 h) were varied; keeping the SiO_2/Al_2O_3 (40.05) and H_2O/SiO_2 (60) molar ratios constant. In the case of the syntheses where used seed, this was 10% of the mass of SiO_2 used.

2.3.2.2 Synthesis protocol. In a typical run, 0.9 g of the aluminum precursor and 0.61 g of sodium hydroxide were dissolved in 17.8 g of type I water (0.8 g or 1.1 g of NaOH for the other relations), then mixed using magnetic stirring with an aqueous solution containing 0.29 g of zeolite seed, 32 g of water, and the silicon precursor (7.2 g for Ludox, 2.88 g for Fumed silica and 5 g for TEOS). In the case of Ludox and Fumed silica, when the two solutions were mixed, a dense gel was formed. In contrast, with the TEOS precursor, a suspension was first observed with the presence of two phases, which gradually disappeared thanks to the hydrolysis of TEOS to form a homogeneous solution at the end of 24 hours of magnetic stirring.

After magnetically stirring for 24 hours the final mixes mentioned above, they were deposited in equal parts in two Teflon-lined stainless steel reactors and subjected to a hydrothermal treatment of 24 or 48 h at 180°C, depending on the case. After the above treatment, the solids produced were recovered using gravity filtration with quantitative filter paper and then washed by centrifugation until a neutral pH of the washing water was obtained (Type I water).

2.3.3 Materials characterization

The morphology, crystal size, and chemical composition of the materials were studied with a QUANTA FEG 650 scanning electron microscope (SEM) using an Everhart Thornley detector (ETD) for morphology and an SSD type Back Scattered Electron detector (BSED) for composition. Before the analyses, samples were coated with gold for controlling differential charging effects during the measurements. The crystalline structure of the materials was studied by collecting X-ray diffraction (XRD) patterns with a D8 advanced X-ray diffractometer (Bruker) provided with Cu Kα1 radiation. XRD patterns were recorded between 2θ angles of 3.5-70 with a 0.02 step size.

The porosity and surface area of the materials were estimated from Argon adsorption-desorption isotherms obtained with a 3Flex apparatus (Micromeritics) at 87 K. For the tests, samples of approximately 0.1500 grams of each material were degassed –(apparatus, vacuum pressure: see at 120 ° C for 2 h and then at 300 °C overnight. After optimizing the CBET parameter with the Rouquerol consistency criteria, specific surface areas were calculated with the BET method.

The chemical structure of the materials was analyzed after recording infrared spectra for samples from them. Measurements were made with a Nicolet iS50 Fourier Transform Infrared (FT-IR) spectrometer (ThermoScientific) equipped with an attenuated total reflectance (ATR-FTIR) detector.

2.3.4 Nomenclature

The nomenclature of the samples prepared with TEOS was established as follows: T-Na#-S-X, where T means TEOS, Na corresponds to $NaOH/SiO_2$ molar ratio where Na_1, Na_2, Na_3 means $NaOH/SiO_2$=0.32, $NaOH/SiO_2$=42 and $NaOH/SiO_2$=0.58, respectively; S corresponds to employed seed (Z=ZSM-5, M=mordenite, Y= Y zeolite and 0= no seed added) and X correspond to the hydrothermal time (1 for 24 h and 2 for 48h). The R of in the name of some samples means replica synthesis. For the materials synthetized with Ludox or fumed silica, the first letter of the sample name change to L or F, respectively.

2.4 Results and Discussion

2.4.1 Materials synthesis with $NaOH/SiO_2$=0.32 molar ratio

2.4.1.1. ATR-IR. Shows the influence of silicon precursor, seed type, and hydrothermal time on the IR spectra for synthesized materials with the lowest sodium concentration (NaOH/SiO2=0.32).

Figure 1.

ATR-FTIR spectra of the synthesized samples using the molar ratio NaOH/SiO_2=0.32 with the silicon precursors: a) TEOS, b) Ludox, and c) Fumed Silica.

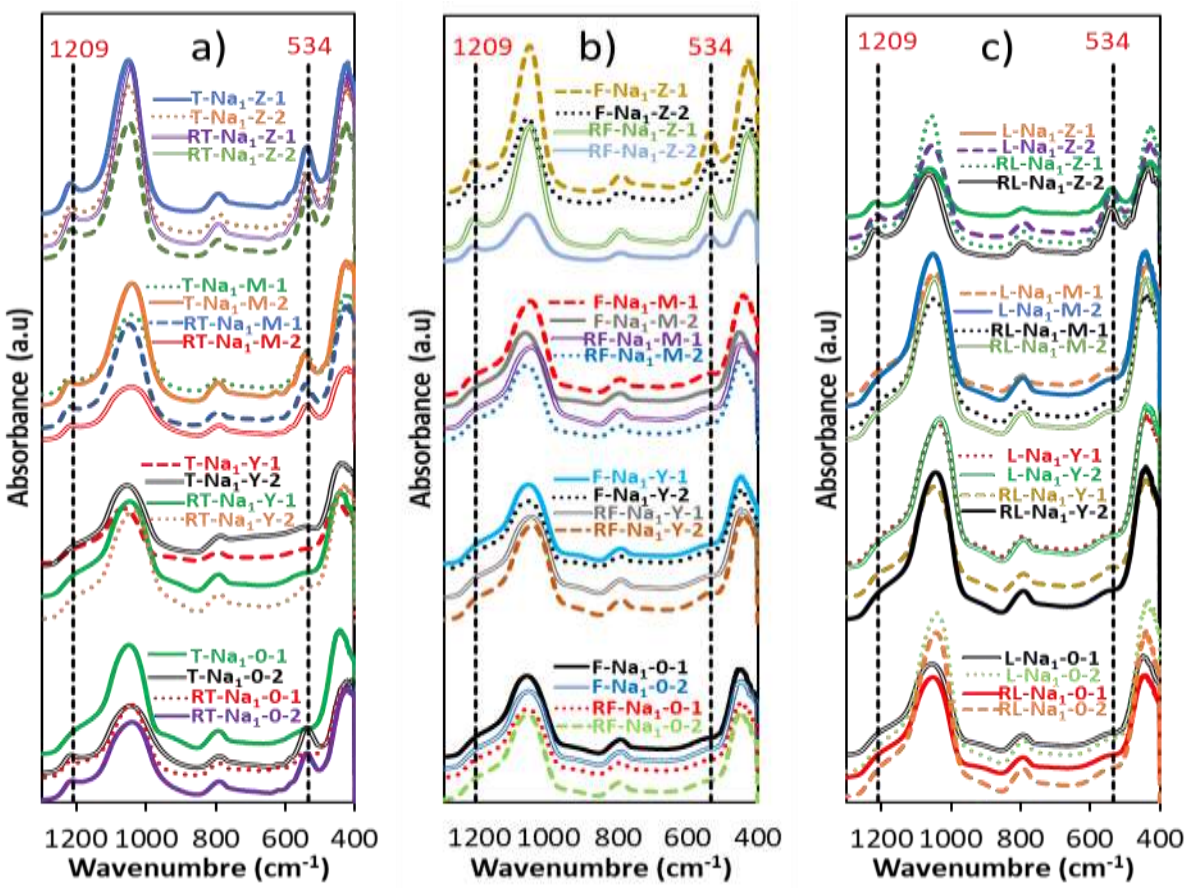

The results shows, for all the materials in which ZSM-5 seed was used, two peaks around 1209 and 534 cm^{-1}, independent of the silicon source and the hydrothermal treatment time used; these peaks refer to the vibration modes of the pentasil rings associated with the MFI structure (534 nm) and the chains formed by said rings (1240 cm^{-1}) (Jansen, et. al., 1984; Trombetta, et. al., 2000; Shukla & Pandya, 1989), and although it is not possible to accurately determine the presence of other phases or the percentage of crystallinity, are a good indicator of the possible formation of ZSM-5 zeolite (Jansen, et. al., 1984; Trombetta, et. al., 2000; Shukla & Pandya, 1989; Flanigen,

et. al., 1974). Since one of the main objectives of the work is to obtain zeolite ZSM-5, the IR results serve as an aid to select those materials where the probability of formation of zeolite ZSM-5 is greater and to discard for future characterization those in which no.

In the cases of the Ludox and silica fume precursors, the two bands mentioned above were only observed when ZSM-5 seed was used; no other experiment with the ratio $NaOH/SiO_2$=0.32 could obtain them. The behavior of the samples prepared with TEOS was different; Although the mentioned bands could not be observed regardless of the crystallization time when zeolite Y was used, they did occur when using zeolite mordenite and in the seedless system (only with 48 h of hydrothermal treatment).

2.4.1.2 X-ray diffraction. Figure 2 shows the diffractograms of some of the synthesized samples whose IR spectra presented bands around 1200 cm^{-1} and 550 cm^{-1}; they also show those of the ZSM-5 and mordenite zeolites used as seeds.

Figure 2.

*XRD patterns of some selected samples whose IR spectra presented bands around 1209 cm^{-1} and 534 cm^{-1}, ZSM-5 (CBV2314) and mordenite (CBV21A) seed. *Mordenite peaks.*

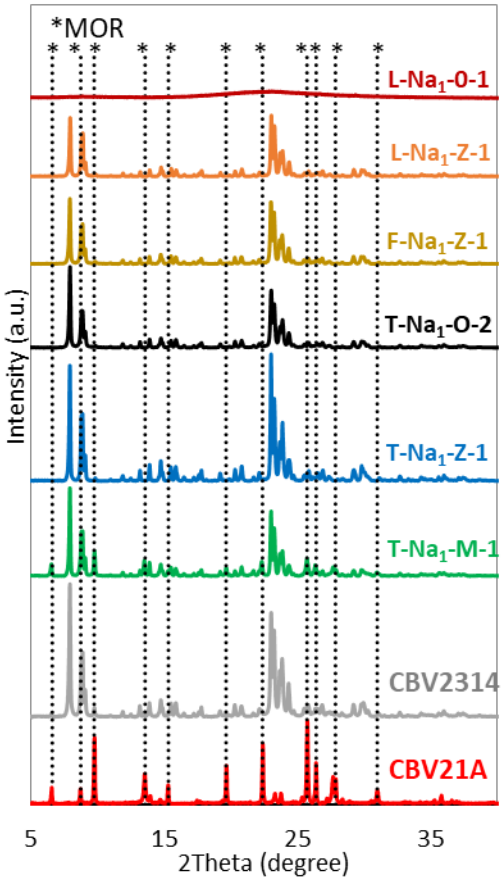

The diffraction peaks of the materials synthesized with the ZSM-5 seed coincide with those of the commercial sample (CBV2314). In the case of the material prepared with mordenite, in addition to the peaks associated with the ZSM-5 phase, bands related to the formation of the crystalline phase of the seed can be observed. Figure 2 also shows the XRD spectrum of one of the samples that did not present IR bands around 550 cm^{-1} and 1200 cm^{-1} (L-Na_1-0-1). No diffraction peaks are observed for this material, evidencing the non-formation of zeolitic material.

The phase percentages for the samples presented in Figure 2 are reported in Table 1, and the materials synthesized with the ZSM-5 seed (CBV2314) present ZSM-5 as the majority phase, independent of the source silicon used. It should be noted that the zeolite used as seed ZSM-5 (CBV2314) has 8.9 % of the mordenite phase and that the materials prepared with it have a lower concentration.

Table 1.

Phase percentages for some of the samples presented in Figure 1

	Material					
	CBV2314	**T-Na$_1$-Z-1**	**T-Na$_1$-M-1**	**T-Na$_1$-0-2**	**LD-Na$_1$-Z-1**	**F-Na$_1$-Z-1**
% ZSM-5	8.9	0.74	19.7	0.7	1.3	1.2
% MOR	91.2	99.26	80.3	99.3	98.7	98.8

From the results reported in Table 1, two assertions can be made: 1) ZSM-5 zeolite seed and their structural composition units exert a directing effect on the structure, considering that with the precursors of Ludox and fumed silica, only zeolitic material could be obtained with said seed. 2) The composition of the system favored the directing effect of ZSM-5 zeolite crystals above those of mordenite (crystals provided as impurity) since there was a decrease in the percentage of the mordenite phase concerning the seed. More evidence related to the second assertion can be found by analyzing the fact that with the TEOS precursor, there was zeolite formation without using seed.

The effect that exerts the initial synthesis composition and the seed CBUs on the prepared material is highlighted in the experiment where TEOS is used as a silicon precursor and mordenite zeolite as a seed. When mordenite zeolite was added, the percentage of that phase increased

compared to the experiment where no seed was used or mordenite zeolite was used, but the ZSM-5 phase remained the main. The results show a direct effect of the zeolite mordenite that provides the synthesis mixture of composite building units that direct a new structure, and a thermodynamic effect (synthesis conditions) favorable to zeolite ZSM-5 (Wu et al., 2014; Razavian, et. al., 2015; Corregidor, 2018). It could be thought that there are regions in the synthesis mixture guided by the effect of the seed and other regions where the thermodynamic aspect that favors the formation of zeolite ZSM-5 prevails.

The synthesis with the precursor TEOS also allowed us to observe that the seed zeolite presence affects the kinetics of crystallization; in the seedless experiment with the TEOS precursor, more than 24 h was needed to form the ZSM-5 zeolite (IR band formation at 550 and 120 cm^{-1}), when ZSM-5 seed was used, this result is achieved within 24 h of synthesis. And that although the synthesis conditions may be appropriate for the formation of the ZSM-5 structure, the use of seed Y does not lead to obtaining a zeolitic material.

2.4.1.3 Argon physisorption. The textural properties of the materials analyzed in XRD are presented in Table 2. **Ar** adsorption-desorption curves and pore size distribution calculated by the DFT method are presented in the supplementary information (Figure S1).

Table 2.

Textural properties of some of the samples synthesized using the $NaOH/SiO_2$=0.32 molar ratio with the silicon precursors

Properties / Sample	BET Surface Area (m^2/g)	T-Plot Micropore Area (m^2/g)	t-Plot external area (m^2/g)	Pore diameter (nm)	t-Plot Micropore Area (m^2/g)
T-Na_1-Z-1	423	395	28	0.54	0.15
L-Na_1-Z-1	388	377	11	0.58	0.13
F-Na_1-Z-1	390	370	20	0.51	0.13
T-Na_1-M-1	388	377	11	0.61	0.13
T-Na_1-0-2	278	267	11	0,51	0.14
CBV2314	406	367	39	0,57	0,17
CBV21A	497	439	58	0,61	0,21

Table 2 shows that textural properties of the materials in which the seed was used presented values relatively close to those of the commercial ZSM-5 zeolite; it also allows to point out that in the case of the preparation without seed, its surface area was 35% lower than the value reported for its counterpart with seed. This implies that the seed, in addition to achieving a decrease in the synthesis time, also improves the physicochemical properties of the material.

2.4.1.4 Scanning electron microscopy (SEM). Figure 3 shows the SEM images of the materials reported in Table 2.

Figure 3.

Micrographs of samples prepared with TEOS a) T-Na1-Z-1, d) T-Na1-M-1, e) T-Na1-0-1. With Ludox b) L-Na1-Z-1, Fumes silica c) F-Na1-Z-1. See zeolites f) CBV2314(ZSM-5), g) CBV21A (MOR) and h) CBV100 (Y).

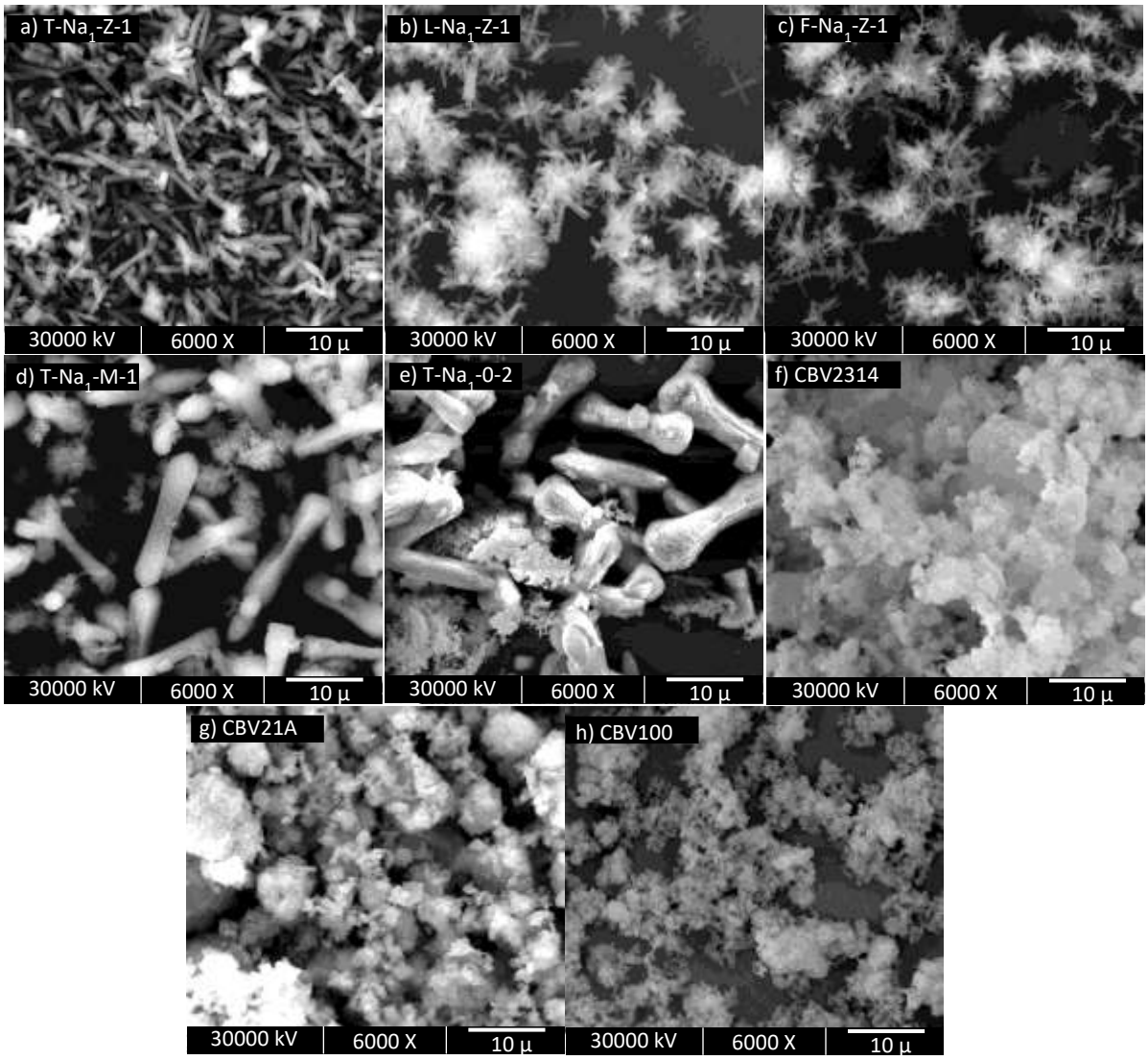

In the case of the sample prepared with TEOS without the help of seed (T-Na_2-0-2), it can be seen crystals with different shapes, in some cases they are elongated with a narrow half and round tips, in other cases they are like those presented with the sample prepared with TEOS and

ZSM-5 seed. It is also worth noting the presence of amorphous material surrounding some of these crystals and that their size is much larger than that observed with the samples prepared with ZSM-5 seed**.**

About the sample in which zeolite mordenite (T-Na_1-M-1) was used, crystals with an elongated hexagonal shape and tiny crystals around them can be observed. Those with an elongated hexagonal shape have a size comparable to those found in the sample prepared without seed (> 10 µ) and can be associated with the ZSM-5 phase; in comparison, the smaller crystals (< 5 µ) can be associated with the mordenite phase detected through XRD. These two crystalline environments reinforce the assumption that the added MOR zeolite crystals direct crystallization in the zones of the synthesis mixture in which they are embedded. In contrast, in those zones where they are not present, crystallization will be governed by the composition of the synthesis mixture.

2.4.2 General discussion of the results for the materials obtained with the molar ratio $NaOH/SiO_2$=0.32

The results presented above show differences in the formation processes of the ZSM-5 zeolite when using TEOS, fumed silica, and ludox. For the first, the margin for obtaining zeolite is wider (obtaining ZSM-5 without the presence of seed); for the other two, the margin is reduced to the point of requiring the presence of ZSM-5 seed to obtain it. The physicochemical characteristics of the silicon precursors and the phenomena generated during their mixing with the solution containing the aluminum precursor could be the reason for these differences.

Ludox consists of colloidal silica with a particle size of around 12 nm (Doroganov, 2012; Van der Meeren, et. al. 2004), while Fumed silica consists of aggregates of silicon particles with

sizes between 7 and 12 nm (Gun'ko et al., 2015; Liu and & Maciel, 1996) in both cases, the SiO_2 particles are already formed in the precursors. When the solutions containing the above precursors encountered the one containing the **Al** source, a gel with a viscous appearance was rapidly generated. Possibly the rapid reaction of the silicon species with those of aluminum can lead to the generation of aluminosilicates with Si/Al ratios that are not suitable for self-nucleation to occur, and the zeolite can be obtained without the addition of structure directing agent; a role that the composition units would come to play by providing the composition units of the MFI structure provided by the seed zeolite, acting as nucleation centers of new zeolitic material (Li et al., 2018; Gabelica, et. al, 1984). This supposed role as a crystallization nucleus that the zeolite plays may be responsible for the morphology observed in the SEM images, where the samples prepared with the Ludox and Fumed silica precursors lead to obtaining agglomerates of square bars joined at a central point forming a star.

Unlike Ludox and fumed silica, the formation of the aluminosilicate with TEOS takes place in a more controlled manner. TEOS consists of a monomeric silica source that, through hydrolysis and condensation reactions, can produce monodisperse silica particles and then react with aluminum species in solution. Since the rate of hydrolysis and condensation controls the silicon particles' release process, the aluminosilicate's formation is slower than other precursors. How the synthesis mixture was generated with the TEOS precursor, and considering that crystallization is also possible with this silicon precursor without the presence of seed particles, allows inferring that a Si/Al ratio was obtained in the synthesis mixture suitable for auto nucleation and the formation of zeolite ZSM-5 without the presence of seed (T-Na1-Z-0 synthesis); the addition of ZSM-5 seed accelerates the crystallization of this structure as shown by the comparison between the seeded and seedless samples (Grand, et. al., 2016; Mintova, et. al., 1992; Majano, et. al., 2009;

Derouane, et. al., 1981). Due to how the mixture was formed with TEOS, it can be inferred that the dispersion of the seed particles was also better than Ludox and Fumed silica precursors; this added to self-nucleation, which can explain why the images of the samples prepared with TEOS and ZSM-5 seed presented less agglomeration and a different shape than the samples prepared with the other two precursors.

Another aspect to highlight from the results is the influence the seed can exert on zeolite, considering the composition of the synthesis gel. With the Ludox and Fumed silica precursors, the presence of ZSM-5 zeolite, and only this zeolite, was crucial to obtain a zeolitic material. In this case, one could hypothesize about a "recognition" between the units of the synthesis gel, suitable for the formation of zeolite ZSM-5, and the seed zeolite that precisely contain that phase. This "recognition" effect has been proposed in the literature as a key to explaining the directing effect of the seed, in which the units in the gel are attached to the seed through the OH groups (Iyoki, et. al., 2014; Itabashi, et. al., 2012).

In the case of synthesis with TEOS and mordenite zeolite, both the directing effect exerted by the seed and the conditioning given by the synthesis gel can be evidenced. In this preparation, two phases were obtained: mordenite, promoted by the seed, and ZSM-5, which is probably produced thanks to the conditions of the medium. This would indicate seed has an effect in a defined range around it, while in the areas where it is not affected by the seed, there is self-nucleation and zeolite formation due to the system's composition (Zhu et al., 2017; Itabashi, et. al., 2012).

2.4.3 Synthesis of materials with a molar ratio NaOH/SiO₂=0.42

2.4.3.1. ATR-IR. The ATR-IR spectra of the samples synthesized with the molar ratio NaOH/SiO_2=0.42 and the three silicon precursors are presented in Figure 4.

Figure 4.

ATR-FTIR spectra of the synthesized samples using the molar ratio NaOH/SiO_2=0.42 with the silicon precursors: a) TEOS, b) Ludox, and c) Fumed Silica.

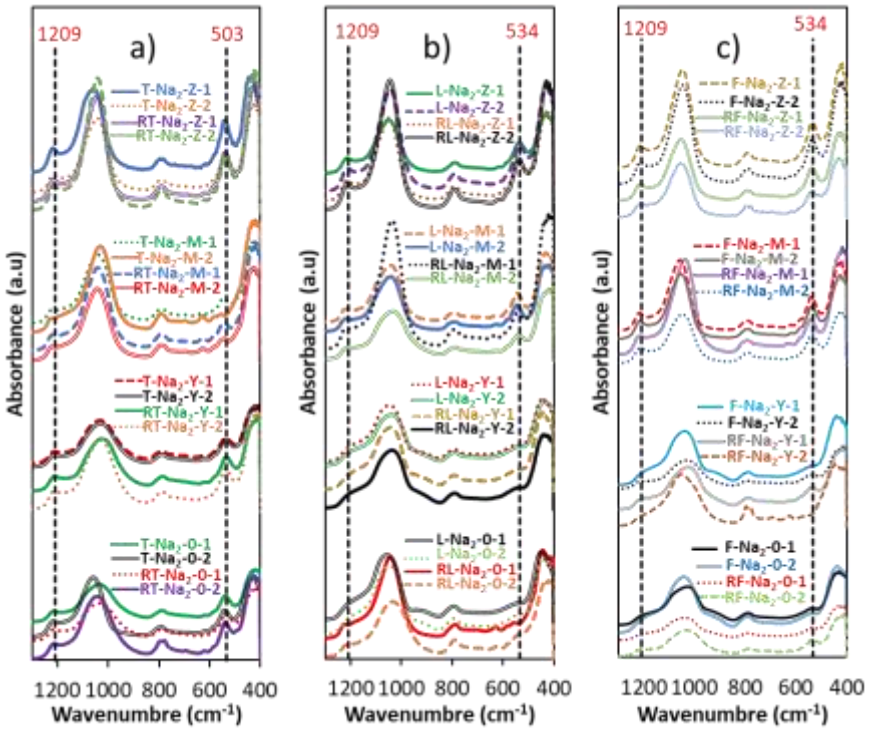

The results show all materials prepared with TEOS have bands around 550 and 1200 cm^{-1} regardless of the seed used and the crystallization time (Figure 4a). These bands can be observed within 24 h of crystallization with the not seeding sample, which could not be achieved with the

$NaOH/SiO_2$=0.32 ratio. Furthermore, samples prepared using zeolite Y as seed show bands associated with forming the MFI structure.

With the Ludox and Fumed silica precursors, the behavior was different (Figures 4b and c); although the bands related to the formation of the MFI structure can be observed for the materials synthesized with ZSM-5 and mordenite seeds; these were not formed, or they were of very low intensity for the materials synthesized using Y seed or in the seedless system.

However, the fact that the bands around 550 and 1200 cm^{-1} are present when using mordenite seed, with which their appearance was not possible with the ratio $NaOH/SiO_2$=0.32, indicates a positive effect on the increase in NaOH concentration in the synthesis.

2.4.3.2 X-ray diffraction. Figure 5 shows the XRD spectra for the materials obtained using TEOS as a silicon precursor (Figure 5a). In this, it can be observed that the samples synthesized with ZSM-5 seed present the characteristic peaks of the ZSM-5 phase, coinciding with those of the seed zeolite (CBV2314). Additionally, peaks related to the mordenite phase can also be observed.

The quantification presented in Table 3 indicates that the ZSM-5 phase is found in the highest proportion, regardless of the seed used or the hydrothermal time. Which reaffirms what was stated when analyzing the IR of said samples, the increase in the $NaOH/SiO_2$ ratio favored the formation of zeolite ZSM-5. However, the increase in NaOH concentration also favored the action of the mordenite zeolite crystals; in the experiments in which it was used as seed, the percentage of that phase increased by 13% compared to the experiment performed using a ratio of $NaOH/SiO_2$=0.32. Regarding the use of Y zeolite as seed, the results reported in Table 3 evidence that its presence in the synthesis led to a material with a lower percentage of the ZSM-5 phase

compared to the experiment in which no seed was used. This result suggests that the formation of ZSM-5 zeolite crystals was due more to the conditions of the synthesis mixture than to the use of Y seed.

Figure 5.

*XRD patterns of some selected samples whose IR spectra presented bands around 1209 cm-1 and 534 cm^{-1} for materials prepared with: a) TEOS, b) Fumed Silica and c) Ludox. *Mordenite peaks.*

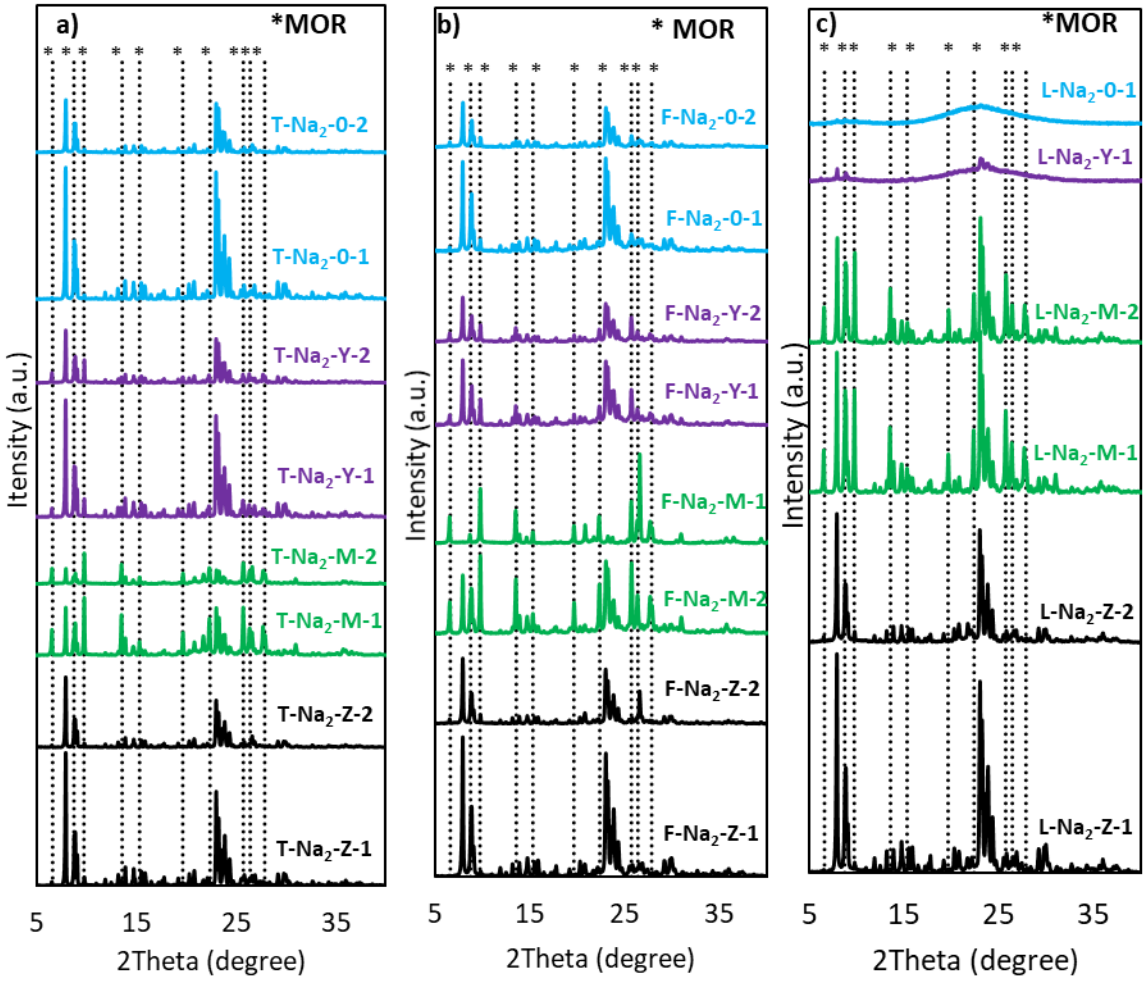

Regarding the hydrothermal treatment time, its increase generated an increase in the percentage of the mordenite phase; the most significant change occurred with the material prepared with zeolite Y, in which the percentage of the mordenite phase increased by around 5%. The X-rays for the experiments with Fumed Silica and Ludox are presented in Figures 5b and c. Except for the samples prepared using Ludox precursor, without seed and with Y zeolite, all the materials show the characteristic peaks of the ZSM-5 zeolite.

Table 3.

Phase percentages for some of the samples presented in Figure 5 Material

	Material							
	F-Na2-Z-1	**F-Na2-Z-2**	**F-Na2-M-1**	**F-Na2-M-2**	**F-Na2-Y-1**	**F-Na2-Y-2**	**F-Na2-0-1**	**F-Na2-0-2**
% MOR	2.0	5.0	25.5	41.7	13.2	16.2	8.2	26.3
% ZSM-5	98.0	95.0	74.5	58.3	86.8	83.8	91.8	73.7
	T-Na2-Z-1	**T-Na2-Z-2**	**T-Na2-M-1**	**T-Na2-M-2**	**T-Na2-Y-1**	**T-Na2-Y-2**	**T-Na2-0-1**	**T-Na2-0-2**
%MOR	4.1	4.4	32.9	35.8	7.2	12.1	2.9	3.4
% ZSM-5	95.9	95.6	67.1	64.2	92.8	87.9	97.1	96.6
	L-Na_2-Z-1	**L-Na2-Z-2**	**L-Na2-M-1**	**L-Na2-M-2**	**T-Na2-Y-1**	**T-Na2-Y-2**	**F-Na2-0-1**	**F-Na2-0-2**
%MOR	2.6	3.8	26.7	29.9	-----	-----	-----	-----
% ZSM-5	97.4	96.2	73.3	70.1	-----	-----	-----	-----

The percentage of the phases present in the samples is reported in Table 3; in this, it is possible to observe that the materials prepared with the ZSM-5 seed present the highest percentage of that phase, although it also presents a lower percentage of the mordenite phase that increases with increasing synthesis time. The presence of zeolite mordenite leads to the formation of this phase in the materials in which it was used, but the ZSM-5 phase continues to be the one with the highest percentage. This phenomenon occurred with the TEOS precursor but with the $NaOH/SiO_2$

ratio. Still, it should be noted that with the same NaOH concentration, the use of mordenite zeolite with the Ludox and silica fume precursors did not lead to the formation of zeolite. Concerning seedless systems and using **Y** seed with the fumed silica precursor, the main phase is ZSM-5. For 24 hours, this percentage is higher in the system without seed that in the system where zeolite **Y** was used.

It can also be observed in Table 3 that the increase in the synthesis time generates an increase in the percentage of the mordenite phase. The quantification of the samples prepared without seed and with seed Y but using the Ludox precursor; could not be reported due to the low intensity of their diffraction peaks, as can be seen in Figure 3.

2.4.3.3. Argon physisorption. Supplementary information Figure S1 and Table 4 report the Ar adsorption-desorption pore size distribution curves and the samples' textural properties, respectively. Generally, the samples prepared with the ZSM-5 seed have the highest surface area regardless of the silicon precursor. They also present a pore size distribution around 0.57 nm, characteristic of ZSM-5 zeolite.

Table 4.

Textural properties of some of the samples synthesized using the $NaOH/SiO_2$=0.42 molar ratio with the three silicon precursors

Properties / **Sample**	**BET Surface Area (m^2/g)**	**t-Plot Micropore Area (m^2/g)**	**t-Plot external area (m^2/g)**	**Pore diameter (nm)**	**t-Plot Micropore Area (m^2/g)**
T-Na_2-Z-1	416	402	14	0.57	0.14
T-Na_2-Z-2	324	310	14	0,61/1,08/0,84	0,10
T-Na_2-M-1	342	324	18	0,61/0,84/1,08	0,12
T-Na_2-M-2	84	81	3	0,84/1,08	0,03

Properties Sample	BET Surface Area (m^2/g)	t-Plot Micropore Area (m^2/g)	t-Plot external area (m^2/g)	Pore diameter (nm)	t-Plot Micropore Area (m^2/g)
T-Na_2-Y-1	338	315	23	0,54	0,13
T-Na_2-Y-2	274	263	11	0,51	0.12
T-Na_2-0-1	352	346	6,9	0,57//0,81/1,08	0,11
T-Na_2-0-2	343	335	8.14	0.51/0.84	0.10
L-Na_2-Z-1	402	374	28	0,51	0,13
L-Na_2-Z-2	328	310	18	0,51	0,11
L-Na_1-M-1	357	337	20	0,61/0,71//1,08	0,12
L-Na_1-M-2	156	147	9	0,61/0,88/1,045	0,05
L-Na_2-Y-1	18	15	3	---	0,01
L-Na_2-0-2	19	15	4	---	0,01
F-Na_2-Z-1	404	378	26	0,54	0,15
F-Na_2-Z-2	319	303	16	0,54/1,11/1,42	0,11
F-Na_2-M-1	294	283	11	0,71/0,88/1,08	0,1
F-Na_2-M-2	214	212	2,5	0,71/0,84	0,1
F-Na_2-Y-1	184	175	9	0,51/0,54/0,84	0,07
F-Na2-0-1	71	63	8	0.8	0.02
CVB2314	406	367	39	0,57/1,018	0,17
CBV21A	497	439	58	0,61	0,21

When MOR zeolite is used as seed, there is a change in the pore size distribution, focusing on 0.61 nm, 0.81, and 1.085, which occurs for all precursors. For the samples that presented surface areas greater than 100 m^2, the synthesis time of 48 h led to a deterioration of the textural properties; with all the precursors, there was a reduction in the surface area and the pore volume.

The lowest surface areas were found for the Ludox precursor with the materials prepared with zeolite Y and without using the seed. In the case of the Fumed silica precursor, even though the materials prepared with zeolite Y and in the seedless system presented diffraction peaks (Figure 5), their area surface was less compared to those obtained using the precursor of TEOS, and all those materials where ZSM-5 and mordenite zeolite were used as seed.

2.4.3.4 Scanning electron microscopy (SEM). Figure 6 shows the SEM images for the samples prepared with the three silicon precursors within 24 hours of hydrothermal treatment and whose phase percentage was reported in Table 3. Materials synthesized with the TEOS and the ZSM-5 seed, mainly crystal agglomerates with an elongated hexagonal shape and well-defined edges can be observed; the crystals are less than 5 microns, and both size and shape are homogeneous in the images obtained. In addition to observing hexagonal-shaped crystals, smaller crystals with a less defined shape are observed when using mordenite seed. Particles with a spherical shape can also be observed in some areas, which account for the heterogeneity in the forms of crystallization of the material when introducing the zeolite mordenite in comparison with the use of zeolite ZSM-5. With the use of Y seed and in the absence of seed, the predominant shape of the crystals coincides with those shown by the sample in which ZSM-5 seed was used, elongated hexagonal, but in these last two cases, the size of crystals can be up to three times larger.

Figures 6b and c show the similarity in morphologies of the materials prepared using Ludox and Fumed silica precursors with the ZSM-5 seed; in both cases, agglomerates of grain-shaped particles are present, whose size reaches less than 5 microns. These grains have a rough surface and undefined edges, unlike the material obtained using TEOS and the same seed. The use of mordenite seed also leads to morphological similarities between the materials synthesized with ludox and pyrogenic silica. The formation of two types of crystals can be observed for the two precursors, one with the form grain and more thin crystals shaped. This result is consistent with the presence of two phases reported in X-rays, in which the mordenite and ZSM-5 phases are detected. About the use of Y zeolite and in the seedless system, the formation of some crystals with granular shape can be observed for both, the Fumed silica and the Ludox precursor; in these

experiments, can also be detected the presence of amorphous material surrounding mentioned crystals.

Figure 6.

Micrographs of samples prepared with a-d) TEOS, e-h) Ludox and i-l) Fumed silica

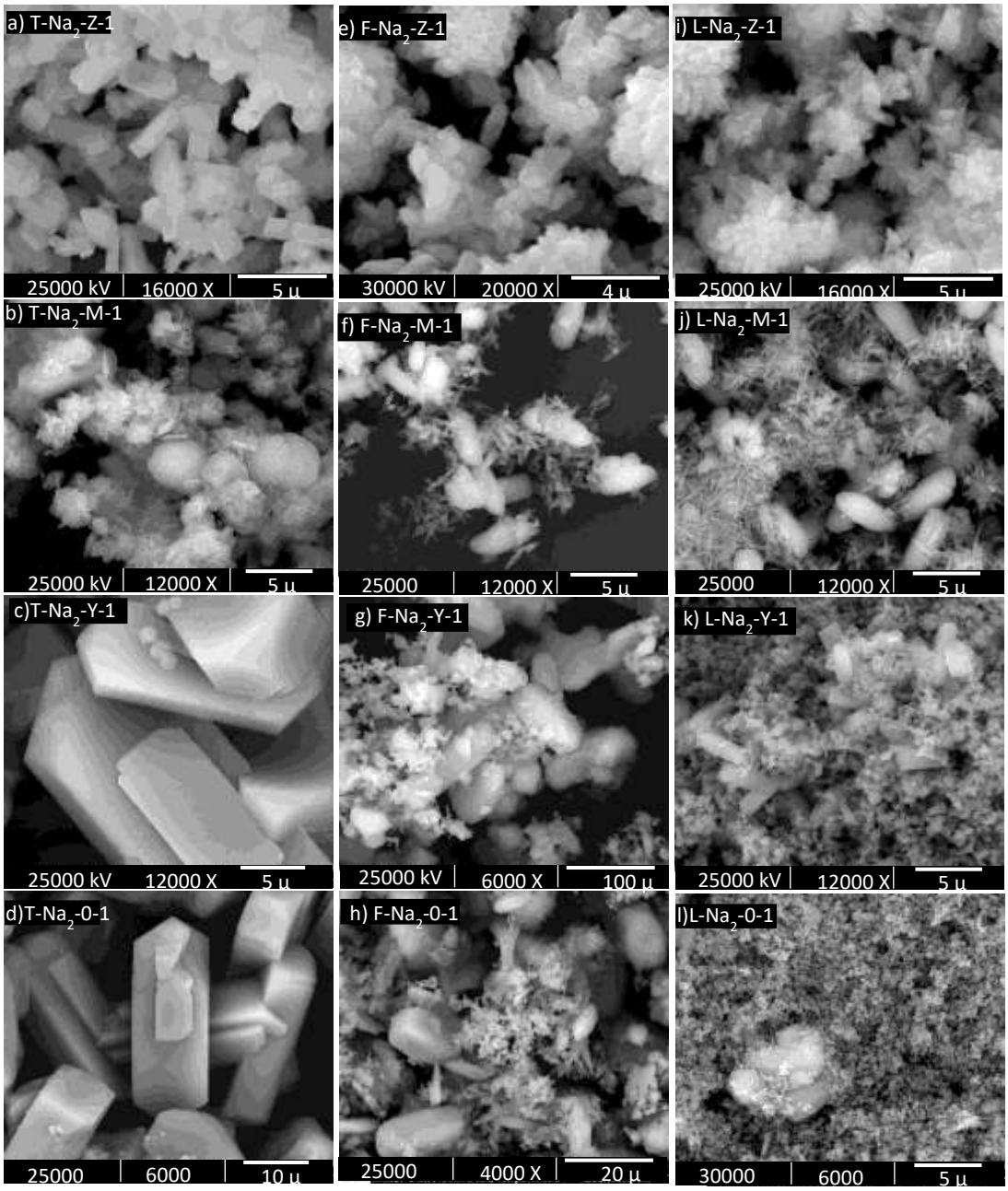

According to the SEM images, the proportion of amorphous material is always more significant when the Ludox precursor is used; the results agree with those presented in the X-ray section.

2.4.4 General discussion of the results for the materials obtained with the molar ratio $NaOH/SiO_2=0.42$

As a general analysis, the $NaOH/SiO_2$ ratio enhances the probability of obtaining a zeolitic material with all silicon precursors. An increase in the concentration of NaOH in the initial mixture leads to an increase in the concentration of hydroxyl groups OH^- and sodium cations Na^+ (Cundy & Cox, 2003; Kang, et. al., 209). It has been reported that the increase in the former in solution promotes the solubility and depolymerization of silicon sources, favors reactions between silicate and aluminate species in solution, and increases nucleation rate and crystallization during the synthesis of zeolites. As for the Na^+ cations, these have been reported as inorganic structure directors, which help to balance the negative charges of the zeolite network generated by the presence of aluminum (Cundy & Cox, 2005; Iyoki, et. al., 2014; Kadja, et. al., 2021; Culfaz & Sand, 1973).

Regarding the Ludox and Fumed silica precursors, the increase in the solubility and the depolymerization of the SiO_2 particles can help to obtain a more suitable Si/Al ratio for obtaining zeolite with greater homogeneity throughout the synthesis gel; this added to the structure-directing effect provided by a higher amount of Na^+ ions, can increase the probability of zeolite formation. Concerning the TEOS precursor, in addition to the benefits mentioned above, a higher amount of

OH^- can facilitate the precursor hydrolysis and obtain SiO_2 particles that will subsequently form part of the zeolite structure (Dos Santos, 2020; Grand, et. al., 2016).

In addition to the increase in the margin for obtaining zeolite, the increase in NaOH concentration also leads to an increase in the percentage of the modernite phase in the materials. Given that the mordenite structure can contain more aluminum atoms than zeolite ZSM-5 (Nada, et. al., 2019; Ren, et. al., 2012), obtaining it benefits from a higher amount of Na^+ that can compensate negative charge generated by said atoms. If we add the mordenite zeolite, the CBUS that it provides will also facilitate the formation of mentioned structure. It should be noted that, although there was an increase in the mentioned phase when using mordenite zeolite, the majority phase was always ZSM-5, which highlights what was mentioned in the previous section: the seed zeolite exerts a structure-directing effect in each environment that surrounds it, but if the composition of the synthesis gel can crystallize without the presence of seed, the phase will be determined by its composition (Iyoki, 2014; Itabashi, et. al., 2012).

Additionally, increasing the range for obtaining zeolitic material with all precursors, the increase in NaOH concentration also affects the morphology of the samples. In the case of the TEOS precursor, we can observe how the synthesized material with the molar ratio $NaOH/SiO_2$=0.21 and the ZSM-5 seed (T-Na_2-Z-1), present crystals with more defined edges and a less rough surface. than those obtained with the same seed, but with the ratio $NaOH/SiO_2$=0.21. These morphological differences may be related to an increase in the mobility of the aluminosilicate species, thanks to a greater solubility of the precursors due to the increase in NaOH concentration, which allows a greater ordering of the structure.

In relation to the difference in size of the crystals of the samples T-Na_2-Z-1 and T-Na_2-0-1, this may be related to the difference in the amount of crystallization nuclei dispersed in the

synthesis mixture, the amount was greater thanks to the seed in sample T-Na_2-Z-1 than in the sample prepared without seed T-Na_2-0-1, a greater amount of crystallization nuclei would imply more sites in which the particles can be adsorbed. aluminosilicate species, thus having a lower amount of nutrients per nucleus compared to the sample prepared without seed, where the nuclei are fewer.

Regarding to the use of zeolite Y as seed, although in the literature it has been reposted that it can help to obtain zeolite ZSM-5, playing a role of seed or undergoing an interconversion towards that zeolite (Qin, et. al., 2019; Dos Santos, 2020; Goel, 2015; Pan, 2010), the results found under the conditions studied in this work show that zeolite Y did not play a role in the synthesis. In the cases in which zeolitic material was obtained with its presence, it was also obtained without the presence of seed, in fact, properties such as the surface area or the percentage of the ZSM-5 phase were higher in the absence of seed. The results with the $NaOH/SiO_2$ ratio=0.32 show that it was not possible to obtain zeolite with this seed, while it was possible to obtain it in the system without seed.

2.4.5 Synthesis of materials with a $NaOH/SiO_2$=0.58 molar ratio

2.4.5.1 ATR-IR. Figure 7 presents the IR spectra of the materials synthesized with the highest concentration of NaOH.

Figure 7.

ATR-FTIR spectra of the synthesized samples using the molar ratio NaOH/SiO_2=0.58 with the silicon precursors: a) TEOS, b) Ludox, and c) Fumed Silica.

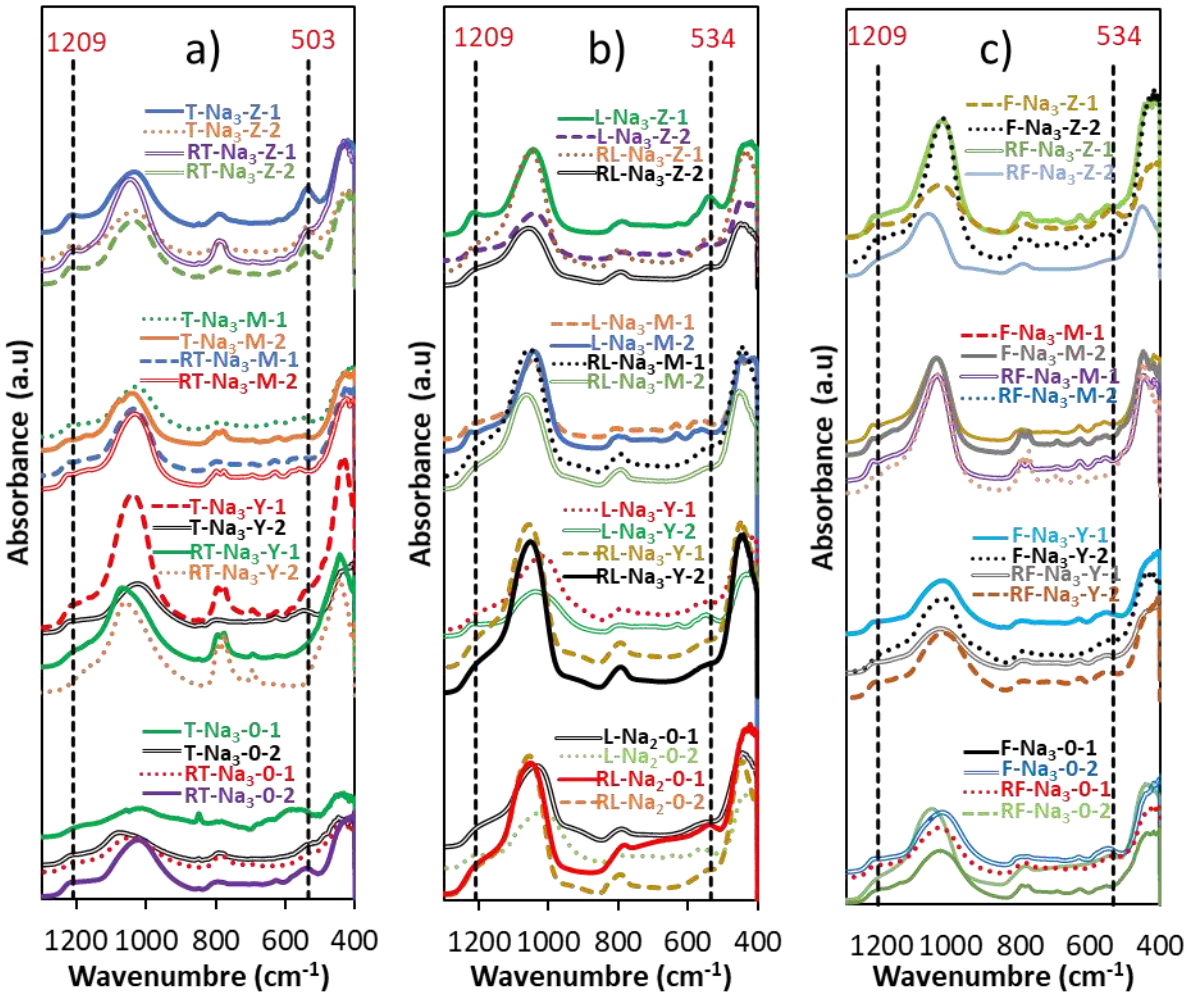

It was observed that the bands at 550 and 1200 cm^{-1} appeared with greater intensity in the samples prepared with zeolite ZSM-5; for the remaining samples, they were of low intensity or absent. This result was similar for the three silicon precursors regardless of the crystallization time. The results then indicate that this concentration of NaOH is not favorable for ZSM-5 zeolite obtention.

2.4.5.2 X-ray diffraction. Based on the IR results, three samples prepared with ZSM-5 seed were analyzed by X-ray. The results are presented in Figure 8, and show the characteristic peaks of the mordenite phase with greater intensity than the characteristic peaks of the ZSM-5 phase, indicating that despite the presence of CBU contributed by ZSM-5 zeolite, the synthesis composition favors the formation of mordenite zeolite.

Figure 8.

*XRD patterns of some selected samples prepared with TEOS (T-Na3-Z-1), Ludox (L-Na3-Z-1) and Fumed Silica (F-Na_3-Z-1) prepared with ZSM-5 seed. *Mordenite peaks.*

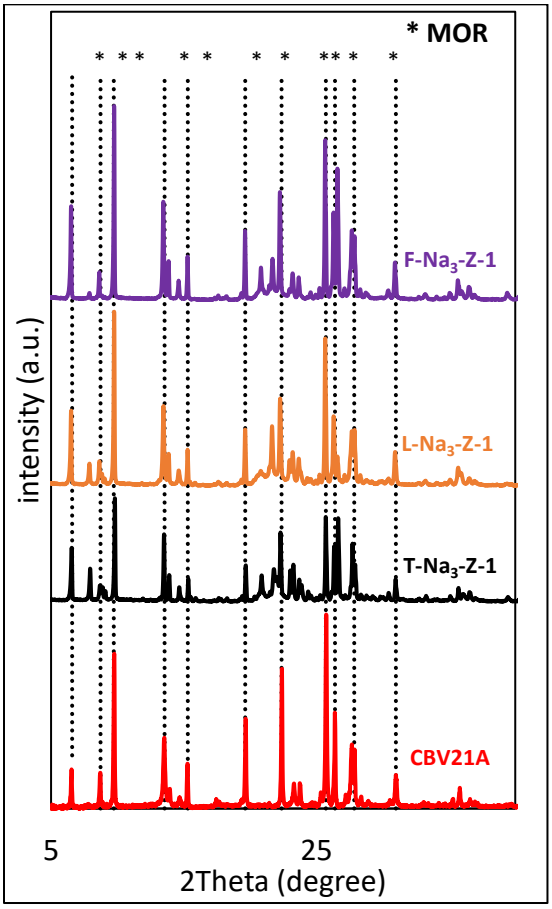

The quantification of the phases of the samples presented in Figure 8 is presented in Table 5, where the is confirmed: the percentage of the mordenite phase in the three samples is greater than 80 %.

Table 5.

Phase percentages for some of the samples presented in Figure 9

	Material		
	T-Na_3-Z-1	**LD-Na_3-Z-1**	**F-Na_3-Z-1**
%MOR	81	85.6	90.4
% ZSM-5	19	14.4	9.6

2.4.5.3 Scanning electron microscopy (SEM). Figure 9 presents the SEM images for the samples prepared with zeolite ZSM-5, whose X-ray results were reported in Table 5. Additional images can be seen in the supplementary information (Figure S2). Different morphologies can be observed by changing the silicon source, even though the majority phase is mordenite in the three samples.

Figure 9.

SEM micrographics sample prepared with highest Na concentration ($NaOH/SiO_2$=0.58), ZSM-5 seed, 24 hours of hydrothermal treatment and with the precursors of a) TEOS, b) Ludox, and c) Fumed silica.

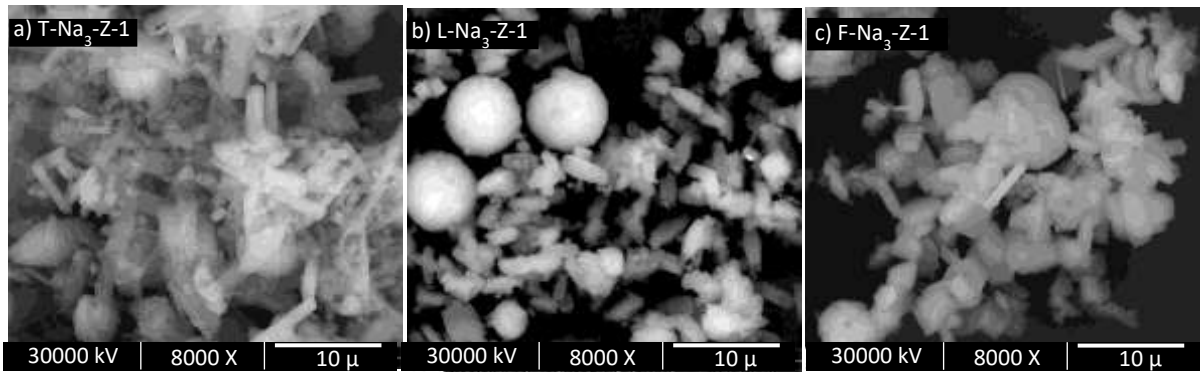

In the case of the TEOS precursor, mainly rod-shaped crystals can be observed; in the sample prepared with Ludox, it is possible to observe elongated hexagonal crystals mixed with irregular crystals. Concerning the sample prepared with Fumed silica, the crystals have a hexagonal shape but, in this case, with sides of similar sizes. Despite the differences in the images presented in Figure 9, species of spheres can be observed in all the samples analyzed.

2.4.5.4 Argon physisorption. Table 6 summarizes the textural properties of the samples for the 3 silicon precursors and prepared using the ZSM-5 seed.

Table 6.

Textural properties of some of the samples synthesized using the $NaOH/SiO_2$=0.32 molar ratio with the silicon precursors

Properties / Sample	BET Surface Area (m^2/g)	t-Plot Micropore Area (m^2/g)	t-Plot external area (m^2/g)	Pore diameter (nm)	t-Plot Micropore Area (m^2/g)
T-Na3-Z-1	242	223	19	0.58, 1.08	0.1
L-Na3-Z-1	228	218	10	0.61, 1.08	0.07
F-Na3-Z-1	224	208	15	0.61, 1.08	0.07

These materials presented a low surface area compared to the ZSM-5 zeolite used as seed and the commercial mordenite zeolite. It is worth mentioning that the samples recovered from the samples prepared with the previous $NaOH/SiO_2$ ratios were powders, most of the samples recovered with the $NaOH/SiO_2$ ratio=0.58 were compact and took the shape of the bottom of the reactor, as can be seen. in the images presented in Figure 10, for the samples presented in Table 6.

Figure 10.

Samples recovered and compacted with the $NaOH/SiO_2$ ratio=0.58.

2.5 Conclusion

The results presented in this work allow us to conclude that the use of the precursor TEOS offers a broader margin for obtaining zeolite ZSM-5 compared to the precursor's Ludox and Fumed Silica. Under the lowest alkalinity conditions, the ZSM-5 zeolite could be obtained with TEOS, even without the help of the seed zeolite, which was not possible with the other two silicon precursors. It was also shown that the seed zeolites can exert a directing effect on the structure of the synthesis mixture around them but that the composition of the said mixture was what determined the majority phase to be formed. Regarding the use of zeolite Y as seed, in this work, it was observed that it did not have a relevant or beneficial effect for obtaining zeolite ZSM-5 since the results without the presence of seed were the same or even better.

In addition, the concentration of NaOH in the synthesis was a crucial factor in obtaining zeolite ZSM-5. At the lowest concentration ($NaOH/SiO_2$=0.32), the presence of ZSM-5 seed was always necessary to obtain crystalline ZSM-5 zeolite with a high surface area, regardless of the silicon precursor. With the intermediate concentration ($NaOH/SiO_2$=0.42), it is possible to obtain zeolite ZSM-5 with the precursor TEOS and fumed silica in the seedless system and with zeolite Y; however, the formation of the mordenite phase is also promoted. Finally, with the highest alkalinity ($NaOH/SiO_2$=0.58), the production of zeolite ZSM-5 is not favored, while the formation of the mordenite phase is promoted.

3. Understanding the mechanochemical synthesis of zeolites: Analysis of the effects of key components

3.1 Abstract

This research seeks to understand some critical aspects of the solvent-free synthesis of zeolite ZSM-5. Aspects such as the influence of the particle size variation of the silicon source on the morphological, textural, and crystallographic properties of zeolite ZSM-5 were analyzed. In the first part of the work, the synthesis of ZSM-5 zeolite was explored with the help of an organic structuring agent (OSDA), finding that the size of the silicon particles only generated morphological changes when silica gel was used. It was also found that the crystals obtained using OSDA are much larger than those obtained using seeds and have larger surface areas. It was found that a high concentration of Na favors the appearance of phases such as mordenite (MOR) and larger silica gel particles. Finally, a comparison was made by varying the crystallization time between mechanochemical and sol-gel synthesis to study the differences and common aspects.

Keywords. ZSM-5 zeolite, mechanochemical, solvent-free, silicon precursor, sodium. concentration.

3.2 Introduction

Zeolites are microporous crystalline materials whose structure is mainly formed by aluminum and silicon tetrahedra and can be used as catalysts, adsorbents, and gas separators

(Cundy & Cox, 2005). ZSM-5 zeolite is widely used in processes such as xylene isomerization, toluene alkylation, and disproportionation, among other (Dawagreh, 2017). Conventionally, the synthesis is carried out through solvothermal processes involving ammonium based cationic reactants as organic structure directing agents and solvents such as water or alcohol (Cundy & Cox, 2005; Liu & Yu, 2016; Ma, et. al., 2020; Pan, et. al., 2016). Among the drawbacks that conventional synthesis are the generation of liquid residues in which reagents can be wasted, low yields related to the fact that the volume occupied by the solvent that can be up to fifty percent of the total reactor volume, and the need for eliminating the organic structuring agent via calcination thence requiring energy consumption and producing NO_x. Therefore, research has focused on producing zeolites by alternative routes such as the seed-assisted and the solvent-free synthesis via mechanochemistry (Liu & Yu, 2016; Pan, et. al., 2019; Asgar Pour & Sebakhy, 2022; Xu & Wu, 2022; Wang, et. al., 2020; Mei, et. al., 2021).

In the seed-assisted synthesis, usually a small amount of the targeted zeolite is added during the synthesis is added to fulfill the role of structure directing agent (Grand et al., 2016)(Wu et al., 2019)(dos Santos et al., 2020).The seed provides crystallization nuclei that promote the formation of a structure with similar composite construction units. Zhang et al., (2013) studied how the modification of the Si/Al ratio and the crystallization time of ZSM-5 led to the formation of intracrystalline mesopores in the zeolite.

On the other hand, the mechanochemical method for mixing zeolite precursors (also called reactive grinding) has been found to be an alternative to reduce or eliminate solvent usage during the zeolite's synthesis(Wu et al., 2019)(Ren et al., 2012). Indeed, grinding provides the energy to carry out the reactions needed to form the compounds that will further crystallize during thermal treatment (Nada, et. al., 2019; Nada, et. al., 2019; Wang et. al., 2020). Furthermore,

mechanochemical processing has been combined with seed-assistance to produce ZSM-5. Wu et al., (2014) studied the seed-assisted synthesis of ZSM-5 and beta zeolites via reactive grinding using mortar and pestle. They found that small amounts of water were needed to produce these zeolites with this method. They proposed that water is required to facilitate the hydrolysis and condensation of the Si-O-Si bonds that will further produce the zeolite. They also found that zeolites were not produced when seeds were not added. Later on, Nada et al., (Nada, et. al., 2019; Nada, et. al., 2019) studied this kind of synthesis using a planetary ball mill and analyzed the role of the operating conditions of the mill on the properties of the produced materials (Goel et al., 2015). Particularly, they found that found that ball milling should be done for at least 50 min to obtain crystalline ZSM-5 after hydrothermal treatment. Recently, we presented a study on how the milling time and speed as well as the Na_2O/SiO_2 and H_2O/SiO_2 molar ratios influence the properties of materials of the ZSM-5 type produced via seed-assisted mechanochemical processing (García-Sánchez, et. al., 2021). Our results allowed concluding that, on the one hand, the non-linear combination of milling time and speed leads to supplying different amounts of energy during milling where the latter is key to determine the morphology, porosity, and acid properties of the zeolites. Besides, sodium was found to perform the role of structure directing agent while also promoting the aluminum enrichment of the materials.

In this contribution, we systematically studied the following aspects of the seed-assisted mechanochemical synthesis method: (i) what is the role of the type of silicon precursor on the properties of the materials? (ii) How does the use of a ZSM-5 seed changes the properties of the materials produced with the different silicon precursors? (iii) Does sodium also play a role as structuring agent under the conditions of the present study? (iv) What is the influence of water on the apparent kinetics of the crystallization stage of the process?

The investigations presented so far show the great potential of the solvent-free synthesis of zeolites as an alternative to the conventional way. Possible benefits include reducing waste generation and greater use of the volume available in the synthesis reactors. However, for this synthesis route to replace the conventional one, it is necessary to delve into aspects that allow the identification of crucial synthesis parameters and how they can affect the physicochemical characteristics of the final material (Liu & Yu, 2016; Wang, et. al., 2020).

One of the aspects to be considered in the synthesis without solvents is that the size of the crystals produced by this route is comparatively more significant than those obtained by the Sol-Gel route.

On the other hand, Mintova et al., (2002) showed how the size of the zeolite obtained. They obtained zeolites with sizes of 15, 25, and 50 nanometers using tetraethyl orthosilicate silicon precursors, Ludox LS-30, and Fumes silica (Cab-O-Si), through the variation of the silicon source.

However, Zhang et al., (2018) produced ZSM-5 crystals with sizes between 100 to 6000 nm by changing the amount of water during the hydrothermal stage of the synthesis process. The authors found a linear correlation between the H_2O/SiO_2 ratio of the synthesis and the size of the crystals.

3.3 Experimental section

3.3.1 Materials

The following materials were used in this research: sodium metasilicate pentahydrate ($Na_2SiO_3.5H_2O$, > 99.9%, Aldrich), sodium metasilicate nonahydrate ($Na_2SiO_3.9H_2O$, > 99.9%,

Aldrich), fumed silica 1 (SiO_2 with average particle size of 0.007 μm, > 99.9 %, Aldrich), fumed silica 2 (dry SiO_2 with average particle of 0.2 μm, > 99.9 %, Aldrich) as silicon precursors; aluminum sulfate ($Al_2(SO_4)_3.18H_2O$, 97 %, Merck) as aluminum precursor; tetrabutylammonium bromide (TPABr, > 98 %, Aldrich) as organic structure directing agent, and CBV2314 (Brand, type) and homemade ZSM-5 zeolite used as seeds; sodium hydroxide (NaOH, > 99 %, Merck) and ammonium chloride (NH_4Cl, > 99.5%, Aldrich) as inorganic reactants, and type I water as solvent.

3.3.2 Zeolites synthesis

3.3.2.1 Preparation of the seed zeolite. The seeds used for the mechanochemical synthesis process were prepared via Sol-Gel as follows. For this purpose, aluminum sulfate and sodium hydroxide were dissolved in type I water and mixed with an aqueous mixture containing sodium metasilicate pentahydrate ($Na_2SiO_3.5H_2O$, > 99.9%, Aldrich), sodium metasilicate nonahydrate ($Na_2SiO_3.9H_2O$, > 99.9%, Aldrich) and commercial zeolite seed (CBV2314). The mixture of these two fluids, whose molar composition was SiO_2: 0.025 Al_2O_3: 0.157 Na_2O: 60 H_2O, whle using a seed/SiO_2 mass ratio was 0.1, was made by stirring for 24 h. Afterwards, the mixture was deposited in a stainless steel reactor provided with a PTFE coating and underwent a hydrothermal treatment for 24 h under autogeneous pressure. After this process, the produced solid was recovered by filtration and then washed with type I water through centrifugation.

3.3.2.2 Mechanochemical synthesis using tetrabutylammonium bromide as structure directing agent. This synthesis was made with fumed silica 1, fumed silica 2, silica gel, and sodium metasilicate pentahydrate ($Na_2SiO_3 \cdot 5H_2O$) as silicon precursors. Each one of the silicon

precursors was mixed with aluminum sulfate, tetrapropylammonium bromide, and ammonium chloride (NH_4Cl), were subjected to a milling process for 20 min at a speed of 400 rpm in a planetary mill (Retsch- PM100) using 29 balls of 1 cm diameter and a 125 mL stainless steel container. The molar ratios in the initial grinding mix were as follows: H_2O/SiO_2= 3.2, $TPABr/SiO_2$= 0.15, NH_4Cl/SiO_2= 0.7, SiO_2/Al_2O_3= 40. The amount of sodium metasilicate was calculated considering that it provides the Na cations in the mixture and that some react with the anions released by the NH_4Cl forming NaCl salt, Na_2O/SiO_2= 0,56 (Without reacting with NH_4Cl), Na_2O/SiO_2= 0,21 (Taking into account the reaction with NH_4Cl). The ground product was put into a sealed autoclave where it was maintained under autogenous pressure while heating at 180 °C for 24 h in a static oven. Afterward, the autoclave was cooled to room temperature by putting them in cold water. The produced solids were recovered and washed with type I water, centrifuging them to remove any unreacted soluble precursors after each wash. Calcination of the recovered powders at 550 °C for 6 h ensured the removal of the organic template from produced aluminosilicates.

3.3.2.3 Mechanochemical synthesis using ZSM-5 seeds. For this synthesis, the grinding conditions were the same as those used in section 2.2.2, and the silicon precursors, the sodium concentration (Na_2O/SiO_2), and the amount of water (H_2O/SiO_2) were varied. A definite amount of the ZSM-5 zeolite synthesized in 2.2.1 was used as seed. The H_2O/SiO_2 ratio variation was made using $Na_2SiO_3 \cdot 5H_2O$ and $Na_2SiO_3 \cdot 9H_2O$.

3.3.3 Experiments to analyze the evolution of the materials during crystallization

A series of experiments were done for studying the apparent kinetics of crystallization of ZSM-5 synthesized via the seed directed mechanochemical route. For comparison purposes, a similar set of tests were done for the seed directed synthesis of ZSM-5 by sol-gel described in section 2.2.1. The initial molar composition of both syntheses was: SiO_2: 0.025 Al_2O_3: 0.157 Na_2O: 60 H_2O, and the seed/SiO_2 mass ratio was 0.1. Tests consisted of dividing into eleven samples. Then, these materials were submitted to the same hydrothermal treatment described earlier but, this time, such process was stopped at different times; namely, 2, 4, 6, 8, 10, 12, 14, 16, 18, 20, and 24 h.

3.3.4 Materials nomenclature: summarize and give an example

The names of the samples were assigned following the following terminology: X-Na_{1-2}-$W_{5-9,}$ where X can be FS1, FS2, or SG depending on whether the silicon precursor was 7 nm particle size fumed silica (FS1), 200-300 nm particle size fumed silica (FS2), or silica gel with 63.0-300.0 µm of particle size (SG). Regarding the alkalinity, Na_1 indicates a Na_2O/SiO_2 molar ratio of 0.16 and Na_2 a molar ratio of 0.21. In the case of water content, W_5 means an H_2O/SiO_2 ratio of 1, and W_9 means an H_2O/SiO_2 ratio of 2.

3.3.5 Materials characterization

The morphology, crystal size, and chemical composition of the materials were studied with a QUANTA FEG 650 scanning electron microscope (SEM) using an Everhart Thornley detector (ETD) for morphology and an SSD type Back Scattered Electron detector (BSED) for composition. Before the analyses, samples were coated with gold for controlling differential charging effects during the measurements. The crystalline structure of the materials was studied by collecting X-ray diffraction (XRD) patterns with a D8 advanced X-ray diffractometer (Bruker) provided with Cu Kα1 radiation. XRD patterns were recorded between 2θ angles of 3.5-70 with a 0.02 step size.

The porosity and surface area of the materials were estimated from argon adsorption-desorption isotherms obtained with a 3Flex apparatus (Micromeritics) at 87 K. For the tests, samples of approximately 0.1500 g of each material were degassed –(apparatus, vacuum pressure: see at 120 ° C for 2 h and then at 300 °C overnight. After optimizing the CBET parameter with the Rouquerol consistency criteria, specific surface areas were calculated with the BET method.

The chemical structure of the materials was analyzed after recording infrared spectra for samples from them. Measurements were made with a Nicolet iS50 Fourier Transform Infrared (FT-IR) spectrometer (ThermoScientific) equipped with an attenuated total reflectance (ATR-FTIR) detector.

3.4 Results and discussion

This section is divided into four subsections. Each one of them is devoted to answer the questions asked in the Introduction of the paper.

3.4.1 What is the role of the type of silicon precursor on the properties of the materials?

To answer this question, the section is divided into two parts. The first one discusses the effects of the type of silicon precursor for the materials synthesized with tetrabutylammonium bromide as structure directing agent and the second for the materials synthesized using a ZSM-5 seed as structure directing agent.

3.4.1.1 Materials synthesized with tetrabutylammonium bromide as structure direct agent. Figure 1 shows selected micrographs taken from samples of the materials produced with TPABr as structure directing agent and using different silicon precursors (Figures 1a, 1b, and 1c). Micrographs from samples of the silicon precursors; fumed silica 1, fumed silica 2, and silica gel, are shown in Figures 1d) – 1f), respectively, for reference purposes. Results in Figure 1 show that the materials prepared with both fumed silica precursors presented similar elongated hexagonal shapes and what appears to be an accumulation of sheets in the central part. Although the particle sizes between the two fumed silicas are different, the sizes of the crystals formed with them did not show significant differences.

Figure 11.

SEM micrographs of materials synthetized with OSDA and d) fumed silica 1 (FS1), e) fumed silica 2 (FS2) and f) silica gel (SG).

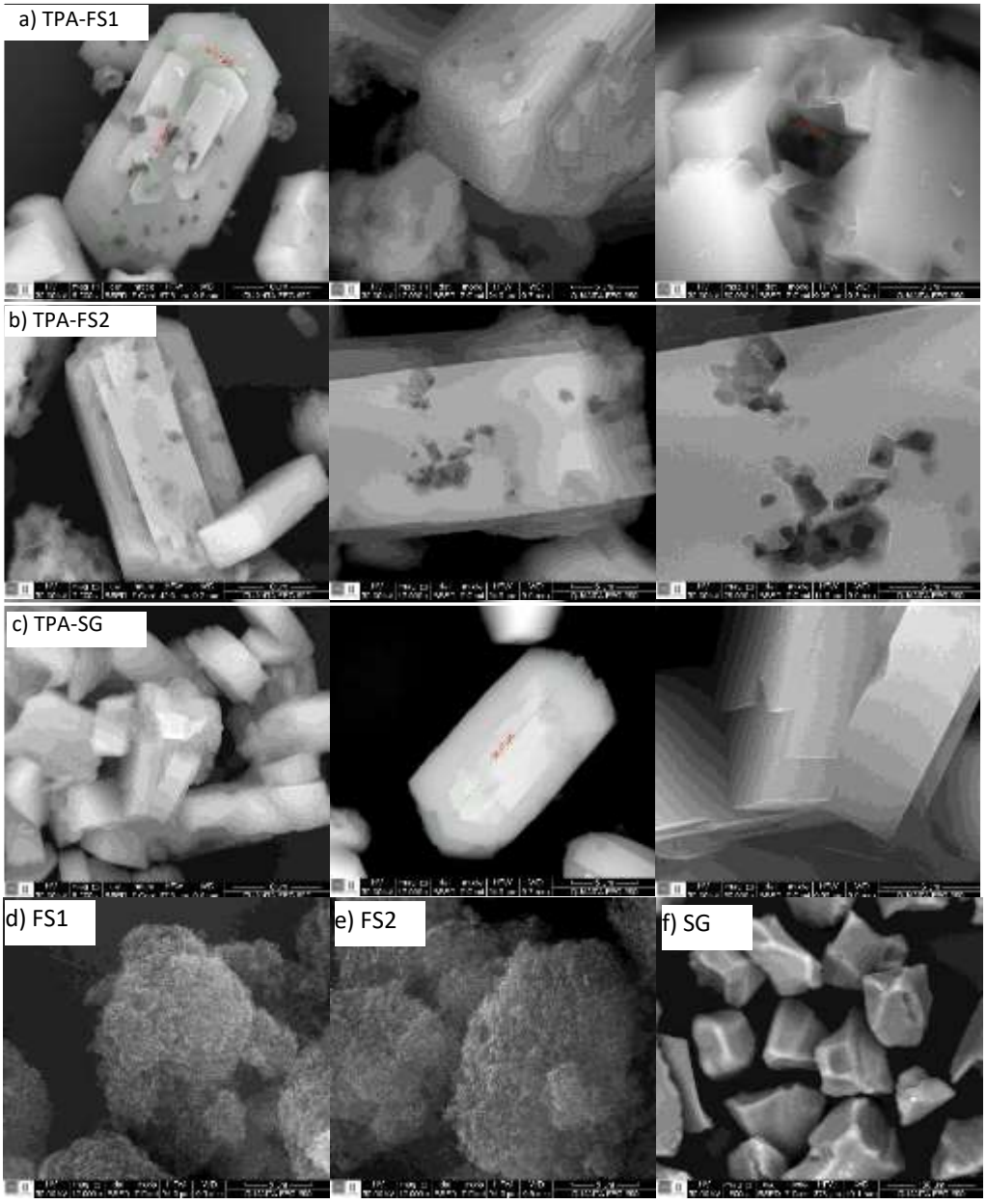

In addition, the materials synthesized with fumed silica showed large crystals with sizes up to 30 mm in length and 15 mm width. These crystals showed macroscopic holes of different sizes.

In addition to the regularly shaped crystals mentioned above, it is possible to observe agglomerates of tiny irregularly shaped particles and broken crystals. In relation to the silica precursors used, the two fumed silicas show similar appearances, they are composed of agglomerates of small particles with a spongy appearance. This contrasts with the images for silica gel, in this case larger particles with a more compact appearance can be observed. The comparison between the images of the starting precursors and the materials obtained with them indicate two different forms for the formation of the crystals; for silica fume precursors, whose particles are in the range of 12-300 nm, an aggregation must occur during crystallization to end up with crystals of sizes up to 30 micrometers. While for the silica gel precursor, which has particles with sizes even greater than 100 microns, a dilution must be present to later form crystals with sizes up to 15 microns. Using the Silica gel precursor, whose particle size is larger than that of silica fume precursors, it is possible to obtain crystals with a smaller size and with a surface with fewer defects than the crystals obtained with silica fume. Hypothetically the silica gel precursor must go through a dissolution process to later form crystals during hydrothermal treatment; with fumed silica, the particles must first be aggregated w to form zeolite crystals later. In addition to the morphological changes, technical differences were also evidenced in this work at the time of performing the syntheses.

Concerning the materials produced from silica gel, About the synthesis using silica gel, Figure 1 shows that the crystals formed with this precursor have a relatively smaller size. Furthermore, the observed crystals did not show inter-micropores as it was the case for the materials synthesized from fumed silica.

Figure 2 shows the diffractograms for samples taken from the produced materials and from the CBV2314 ZSM-5 for reference purposes. All diffraction patterns were basically the same with no peaks other than those corresponding to the MFI structure of ZSM-5 (Alipour et al., 2014). In

conclusions, the mechanochemical synthesis performed with tetrabutylammonium bromide always led to ZSM-5 regardless of the origin of the silicon source.

Figure 12.

X-ray powder diffraction patterns of the material synthesized with OSDA and the three silicon precursors.

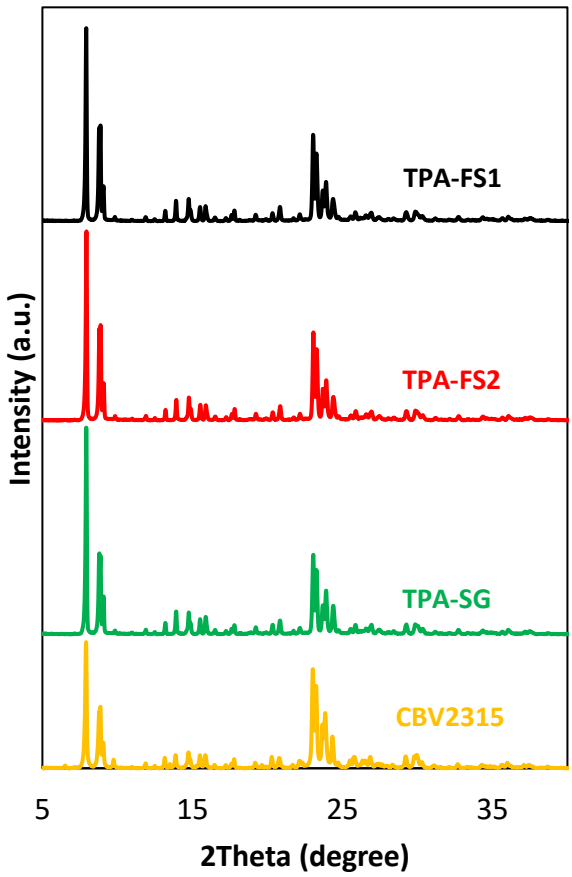

Figure 3 presents the **Ar** adsorption-desorption isotherms, increase for materials synthesized with OSDA using the three silicon precursors. The three samples present Type I isotherms, characteristic of microporous materials (IUPAC classification), and hysteresis loops

that may be associated with a tiny fraction of mesopores generated for the roughness of the crystals or interparticle voids.

Figure 13.

Adsorption desorption argon isotherm of material synthesized with OSDA and a) FS1 (TPA-FS1), b) FS2 (TPA-FS2), and c) SG (TPA-SG1).

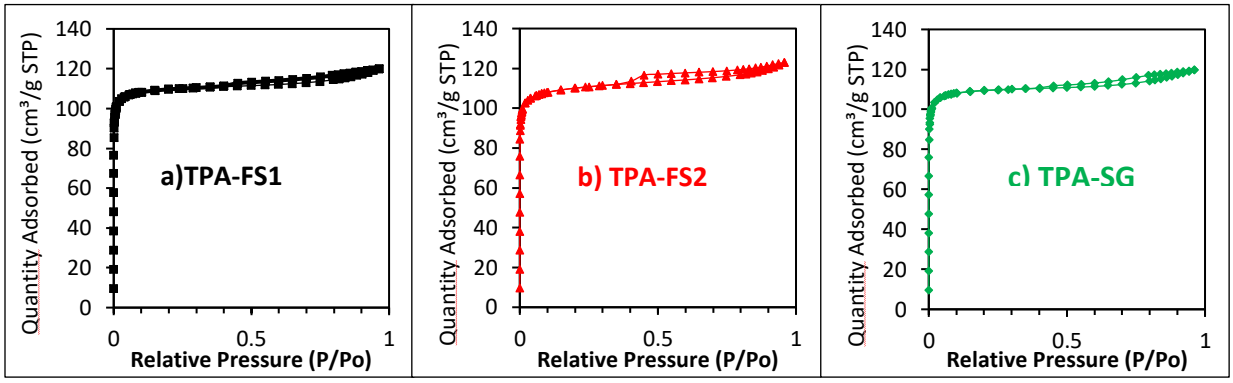

Table 1 presents the values of the textural properties for the materials synthesized with OSDA and for the commercial ZSM-5 zeolite (CBV 2314). The values reported values are consistent with what was observed in the adsorption-desorption isotherms of argon; the three prepared materials are mainly microporous, and their textural properties are similar each other. It can also be seen that regardless of the silicon precursor used, the textural properties are like those of commercial zeolite.

Table 7.

Textural properties for material synthesized with OSDA and commercial ZSM-5 zeolite (CBV2314).

Properties Material code	BET surface area (m^2/g)	t-Plot micropore area (m^2/g)	t-Plot external area (m^2/g)
TPA-FS1	396	370	26
TPA-FS2	392	354	37
TPA-SG	394	371	23
CBV2314	406	367	39

The results presented so far indicate that the size of the silicon source does not affect either the crystal structure or the textural properties of ZSM-5 zeolite produced through the mechanochemical route using organic structuring agent; however, morphological differences do occur.

Considering that ZSM-5 can be produced mechanochemically under the same conditions with both fumed silica and silica gel, one may wonder which one is more convenient from the operative point of view. Figure 4 shows pictures of the state of the milling jars during the reactive grinding stage of the synthesis. One may easily notice that the same mass of fumed silica occupies the entire volume of the grinding vessel while the silicon precursor only occupies a quarter.

Figure 14.

State of the milling jars during the reactive grinding stage of the synthesis a) Silica gel (SG) before and after milling and, b) Fumed Silica 2(SF2) before and after milling.

3.4.2 Materials synthesized using ZSM-5 seeds as structure direct agent

This section will be divided into two subsections as in agreement with the two different Na_2O/SiO_2 molar ratios that were used.

3.4.2.1 What is the role of sodium on the properties of the materials?

3.4.2.1.1 Syntheses made at Na2O/SiO2=0.16. Figure 5 shows the SEM images for the samples prepared with the molar ratio Na_2O/SiO_2=0.16, the three silicon precursors, and sodium silicate (nona and pentahydrate). In general, the three samples are made up of agglomerates of crystals in which a high quantity is observed in the form of hexagons with sides ranging from 400

to 1000 nm. The modification in the concentration of water using the precursors nona and pentahydrate, did not generate a significant change in the morphology of the samples.

Figure 15.

SEM micrographs of materials synthetized without OSDA, Na_2O/SiO_2=0.16 molar ratio and nona or pentahydrate sodium silicate (W9and W5).

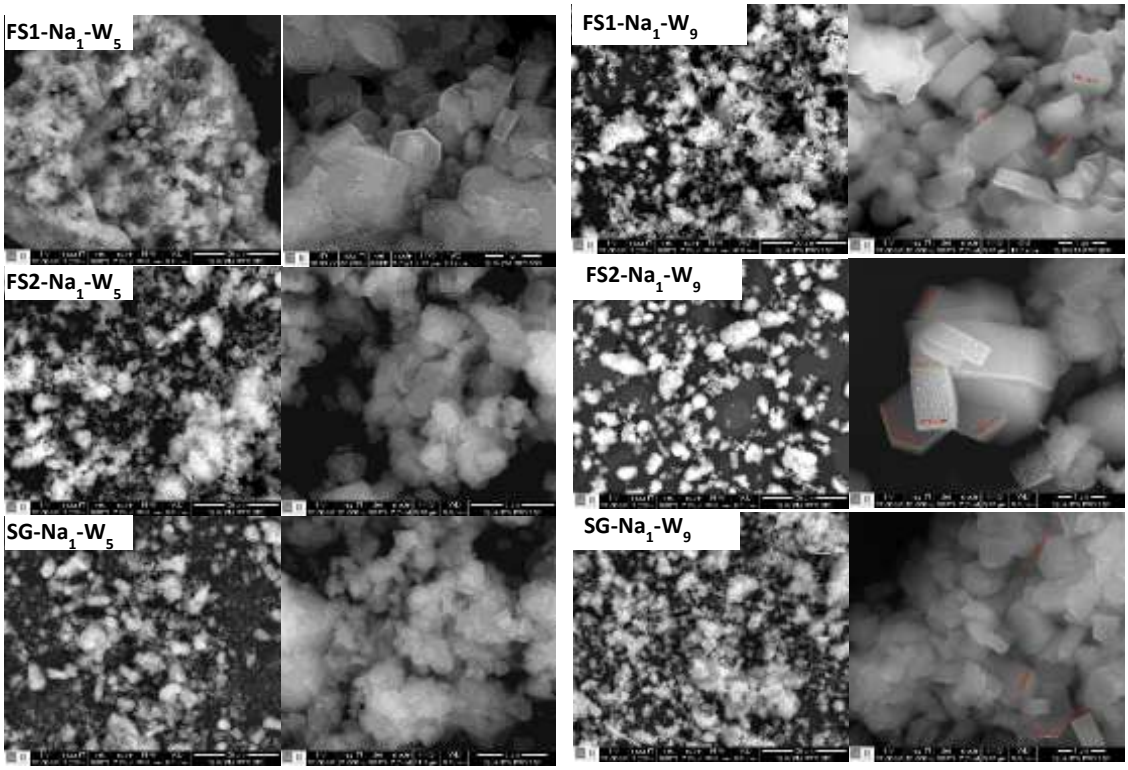

In the micrographs of the samples prepared with the precursors FS1 and FS2, no rod-shaped crystals associated with the mordenite phase were observed; this result, in agreement with the XRD results, indicates the absence of said phase. The rod-shaped crystals can be observed in the samples prepared with the silica gel precursor, confirming its use favors the mordenite phase's appearance.

The diffractograms of the samples prepared with the ratio Na_2O/SiO_2=0.16, the three silicon precursors, and using penta and nonahydrate sodium silicate are presented in Figure 6. The characteristic peaks of the ZSM-5 phase, which is the main phase, are observed for all materials. In the case of the FS1 and FS2 precursors, the peaks related to the mordenite phase were not observed, indicating that the decrease in Na^+ concentration is detrimental for the formation of the mordenite phase and reinforcing what was established in the previous section, an excess of sodium ions can favor the formation of the mordenite phase (Aly, et. al., 2012; Huang, et. al., 2012).

Figure 16.

*Diffractograms of the samples prepared with the ratio Na_2O/SiO_2=0.16, the three silicon precursors, and using nona and pentahydrate sodium silicate (a and b). *Peaks of mordenite phase.*

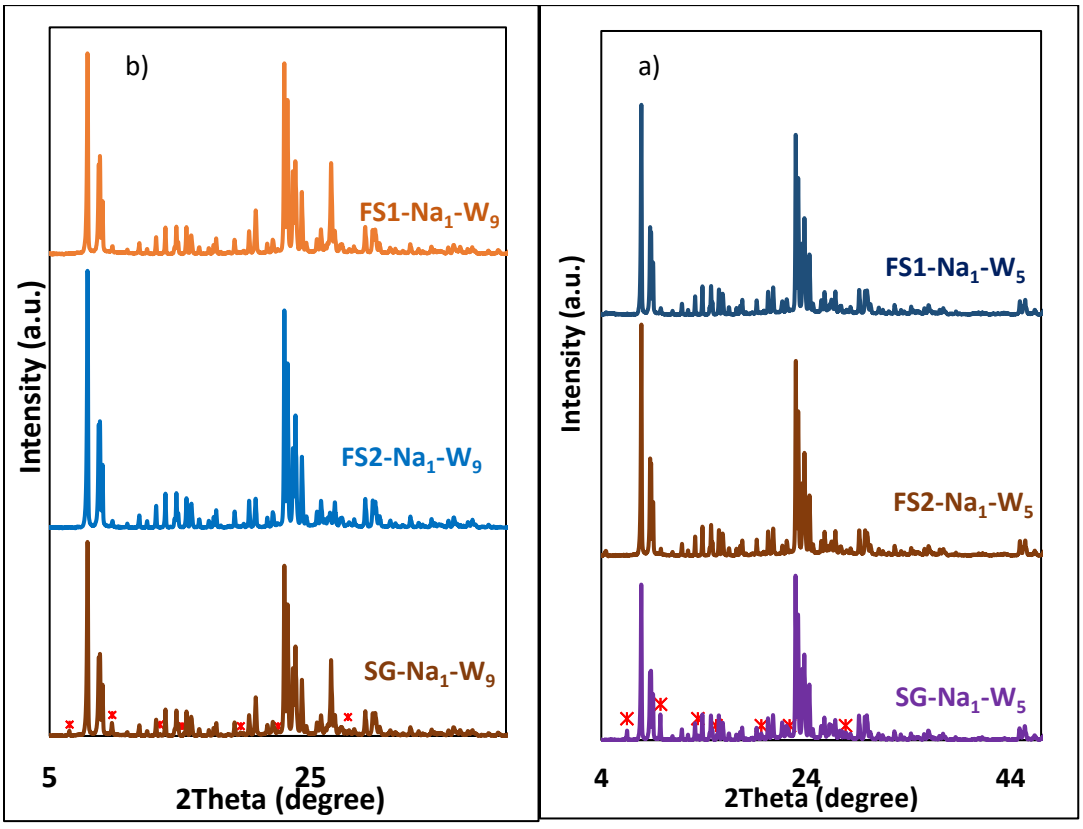

In the case of the silica gel precursor, Figure 6 shows that its use favors the appearance of peaks related to the mordenite phase, with the silicate pentahydrate and the nonahydrate precursor. The quantification of this phase yields 2.1 % for the SG-Na1-5W sample and 2.2 % for the SG-Na1-9W sample, lower than those recorded for the material prepared with the same precursor but using the higher concentration of Na^+ (SG-NA_2-W_5). These results indicate that a higher concentration of sodium it is more suitable for the formation of mordenite and that the use of larger particles, such as silica gel, favors the appearance of this phase.

Regarding the textural properties, the adsorption isotherms of the synthesized samples with lower sodium content (Na_2O/SiO_2=0.16) are presented in Figure 7.

Figure 17.

Adsorption desorption argon isotherm and cumulative pore volume and pore-size distribution of materials synthetized without OSDA, Na_2O/SiO_2=0.16 molar ratio and a) FS1 (FS1-Na1-W9), b) FS2 (FS2-Na1-W9), and c) SG (SG-Na1-W9).

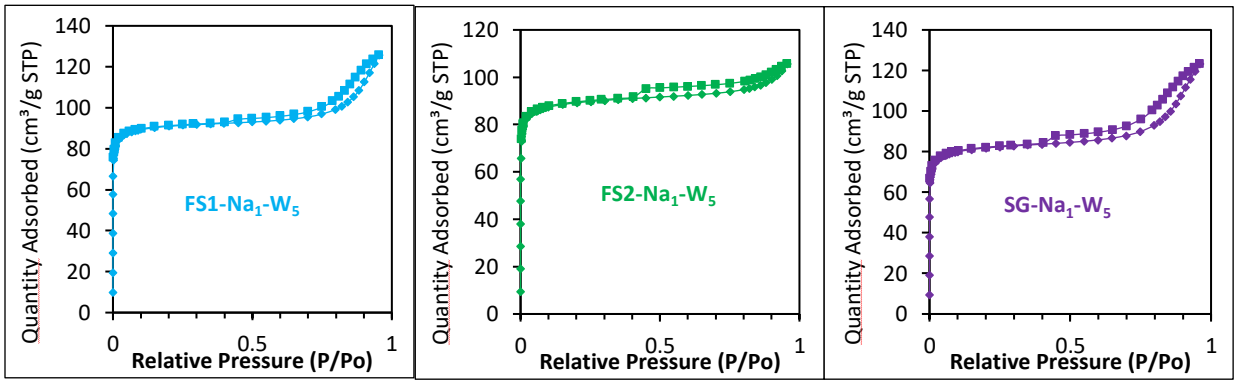

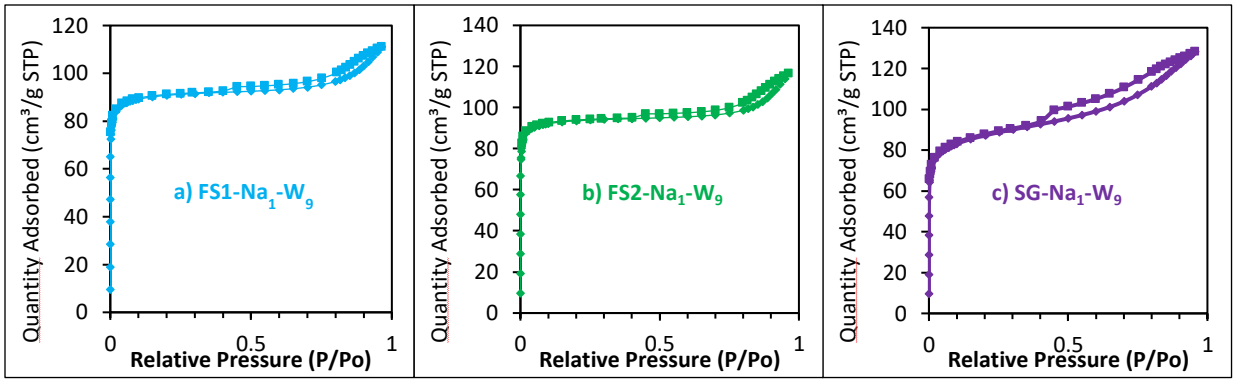

The adsorption isotherms for all samples are type I, typical of microporous materials; all present hysteresis loops that may be due to spaces between particles. Both the shape of the isotherms and the hysteresis loops are like those presented by the materials synthesized with the highest concentration of sodium (Na_2O/SiO_2=0.21). Regarding the values of the textural properties presented in Table 2, the BET area of all the materials prepared with the ratio Na_2O/SiO_2=0.16 is greater than 300 m^2/g, with the microporous area having the highest proportion. In the case of the external area recorded, this can be attributed to interparticle spaces generated due to crystal agglomerates, as seen in the micrographs of the samples.

Table 8.

Textural properties for materials synthetized using zeolite seed and Na_2O/SiO_2=0.16 molar ratio

Properties / Sample	BET Surface area (m^2/g)	t-Plot Micropore area (m^2/g)	t-Plot external area (m^2/g)
FS1-Na1-W5	323	294	28
FS2-Na1-W5	316	284	32
SG-Na1-W5	300	267	33
FS1-Na1-W9	323	295	28
FS2-Na1-W9	323	295	28
SG-Na1-W9	336	311	250

Syntheses made at Na_2O/SiO_2=0.21. Figure 8 shows images of the samples from the materials synthesized using Na_2O/SiO_2=0.21 with the two fumed silicas and silica gel. Bars, hexagons, and irregular particles were found in all instances. The SEM images also highlight that despite the differences in size and morphology between the silicon precursors, the shape and size of the crystals obtained with them are very similar. Overall, the type of silicon precursor had no effect on the distribution of produced particles as it was also the case when tetrabutylammonium bromide was used as structure directing agent.

Further analysis of the chemical composition of some of the hexagonal and bar particles observed with SEM was made with EDS. Results are shown in Table 3. Comment on the results.

Table 9.

*SiO_2/Al_2O_3 molar ratio calculated from EDS results. *Analysis on crystal in the form of a bar*

Sample	Zone 1	Zone 2	Zone 3	Zone 4
FS1-Na2-5W	19.69	23.57	14.96*	14.53*
FS2-Na2-5W	23.17	20.68	30.12	14.58*
SG-Na2-5W	22.31	22.33	23.83	16.68*

Figure 18.

SEM micrographs of materials synthetized without OSDA, Na_2O/SiO_2=0.21 molar ratio and a) FS1 (FS1-Na2-W5), b) FS2 (FS2-Na2-W5), and c) SG (SG-Na2-W5).

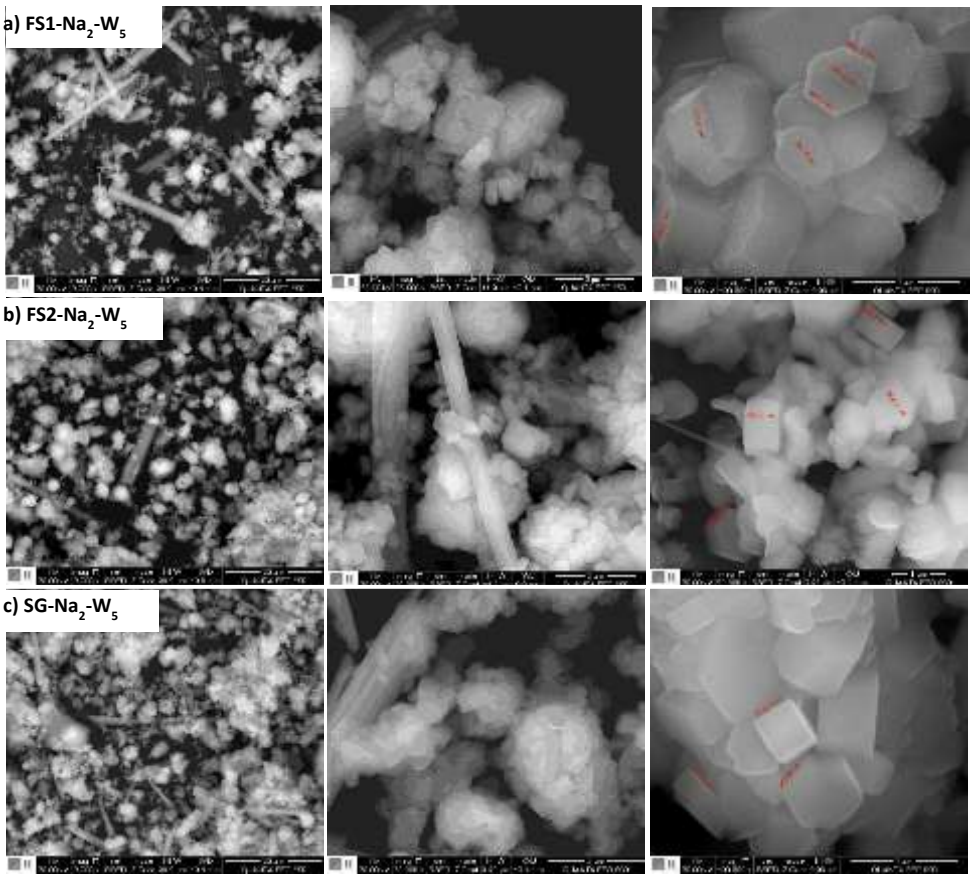

The diffractograms of the samples prepared with the ratio Na_2O/SiO_2=0.21 and the three silicon precursors are shown in Figure 9.

Figure 19.

X-ray powder diffraction patterns of the of materials synthetized without OSDA and Na_2O/SiO_2=0.21 molar ratio

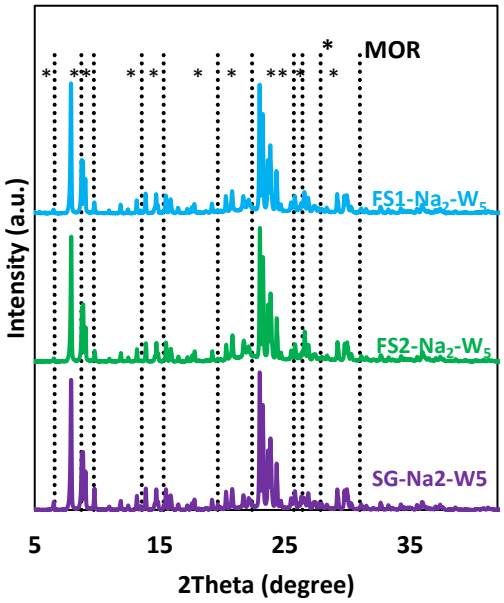

The characteristic peaks of the ZSM-5 phase are observed for the three synthesized samples. It is also possible to note the presence of peaks associated with the mordenite phase in a smaller proportion.

The quantification of these two phases is presented in Table 4. It was found that the majority phase is the ZSM-5 and that the maximum percentage of the mordenite phase occurs when the silica gel is used as precursor.

Table 10.

Phase percentages for samples prepared with the ratio Na_2O/SiO_2=0.21 and the three silicon precursors

	Material		
	FS1-Na_2-W_5	**FS2-Na_2-W_5**	**SG-Na_2-W_5**
% MOR	4.5	3	6
% ZSM-5	95.5	97	94

The adsorption isotherms for the three samples that were prepared with the ratio Na_2O/SiO_2=0.21 and assisted with seed are presented in Figure 10. Regardless of the silicon source, the three samples present type I isotherms, characteristics of microporous materials according to IUPAC (Alothman, 2012).

These results reinforce the phase assignment to the crystals mentioned above; a higher concentration of Al is observed in the rod-shaped crystals than in the hexagonal-shaped crystals. This coincides with what was established for the mordenite phase, this being richer in aluminum than ZSM-5.

Figure 20.

Adsorption desorption argon isotherm of materials synthetized without OSDA, Na_2O/SiO_2=0.21 molar ratio and a) FS1 (FS1-Na2-W5), b) FS2 (FS2-Na2-W5), and c) SG (SG-Na2-W5).

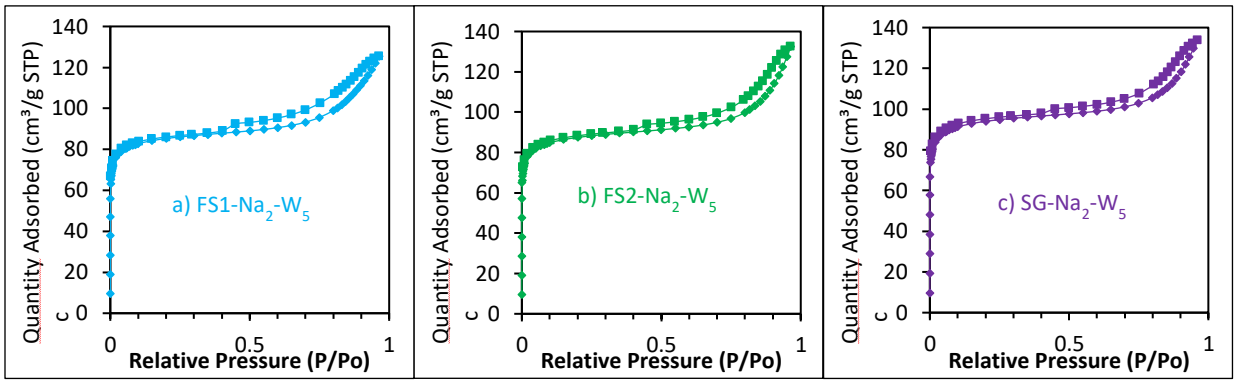

The materials also exhibited similar hysteresis, which can be attributed to interparticle gaps. As it was possible to analyze in the SEM images, the three samples are formed by agglomerates of tiny crystals that can give rise to the interparticle spaces mentioned above.

Table 5 presents the values of the textural properties for the materials synthesized without OSDA using Na_2O/SiO_2=0.21 molar ratio.

Table 11.

Textural properties for materials synthetized using zeolite seed and Na2O/SiO2=0.21 molar ratio .

Properties / Sample	BET Surface area (m^2/g)	t-Plot Micropore area (m^2/g)	t-Plot external area (m^2/g)
FS1-Na2-W5	296	251	45
FS2-Na2-W5	303	257	47
SG-Na2-W5	325	277	48

The BET surface area values for the three materials are around 296 m^2/g and 330 m^2/g, in a more significant proportion in the micropores, confirming what was observed in the isotherms that refer to microporous materials. It is also noteworthy that the external area is similar in the three samples, which is consistent with the fact that this area is attributed to interparticular voids and that the morphologies of these samples are similar, SEM micrographs, Figure 8.

3.4.3 What is the role of the amount of water on the properties of the materials?

As general observations, the variation of the particle size of the silicon source did not generate significant changes in the morphology or the textural properties of the materials synthesized with the ZSM-5 seeds. However, using silica gel (the precursor with the largest particle size) led to a higher percentage of the mordenite phase. It is possible that, since the size of the silica gel precursor particles is greater than that of the other two precursors, zones with a higher concentration of aluminum are generated, thus favoring the mordenite phase over the ZSM-5 (Aly, 2012; Zhang, 2009; Zhu et al., 2017).

Additionally, the comparison between the crystals obtained with the help of the organic structuring agent and those presented with the seed-assisted synthesis shows a difference between the sizes of the produced crystals. These differences can be attributed to the influence, as directing agents of structure, of the seed and the TPABr. For the crystallization of zeolite ZSM-5 with seeds, it is considered that the latter must provide composition units or minute crystals that make crystallization nuclei (Davis, 2014; Ji, et. al., 2016; Kadja, et. al. 2021). Accordingly, the size of the produced crystals would then be limited by the zone of influence of the seed nuclei. When an organic structure directing agent is used, its molecular scale dimensions allow dispersing it more

homogeneously within the mixture of zeolites precursors. Thus, the directing function does not depend on the nuclei present in the mixture but on the distribution of the structuring agent. Since in solventless synthesis, closer proximity of the aluminosilicate precursor species is possible, the size of the agglomerates that can crystallize with the help of OSDA can be larger than those in which the seed crystals can have influence (Cundy & Cox, 2005; Kadja, et. al., 2021; Culfaz &. Sand, 1973).

As a general analysis of this section, it can be mentioned that the decrease in the sodium content did not generate significant changes in the textural or morphological properties of the sample. However, it did lead to a decrease in the presence of the mordenite phase in the materials (Alothman, 2012; Velaga & Peela, 2019). As mentioned in the previous section, the excess Na^+ in the synthesis mixture can lead to the formation of the mordenite phase, so a decrease in this would generate the opposite effect. Regarding the modification in the water content by modifying the sodium silicate precursor (nona and penta hydrate), it was found that it does not generate significant changes in the morphological, crystallographic, or textural properties studied in this section.

Regarding the variation in the size of the silicon precursor, it was observed that the formation of the mordenite phase is favored by using Silica gel, the precursor with the largest silicon particles. As an explanation, it could be said that due to its particle size, now of grinding, it can generate areas with a higher concentration of aluminum, deviating from the adequate one for the formation of zeolite ZSM-5 and favorable for obtaining a zeolite that presents a higher concentration of this element in its structure as mordenite (Jain & Rimer, 2020; Razavian & Fatemi, 2015; Ren, et. al., 2012).

3.4.4 Analysis of the evolution of the materials during the crystallization stage

This section analyzes the evolution of the materials synthesized by mechanochemistry during the crystallization stage and compares it with the evolution of the materials synthesized by sol-gel using seeds. The syntheses were developed under the exact composition of the initial mixture except for the amount of water.

The experiments seek to understand aspects such as the formation of the mordenite phase, described in the previous sections, and if this occurs due to aspects related to the composition of the initial mixture or a prolonged hydrothermal treatment time in which the zeolite ZSM-5 towards mordenite. In addition, they allow a parallel to be drawn to find similarities and differences between mechanochemical synthesis, in which the use of water is restricted to a low quantity; and sol-gel synthesis, where water, in addition to acting as a solvent, also fulfills a function of filling pores, hydrolyzing reagents, and facilitating chemical reactions (Culfaz & Sand, 1973; Davis, 2014; Grand, et. al., 2016).

The evolution of the structure of the materials was followed with the help of Fourier transform infrared spectroscopy (ATR-IR). Figure 11 shows the AT-IR spectra for the materials synthesized by the Sol-Gel route (Figure 11 a) and solvent free route (Figure 11 b) as a function of crystallization time.

Figure 21.

AT-IR spectra for the materials synthesized by the sol-gel route (Figure 10 a) and mechanochemical route (Figure 10 b) as a function of crystallization time.

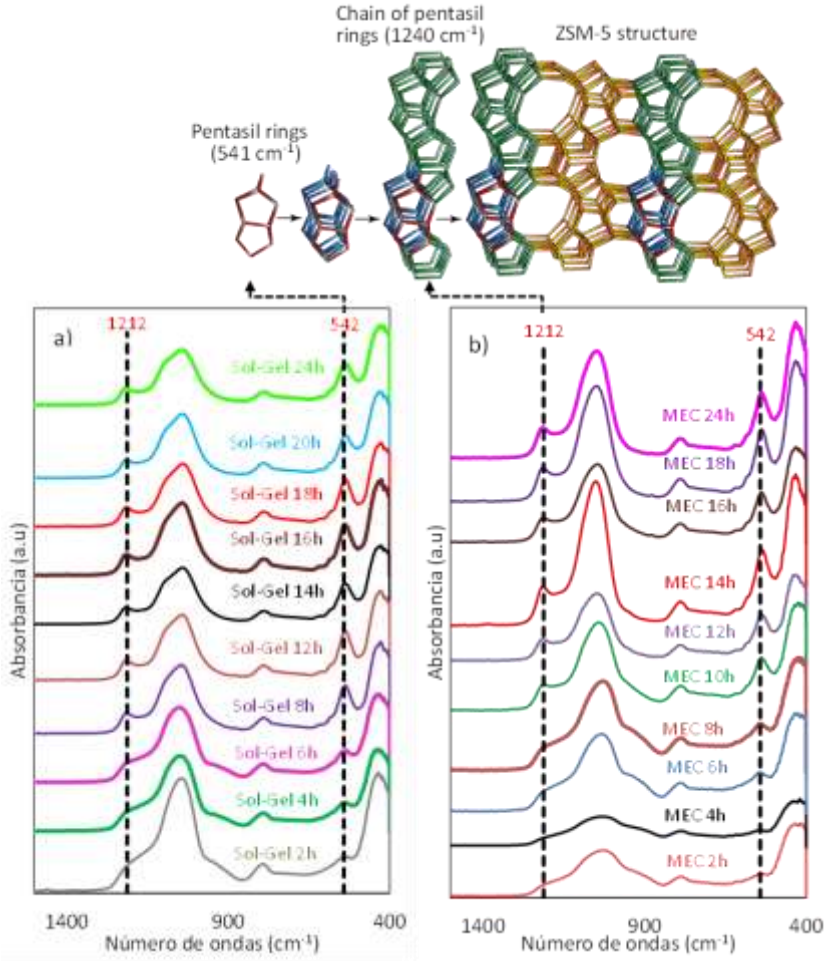

In these spectra, the bands at 542 and 1212 cm^{-1} refer to the vibration modes of the pentasil rings associated with the MFI structure and the chains formed by said rings (Razavian et al., 2015). The illustration presented in Figure 11, indicates the evolution in crystalline structure formation of zeolite ZSM-5, starting from the constitutive unit pentasil to the structure of the material made up of pentasil units and chains. Figures 11 a) and b) show bands (541 and 1200 cm^{-1}) formation occur first for the zeolite synthesized by the sol-gel route. In addition, in both syntheses, the formation

of the pentasils occurs before that associated with the chains that form said rings (1200 cm^{-1}); in Sol-Gel synthesis, it has been found that the formation of crystallization nuclei occurs first and then, from these, zeolite crystals are formed (Cundy & Cox, 2005; Grand, et. al., 2016; Dai, et. al., 1986). The results in this work coincide with this postulate and show a similar phenomenon for mechanochemical synthesis. Regarding the crystallization time in which the completely defined bands at 541 and 1241 cm^{-1} can be observed, we find that for the solvent-free synthesis, this process occurs after 10 h and for the Sol-Gel synthesis after 8 h, which is consistent with a higher rate of Sol-Gel synthesis for the formation of the zeolitic structure.

The evolution of the crystalline structure for both types of synthesis was also analyzed through X-ray diffraction, as shown in Figure 12, which presents the diffractograms for the materials obtained by the Sol-Gel route (Figure 12a) and mechanochemical (Figure 12b).

Figure 22.

X-ray powder diffraction patterns of the samples synthesized at different crystallization times through a) Sol-Gel route and b) solvent-free route.

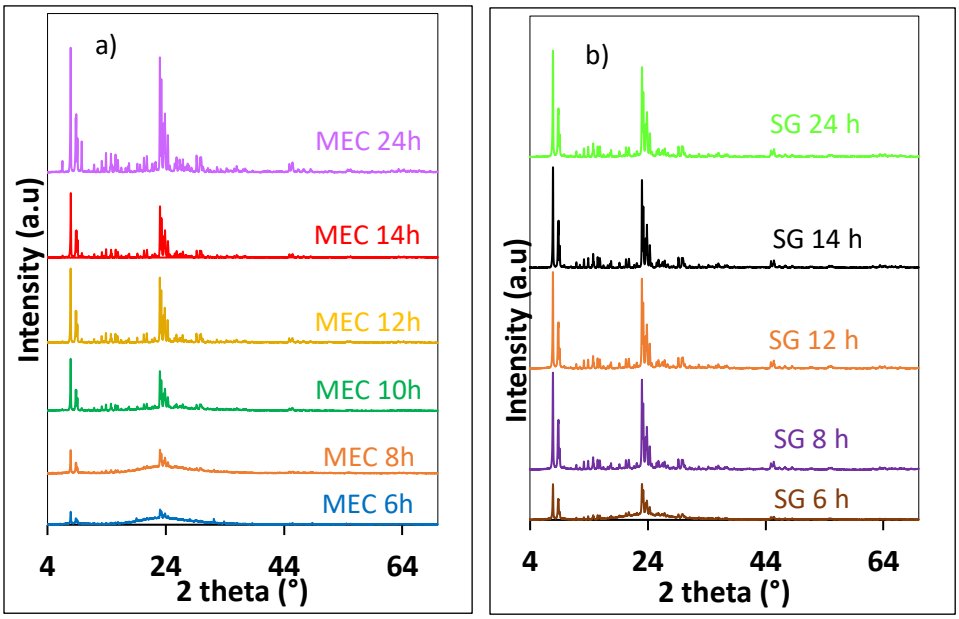

In the diffractograms, it can be observed for the six hours of crystallization, in both types of synthesis, that the intensity of the ZSM-5 diffraction peaks is relatively low, and they are accompanied by a broad hump indicating amorphous material. It is also noteworthy that the diffraction peaks are more intense in the Sol-Gel synthesis at low crystallization times (6 h and 8 h), confirming what was postulated with the results of ATR-IR, that the crystallization of the zeolite using the Sol-Gel method is faster than with the solvent-free method.

Additionally, in the solvent-free synthesis, peaks related to the mordenite phase can be observed after 10 hours of crystallization. It is worth mentioning that in the sample with eight hours of crystallization, these peaks were not found and that the peaks related to the ZSM-5 phase were of low intensity; an increase of two hours in the crystallization time leads to the formation of crystals of zeolite ZSM-5, and possibly at the same time zeolite mordenite crystals are generated. Considering what was postulated at the beginning of the section, the mordenite phase seems to be generated more by the composition of the synthesis mixture than by prolonged times in the hydrothermal treatment. It is also important to note that in Sol-Gel synthesis, there is no presence of this phase, even though the initial composition of reagents is the same. This difference may be related to a more homogeneous distribution of the Si/Al ratio throughout the synthesis gel, thanks to the presence of the solvent. In the mechanochemical synthesis, it is possible that in the mixing process given by grinding, areas with a higher concentration of Al favor the appearance of the mordenite phase.

The morphological study of the materials was carried out through SEM; the images taken for some of the samples are presented in Figure 13.

Figure 23.

SEM micrographs of the samples synthesized at different crystallization times through a) Sol-Gel route and b) solvent-free route.

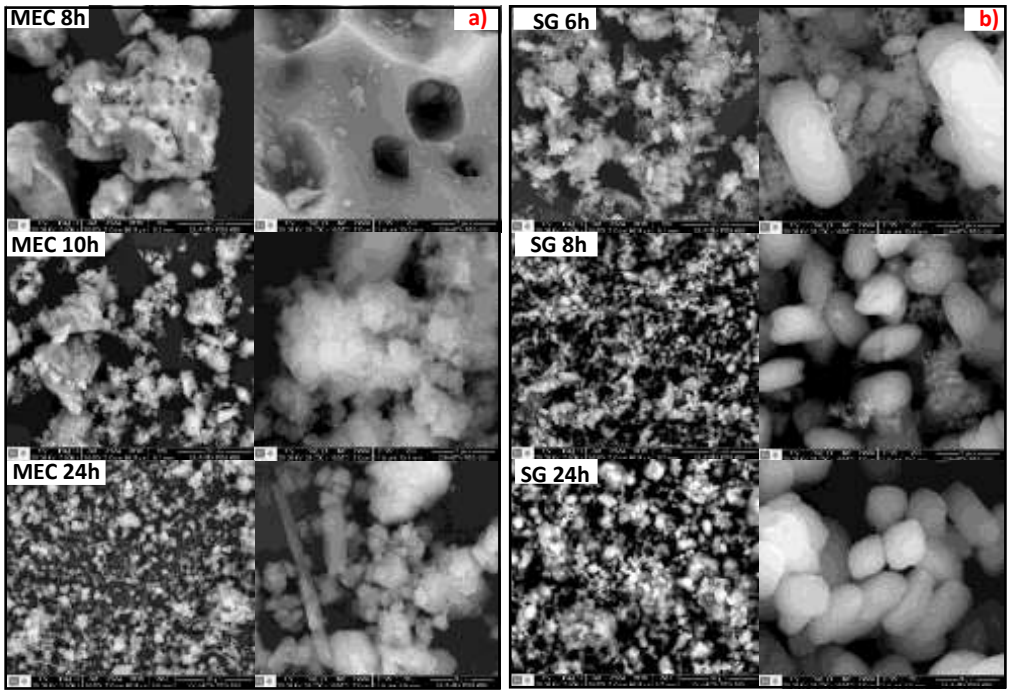

Regarding the solvent-free synthesis Figure 13a, with 8 h crystallization, show particles with sizes that can be greater than 400 microns, with holes that can reach up to 5 microns. For this sample, it is not possible to observe small crystals with hexagonal shapes or bars, but considering the X-ray and ATR-IR results, the particles must contain structural units of the ZSM-5 zeolite. The increase of two hours in the crystallization time leads to a transformation of the particles, the holes present on the surface can no longer be observed; small crystals are also present on the external surface of the particles, hexagonal figures with well-defined edges begin to be observed, which can be attributed to the formation of the zeolite ZSM-5 considering the results of ATR-IR and XRD for this weather. After 24 h of hydrothermal treatment, the absence of particles with sizes

greater than 100 microns can be noted in the micrographs. In this case, agglomerates of small crystals with well-defined edges and a hexagonal shape can be observed; in addition to these, it is possible to observe rod-shaped crystals that can be associated with the mordenite phase.

For the Sol-Gel synthesis (Figure 13b), after 6 h of crystallization, a combination of grain-shaped crystals surrounded by an amorphous shell can be observed. This is consistent with the XRD results, at this time it is possible to observe peaks related to the ZSM-5 phase with low intensity and with the presence of a curvature that can be related to the amorphous portion seen in SEM. The increase in crystallization time up to 10 h leads to an increase in the number of crystals in the form of degrees and a decrease in the amorphous part that surrounds them. Finally, after 24 h of crystallization, it is only possible to observe the grain-shaped crystals mentioned above, there are no evidence of crystals with other shapes or amorphous formations in this sample, indicating that there is no presence of other phases, as was found with the results of X-rays.

Table 6 presents the SiO_2/Al_2O_3 molar ratio for the materials presented in Figure 13, calculated with the SEM-EDS. The variation in the SiO_2/Al_2O_3 ratio in the particles found at 8 h of crystallization for the mechanochemical synthesis can be observed. This variation in composition also occurs when crystallization reaches 24 h. One of the bars associated with the formation of the mordenite phase (SiO_2/Al_2O_3) was also analyzed, finding a higher concentration of Al.

Table 12.

*SiO_2/Al_2O_3 molar ratio calculated from EDS results. +Analysis on crystal in the form of a bar. * Analysis on amorphous material.*

Solvent free synthesis						Sol-gel synthesis					
Sample	**Zone 1**	**Zone 2**	**Zone 3**	**Zone 4**	**Zone 5**	**Sample**	**Zone 1**	**Zone 2**	**Zone 3**	**Zone 4**	**Zone 5**
Mec-cin-8h	40.43	27.55	35.05	-	-	sg-cin-6h	24.31	24.23	24.15	**25.6***	-
mec-cin-10h	27.01	28.91	27.9	28.83	27.28	sg-cin-8h	24.62	24.8	25.2	25.2	**26.19***
mec-cin-24h	20.98	24.29	20.11	18.95	**16.65**+	sg-cin-24h	24.3	23.03	23.03	23.63	-

About the samples prepared by the sol-gel method, it was possible to notice a more homogeneous SiO_2/Al_2O_3 ratio at low crystallization times (6h). Also, the crystals formed after 24 h present a more homogeneous composition than their counterpart in mechanochemical synthesis. These results support the hypothesis that, in the solvent-free synthesis, there may be a less homogeneous distribution of the Al and Si elements than in the Sol-Gel synthesis, being able to generate Al-rich zones and favoring the formation of the mordenite phase. Figure 14 shows the **Ar** adsorption-desorption isotherms of the materials obtained by the solvent-free route (Figure 14a) and Sol-Gel (Figure 14b) at different crystallization times.

Figure 24.

Adsorption desorption argon isotherm of the samples synthesized at different crystallization times through a) Sol-Gel route and b) solvent-free route.

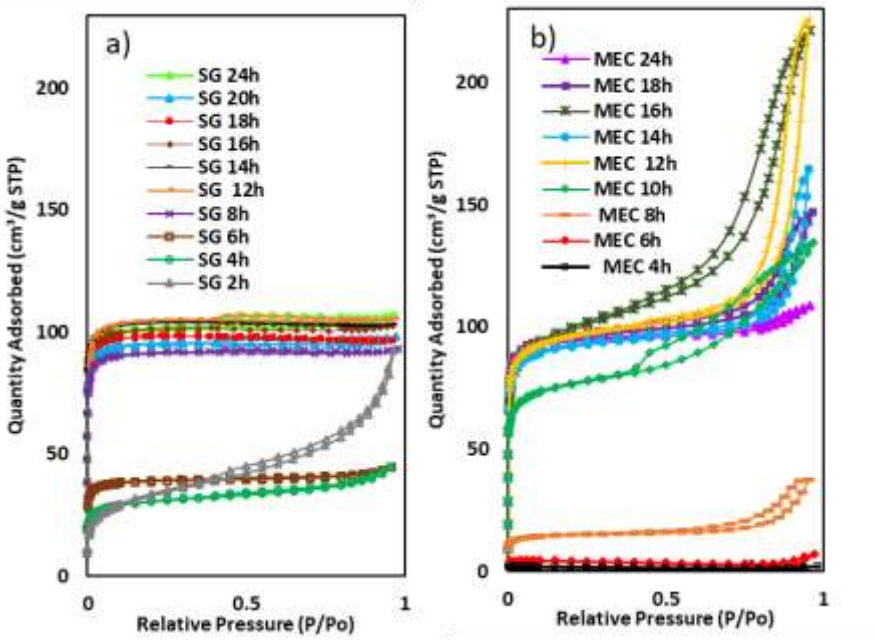

Regarding the sol-gel synthesis, a type II adsorption isotherm can be observed for the sample with 2 hours of crystallization, characteristic of non-porous or macroporous materials; when the crystallization time increases up to 4 h of crystallization, the form of the isotherm changes to a Type I that occurs when the materials are microporous (Alothman, 2012). As the crystallization time increases, the shape of the isotherm is maintained with a significant change in the amount of **Ar** adsorbed between 6 and 8 h of crystallization; after eight hours, the changes in adsorbed **Ar** are less significant.

In the materials synthesized case by the solvent-free route, it is observed in Figure 14b that the isotherms for the crystallization times of four, 4, and 6 h indicate a low **Ar** adsorption; only after 8 h a slight increase is observed. With ten hours of hydrothermal treatment, the material

presents isotherms with a Type H4 hysteresis cycle (Alothman, 2012). After 12 h of crystallization, the adsorbed **Ar** does not change significantly, and the hysteresis loop, which is wide at 12 h (indicating the presence of mesopores), decreases with time up to 24 hours. Finally, after 24 h of crystallization, the material presents a type I isotherm characteristic of microporous materials, with a hysteresis loop that can be attributed to interparticle spaces (Alothman, 2012).

Figure 15 shows the evolution of the BET area of the samples reported in Figure 14. The curves generated from the surface area data presented a sigmoidal shape for both types of synthesis (Davis, 2014; Grand, et. al., 2015).

Figure 25.

Evolution of the BET area of the samples synthesized at different crystallization times through Sol-Gel route and solvent-free route.

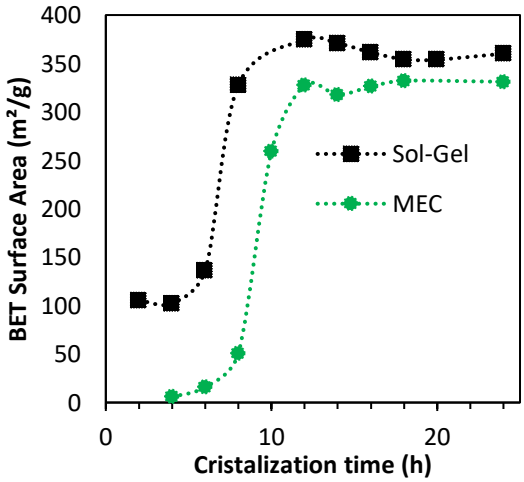

The curve for Sol-Gel synthesis has a similar shape as the mechanochemical synthesis, which may indicate a similar crystallization mechanism. However, at all times of synthesis, the surface area of the materials prepared by the solvent-free route is less than that recorded for the

materials prepared by the sol-gel route. Another difference to highlight when observing the curves is the low surface area of the materials prepared by the solvent-free route at low crystallization times (2h, 4h, 6h) compared to the BET area of the samples prepared by the Sol-Gel. In this case, water can play a space-filling role in the Sol-Gel synthesis, which can generate a specific porosity, which would not be possible in the mechanochemical synthesis due to the absence of it as a solvent (Kadja, 2021; Grand, 2016).

3.5 Conclusions

Silicon size's particle only generated morphological changes when silica gel was used to synthesize zeolite ZSM-5 with the help of an organic structuring agent (OSDA).

The crystals obtained using OSDA are much larger than those obtained using seeds and have larger surface areas. It was found that a high concentration of Na favors the appearance of phases such as mordenite and larger silica gel particles.

Finally, a comparison was made by varying the crystallization time between mechanochemical and Sol-Gel synthesis to study the differences and common aspects.

4. Catalytic evaluation of ZSM-5 zeolite, obtained by the sol-gel method and free of solvent, in the dehydration of glycerol.

4.1 Abstract

The catalytic behavior of various ZSM-5 type zeolites was studied in the gas phase glycerol dehydration reaction using a fixed bed reactor that operated continuously. The analyzed materials were prepared using two methods: 1) the sol-gel method without organic structuring agent (OSDA), using as silicon precursors (Ludox, Fumed Silica 1 and Tetraethyl orthosilicate (TEOS); 2) The solvent-free method and OSDA using three silicon sources with different particle sizes (Fumed Silica 1, Fumed Silica 2 and silica gel). Additionally, the change in the silicon-aluminum ratio with materials prepared with the TEOS precursor and the synthesis method one was evaluated. As result, it was found that the main product for all the materials is acrolein, that the materials prepared by the Sol-Gel method had a catalytic performance like commercial zeolite, and materials prepared by the solvent-free method presented a lower conversion. Regarding the variation of the Si/Al ratio, it was observed that the material prepared with the lowest value presented the lowest catalytic activity.

Keywords. ZSM-5 zeolite, Silicon Precursor, glycerol dehydration, Catalysis

4.2 Introduction

One of the alternatives for replacing fossil fuels with renewable and less polluting fuels is biodiesel. This is produced through the transesterification of vegetable oils (triglycerides) and methanol, using basic catalysts (Asopa et al., 2022)(Huber et al., 2006). The increase in energy consumption over time has led to an increase in the production of biodiesel, which gives rise to the production of glycerol as a by-product of the process. Therefore, the large volumes of glycerol production as a by-product in obtaining biodiesel represent an excellent opportunity to obtain high value-added chemical products (Huber et al., 2006)(Sun et al., 2017). Some of the routes to carry out the valorization of glycerol are presented in Figure 1.

Figure 26.

Possible routes for the use of glycerol taken from Kiakalaieh et al. [4]

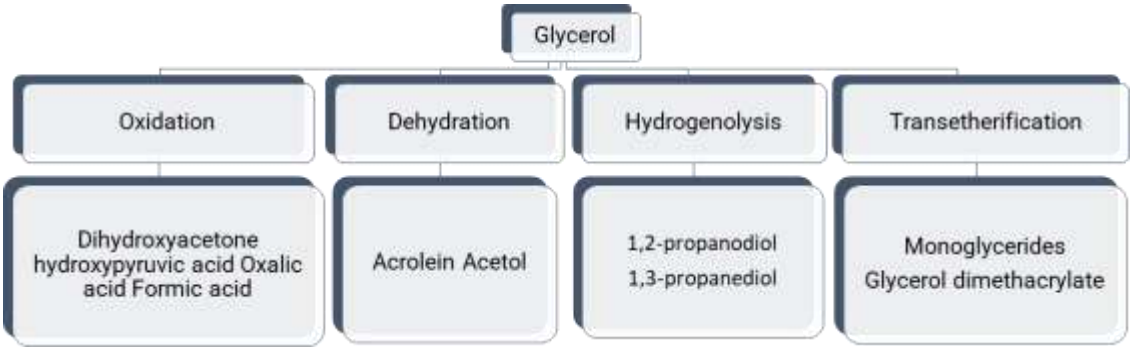

Among the various options for the valorization of glycerol presented in Figure 1, the dehydration of glycerol to acrolein is of particular interest as this molecule is an intermediate in the synthesis of acrylic acid, methionine, and absorbent polymers (Katryniok et al., 2009)(Tan et al., 2013). Conventional processes for the synthesis of acrolein are based on the selective oxidation

of propene at temperatures above 250°C and exhaustive control of the reaction conditions is required to avoid dangerous accidents. In addition, the reaction competes strongly with the production of carbon dioxide, which is why it becomes a source of greenhouse gases (Katryniok et al., 2009)(Talebian-Kiakalaieh et al., 2014). Acrolein can be obtained by decomposing glycerol by heating, where water and other byproducts are generated. The addition of a catalyst to the process provides greater control of the reaction and can increase the yield of acrolein [4]. The first works developed on the dehydration of glycerol using solid acids as catalysts were carried out by Schering-Kahlbaum in 1933 using Cu and Li phosphates as catalysts. The reaction was carried out in the gas phase at temperatures above 300 °C and yields towards acrolein close to 75 % were obtained (Heilig, 1994). In the valorization of glycerol via dehydration, acid solids such as zirconium phosphate, heteropoly acids an zeolites have been studied (Asopa et al., 2022)(Kraleva et al., 2011)(Rao et al., 2014), particularly zeolites, which are crystalline materials composed of interconnected SiO_4 and (AlO_4) tetrahedra, are presented as a very good option thanks to their structural properties, textural and acid-base properties can be modified from their synthesis to match the needs of chemical transformations. Currently around 232 types of zeolites are known, among which ZSM-5 zeolite has been used in the dehydration of glycerol thanks to properties such as its three-dimensional structure of straight and sinusoidal channels, its thermal stability up to 900 °C, and acidity that in total it can reach 490 NH_3 μmol/g (Caldeira et al., 2016; Hoff et al., 2016; Nimlos et al., 2006; Pérez-Page et al., 2016; Rieg et al., 2021).

The ZSM-5 zeolite has been the subject of different investigations on the dehydration of glycerol, among which those carried out by Wang et al. In this, the effect of the type of acidity of the zeolite on the reaction selectivity was studied. The authors propose that the presence of Lewis-type acid sites formed thanks to the introduction of extra-lattice aluminum cations in an H-ZSM-

5 zeolite, combined with a high number of Brønsted-type sites, can significantly increase the glycerol transformation to acrolein.

Aspects related to the textural properties of the ZSM-5 zeolite have also been studied. Investigations such as those carried out by Possato et al.; show the behavior of microporous (ZSM-5) and hierarchical zeolites (with micro and mesopores) in the dehydration of glycerol in the gas phase. In the investigation, it was possible to establish that the generation of mesopores in the zeolite improved the diffusion of the reagents toward the active sites and decreased the blockage of the pores due to the formation of coke. The authors also established that the alkaline treatment for the generation of the mesopores should not be so severe because there was a significant decrease in the concentration of the acid sites, negatively affecting the catalytic performance (Possato et al., 2013).

Park et al., demonstrated that there is a strong influence of the textural properties of the catalysts on their performance in glycerol dehydration. The authors postulated that the deactivation of the catalyst by coke deposition is due to limitations in the migration of carbonaceous compounds towards the external surface of the materials due to its microporous channels (Park et al., 2015).

The articles mentioned above, among others, show how ZSM-5 zeolite is a promising catalyst to carry out glycerol dehydration (*2018 Ren, Gas-Phase Dehydration of Glycerol to Acrolein Catalyzed.Pdf*, n.d.; *2018 Never, Glycerol Dehydration over Micro- and Mesoporous ZSM-5 Synthesized from a Onestep.Pdf*, n.d.; FLANIGEN et al., 1984; Lago et al., 2018; Zhang et al., 2015; Zou et al., 2016). Considering the potential of this zeolite for the valorization of a by-product generated from a process that seeks to reduce environmental pollution, it is consistent that the means for obtaining said zeolite also seeks to reduce the environmental impact.

A classic method of preparing zeolites is the so-called hydrothermal synthesis from silica gels or aluminosilicates (Vermeiren & Gilson, 2009). This type of synthesis is carried out in strongly alkaline media, pH > 9, and at temperatures up to 200 °C. In addition, an aging stage is required to be carried out; during which crystallization occurs under autogenous pressure in autoclaves (Vermeiren & Gilson, 2009)(Cundy & Cox, 2003). During the synthesis, high-cost organic structure directing agents (OSDA) are used, which must then be eliminated by combustion at temperatures above 450 °C, releasing polluting gases such as CO_x and NO_x (Corma & Davis, 2004)(Jones et al., 2001).

The negative environmental impact that ZSM-5 zeolite production can generate traditionally encourages the search for new synthesis methods, in which can: 1) eliminate the use of high-cost and toxic organic structuring agents, and 2) reduce the use of solvents during the synthesis. Different investigations have focused on the study of the two aspects mentioned above, successfully obtaining ZSM-5 zeolite by more environmentally friendly routes. Particularly, our research group has studied the synthesis of ZSM-5 zeolite considering the two sections mentioned above (Tatiana García-Sánchez et al., 2021). The first two chapters of this research focused on studying the synthesis of the zeolite through methods that seek to reduce the pollution generated by obtaining it conventionally, and the catalytic evaluation of the mentioned materials is one of the ways to validate said synthesis methods. As described above, the glycerol dehydration reaction is one of the processes where ZSM-5 zeolite has great potential to be used as a catalyst, and it was chosen as a test reaction for some of the materials synthesized in the first chapters. The synthesis conditions of the materials chosen for the tests were those in which ZSM-5 zeolite could be obtained with the lowest possible percentage of additional phases (mordenite). The purpose of this final chapter was to study the catalytic performance of the ZSM-5 zeolite, obtained by the OSDA-

free Sol-Gel method, and by the mechanochemical route (solvent and OSDA-free), in the glycerol dehydration reaction, comparing them with a commercial ZSM-5 zeolite (CBV2314).

4.3 Experimental section

4.3.1 Materials used in the reaction.

4.3.1.1 Synthesis of the seed zeolite that was used to prepare the catalysts. The zeolite used as a seed to synthesize the materials tested in the reaction was prepared using the Sol-Gel method with TEOS as a silicon precursor. The method used was the sol-gel and the procedure described in section 2.2.2 was followed. The molar ratios used in the synthesis were: Si/(Si+Al) =0.952, $NaOH/SiO_2$=0.32, and H_2O/SiO_2=60. The hydrothermal treatment was carried out in a 500 mL stainless steel reactor protected by a Teflon glass for 24 h at 180 °C. After the hydrothermal treatment, the material was washed with type I water, until the pH of the washing water was neutral, dried, and used as seed.

4.3.1.2 Synthesis of catalysts for reaction

4.3.1.2.1 Sol-Gel method. The materials were prepared using Ludox, Fumed silica 1, and TEOS as silicon precursors named for the reaction as LD, FS-1 and T-0.94, respectively. The material whose preparation is described in section # was used as seed. Regarding the material T-0.94, the number refers to the Si/(Si+Al) molar ratio found by SEM-EDS. The molar ratios used in the synthesis were: Si/(Si+Al) =0.952, $NaOH/SiO_2$=0.32, and H_2O/SiO_2=60. The hydrothermal

treatment was carried out in a 500 mL stainless steel reactor (with Teflon protection on the walls), for 24 hours at 180 °C. After the hydrothermal treatment, the material was washed with type I water, until the pH of the washing water was neutral, dried, and used as seed. Additionally, two materials were prepared with this method using TEOS as silicon precursor, but with different Si/(Si+Al) ratios. The materials were named as T-0.91 and T-0.95, the number refers to the Si/(Si+Al) molar ratio found by SEM-EDS.

4.3.1.2.2 Solvent free method. Three materials were prepared by the solvent-free route following the protocol described in section 2.2.3. Fumed silica 1, Fumed silica 2, and silica gel were used as silicon precursors and named FS-1 MEC, FS-2 MEC, and SG MEC, respectively. The hydrothermal treatment was carried out in a 40 ml stainless steel reactor (with Teflon protection on the walls), for 24 hours at 180 °C. The molar ratios used in the synthesis were Si/(Si+Al) =0.952, $NaOH/SiO_2$=0.32. The hydrated silicon precursor was $Na_2SiO_3*9H_2O$.

4.3.1.3 *Ion* exchange procedure. The synthesized materials were activated by ion exchange of their Na+ cations with a 1 M ammonium nitrate solution (NH_4NO_3, > 99%, PanReac). Such a procedure is mandatory to obtain the acidic zeolite. For the ion exchange, ca. 30 mL/g of zeolite were put in contact with NH_4NO_3. The mixture was heated to 60 °C and kept 16 h under magnetic stirring, and then washed twice. The procedure was repeated thrice, and, subsequently, the sample was dried. Finally, the sample was calcined at 550 °C, heating rate: 1.5 °Cmin 1, for 6 h.

4.3.2 Materials characterization

The morphology, crystal size, and chemical composition of the materials were studied with a QUANTA FEG 650 scanning electron microscope (SEM) using an Everhart Thornley detector (ETD) for morphology and an SSD type Back Scattered Electron detector (BSED) for composition. Before the analyses, samples were coated with gold for controlling differential charging effects during the measurements. The crystalline structure of the materials was studied by collecting X-ray diffraction (XRD) patterns with a D8 advanced X-ray diffractometer (Bruker) provided with Cu Kα1 radiation. XRD patterns were recorded between 2θ angles of 3.5-70 with a 0.02 step size.

The porosity and surface area of the materials were estimated from argon adsorption-desorption isotherms obtained with a 3Flex apparatus (Micromeritics) at 87 K. For the tests, samples of approximately 0.1500 g of each material were degassed –(apparatus, vacuum pressure: see at 120 ° C for 2 h and then at 300 °C overnight). After optimizing the CBET parameter with the Rouquerol consistency criteria, specific surface areas were calculated with the BET method.

The acidity of the materials was evaluated by FT-IR analysis of the adsorption of pyridine (C_5H_5N, J.T. Baker, > 99.9%). For each experiment, ion-exchanged materials were pelletized using 2 metric tons of pressure for 1 min. Pellets of 13 mm diameter and ~10 mg were obtained. The pellets were transferred to a vacuum system composed of a cell with ZnSe windows and a Pfeiffer Hicube Eco Turbo Pumping Station that reaches a pressure of $1x10^{-4}$ Pa. The samples were outgassed at 400 °C for 6 h to desorb water and other contaminants before adsorbing pyridine. Adsorption was carried out at 150 °C for 15 min followed by desorption at 25 °C, as in agreement with well-established procedures reported in the literature (Zholobenko et al., 2020).

After the priridine was adsorbed, desorption was performed at 200°C and at 400°C. The relative concentration of either Brønsted or Lewis acid sites was estimated using equations E1 and E2 (Emeis, 1993).

$$C_B = IA(B)\pi\frac{R^2}{w\varepsilon} \quad \text{E1}$$

$$C_L = IA(L)\pi\frac{R^2}{w\varepsilon} \quad \text{E2}$$

Where, CB is the concentration of Brønsted acid sites [mmol/g], CL is the concentration of Lewis acid sites [mmol/g], IA(B,L) is the Integrated absorbance of the selected Brønsted or Lewis band [cm 1], R is the radius of the sample pellet [cm], w is the weight of the pellet [mg], and e is the extinction coefficient [cm/μmol] for each type of acid site. Herein, e=1.67 was assumed for Brønsted acid sites and e = 2.22 was assumed for Lewis acid sites.

4.3.3 Catalytic test

Glycerol dehydration was carried out in a fixed bed downflow stainless steel reactor at atmospheric pressure and 320 °C. 0.1 g of the catalyst with a particle size ranging from 300 to 180 μm was placed in the reactor. This particle size was chosen considering a previous study where diffusional limitations were ruled in previous laboratory work. To obtain the catalyst particles in the desired size, the materials were first compressed using a hydraulic press (Specac). The granules were made with a depth of 0.3 cm and 1 cm in diameter, the pressure used for each granule was 3 tons and it was maintained at this pressure for 1 min. Subsequently, to obtain the particle diameters to be used in the reactions, the pellets were macerated and sieved to obtain particles with sizes between 180-300 μm.

N_2 was used as stripping gas with a flow of 30 mL/min, the catalytic bed temperature was stabilized with this N_2 flow at 320 °C. Subsequently, an aqueous solution of glycerol at 10% by weight was fed to the reactor with a mass flow of 19.5 g/h. N_2 was used as stripping gas with a flow of 30 mi/min, the catalytic bed temperature was stabilized with this N_2 flow at 320 °C. Subsequently, an aqueous solution of glycerol at 10% by weight was fed to the reactor with a mass flow of 19.5 g/h. The analysis of the reaction products was done with a GC-2010 plus gas chromatograph (Shimadzu), equipped with an FID detector and an automatic injector, using a column (DBWAX UI 30m x 0.25mm x i.d 0.25µm). The results of the catalytic tests were expressed in terms of the conversion of glycerol ($\%C_G$) and yield towards acrolein ($\%Y_{acr}$) or acetol ($\%Y_{ace}$) as follows:

$$\%\boldsymbol{C_G}\frac{\boldsymbol{F_G^0 - F_G}}{\boldsymbol{F_G^0}} \qquad \text{E3}$$

$$\%\boldsymbol{Y_i} = \frac{\boldsymbol{F_i}}{\boldsymbol{F_G^0}} \qquad \text{E4}$$

Where, F_G^0 and F_G are the inlet and outlet molar flow rate of the glycerol, respectively; and F_i is the outlet molar flow rate of the product i (acrolein or acetol).

4.4 Results and Discussion

4.4.1 Scanning electron microscopy (SEM)

The figure 2 shows SEM images of the samples used in the catalytic tests. Figures 2a-c represent samples prepared using the Sol-Gel method. Figures 2c-e are the images of the samples prepared by the mechanochemical route; and Figures 2f-h correspond to the commercial zeolite

(CBV2314) and the samples prepared with TEOS by the Sol-Gel route with Si/Al ratios of 26.6 and 60, respectively.

Figure 27.

SEM images of materials used in catalytic tests. Names beginning with T refer to materials prepared by the sol-gel route using the TEOS precursor. Los materiales nombrados con MEC se prepararon por la ruta libre de solventes. Materials FS-1, LD, and CBV

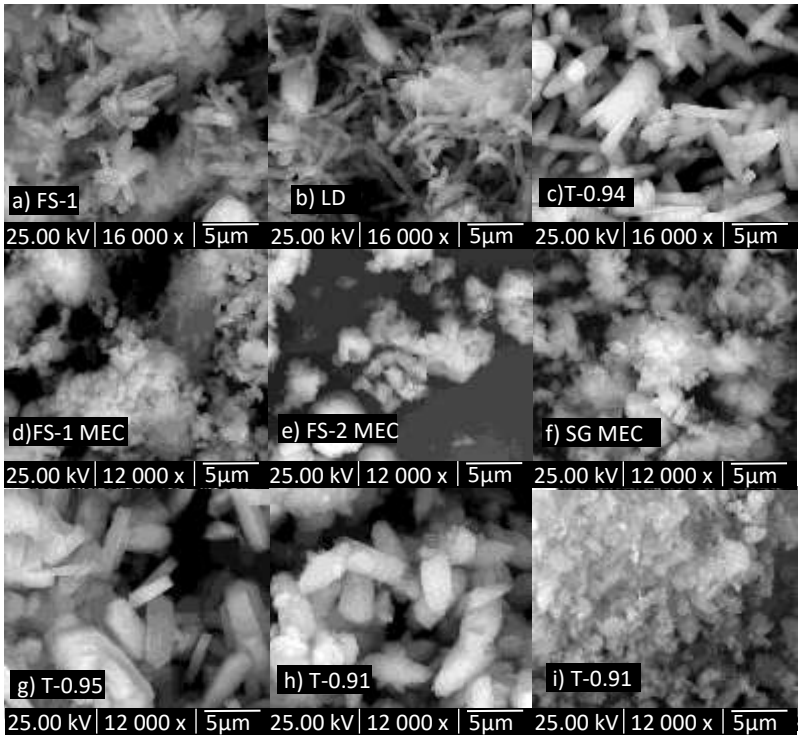

The images show materials prepared by the Sol-Gel method have larger crystal sizes than presented by the mechanochemical method. In the case of the Sol-Gel samples, those prepared with Ludox, and silica fume have similar morphologies, shaped like bars, while the sample prepared with TEOS (T-0.94) has a more oval shape at the tip. Regarding the samples prepared with the solvent-free method, their morphology is similar (aggregates of small crystals), regardless

of the silicon source used for their synthesis. In case T-0.95 material, the crystals have the shape of an elongated hexagon with well-defined edges, unlike the T-0.91 material, whose crystals look like grains and their edges are rough.

Table 13.

Si/(Al+Si) and SiO_2/Al_2O_3 molar ratio calculated from EDS results.

Material	Si/(Al+Si)	SiO_2/Al_2O_3
T-0.91	0.91	20.49
T-0.95	0.95	37.94
T-0.94	0.94	29.55
LD	0.94	29.56
FS-1	0.94	29.08
FS-1 MEC	0.93	25.24
FS-2 MEC	0.92	23.69
SG-MEC	0.93	26.27
CBV2314	0.91	20.62

4.4.2 Textural properties

The textural properties of the materials evaluated in reaction are reported in Table 2.

Table 14.

Textural properties for material synthesized with OSDA and commercial ZSM-5 zeolite (CBV2314).

	LD	FS-1	T-0.94	T-0.95	T0.91	CBV2314	FS-1 MEC	FS-2 MEC	SG MEC
BET Surface Area (m^2/g)	421	415	429	438	390	406	382	396	380
t-Plot Micropore Area (m^2/g)	411	401	421	429	355	367	321	365	341

	LD	FS-1	T-0.94	T-0.95	T0.91	CBV2314	FS-1 MEC	FS-2 MEC	SG MEC
t-Plot external surface area (m^2/g)	10	14	8	9.5	34	39	60.45	27.4	39

4.4.3 X-ray diffraction (XRD)

The Figure 3 shows X-ray diffraction (XRD) patterns of the materials used in catalytic tests. All the materials presented the characteristic diffraction peaks of the ZSM-5 zeolite. As mentioned in the experimental section, except for materials T-0.91 and T0.95, the samples used in the reaction were prepared with the lowest Na_2O/SiO_2 ratio seeking to guarantee a minimum presence of the MOR phase; The diffractograms shown in Figure 2 corroborate that.

Figure 28.

Diffractograms of the of the materials used in catalytic tests.

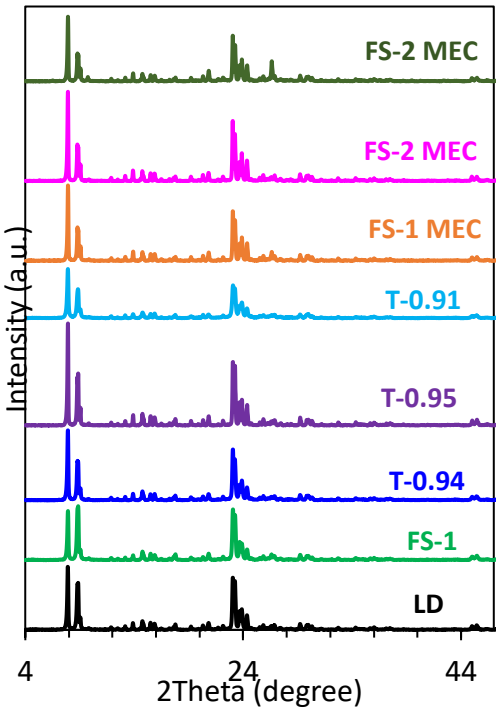

4.4.4 IR of adsorbed pyridine

Figure 4 a) and b) shows the IR spectra recorded for pyridine adsorption on the different materials at room temperature and 400 °C. Bands around 1545 and 1455 cm^{-1} can be observed in the spectra, which correspond to pyridine adsorption at the Brønsted and Lewis acid sites, respectively. The band at 1490 cm^{-1} corresponds to a superposition of the pyridine adsorbed on Brønsted and Lewis sites. Table 3 presents the acidity quantification of the materials using the E1 and E2 equations described in the experimental section.

Figure 29.

FT-IR spectra for pyridine adsorption of the materials tested in reaction. a) desorption at 200 °C b) desorption at 400 °C

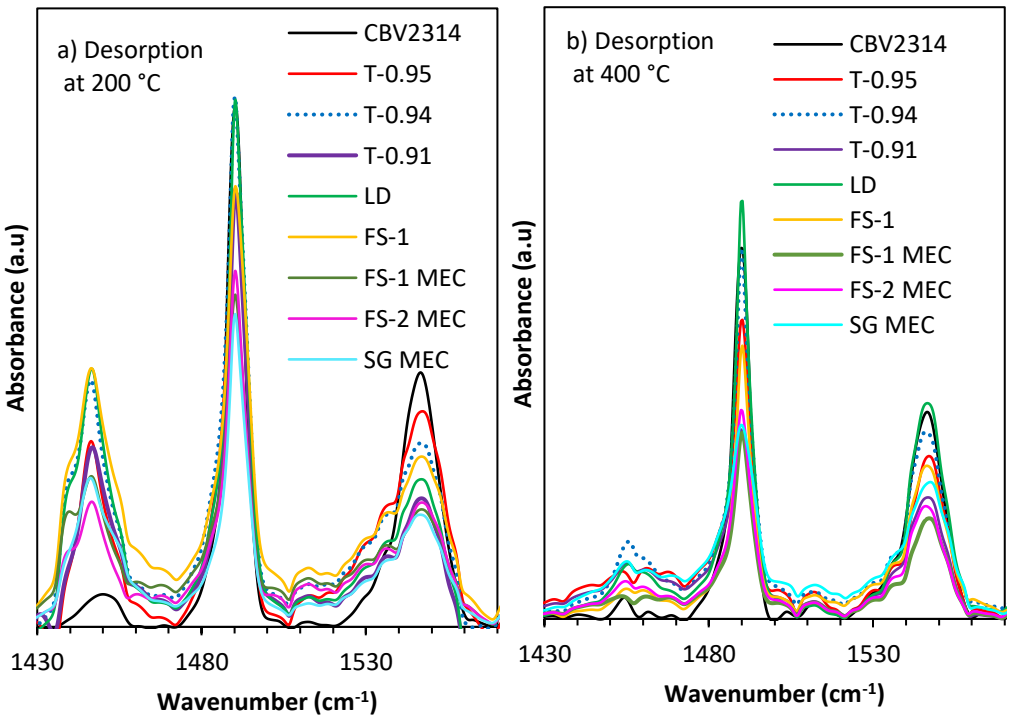

Table 15.

Pyridine quantification as a function of desorption temperature

Sample	Desorption at 200 °C		Desorption at 400 °C	
	Brønsted (mmol/g)	**Lewis (mmol/g)**	**Brønsted (mmol/g)**	**Lewis (mmol/g)**
CBV2314	0.67	0.05	0.44	0.02
LD	0.46	0.42	0.44	0.13
FS-1	0.52	0.46	0.36	0.06
T-0.94	0.57	0.42	0.32	0.14
T-0.95	0.65	0.30	0.32	0.08
T-0.91	0.39	0.38	0.37	0.12
FS-1 MEC	0.36	0.34	0.26	0.06
FS-2 MEC	0.30	0.33	0.34	0.08
SG-MEC	0.31	0.40	0.33	0.06

The results reported in Table 3 also indicate that the materials prepared in this work present a higher concentration of Lewis acid sites than the commercial zeolite. The acidity results also indicate that the strength of the Brønsted acid sites is greater than Lewis acid sites for all materials as the desorption temperature increases from 200 to 400 °C. The intensity of the band associated with Lewis acid sites decreases considerably compared to the band associated with Brønsted acid sites, which is reflected in the quantification of said sites (Table 3). Another notable result is that the sum of the concentration of Brønsted and Lewis acid sites for the materials prepared by the solvent-free method was lower than the rest of the materials tested in the reaction.

4.4.5 Glycerol conversion

Figure 5 presents the conversion as a function of time for all the synthesized materials. It can be observed that the zeolites prepared by the Sol-Gel route present a conversion like that of the commercial zeolite (CBV2314), except for the material with the ratio T-26.6; Whose

conversion after 6 hours was the lowest of the materials prepared by the Sol-Gel route. The catalytic results also show that the activity of the materials prepared by the solvent-free route was lower than those synthesized via sol-gel at any reaction time.

Figure 30.

Glycerol conversion as a function of time for all synthesized material.

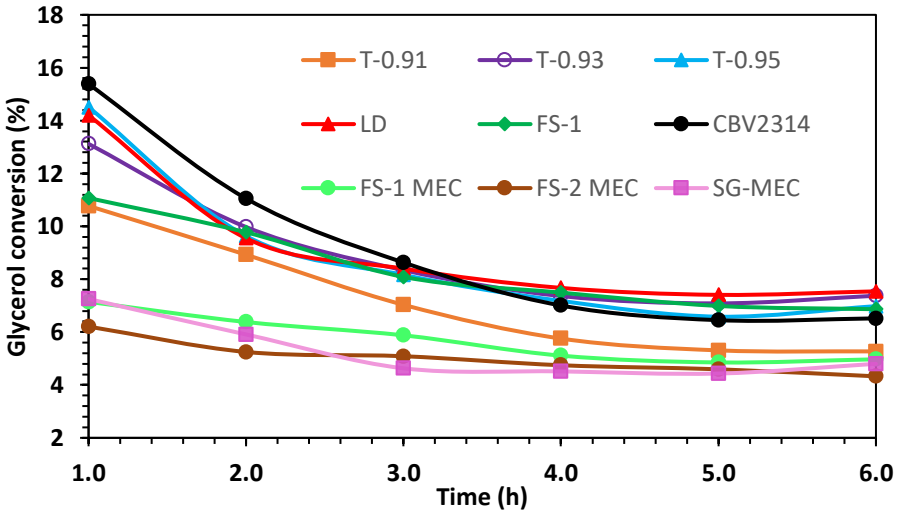

The catalytic results are related to the results obtained with the acidity results, where a lower concentration of acid sites (Brønsted +Lewis) could be observed for the materials prepared by the solvent-free route.

4.4.6 Acrolein and Acetol yield

Figures 6a and b show the yield curves for the materials prepared by the Sol-Gel (a) and mechanochemical (b) routes. The main reaction products were acrolein and acetol, and in the yield graphs, it can be observed that the yield towards acrolein was highest than acetol during the

reactions. However, the yield towards acrolein decreased more rapidly than that of acetol as the reaction time progresses.

Figure 31.

Yield curves for the materials prepared by the Sol-Gel (a) and mechanochemical (b) routes.

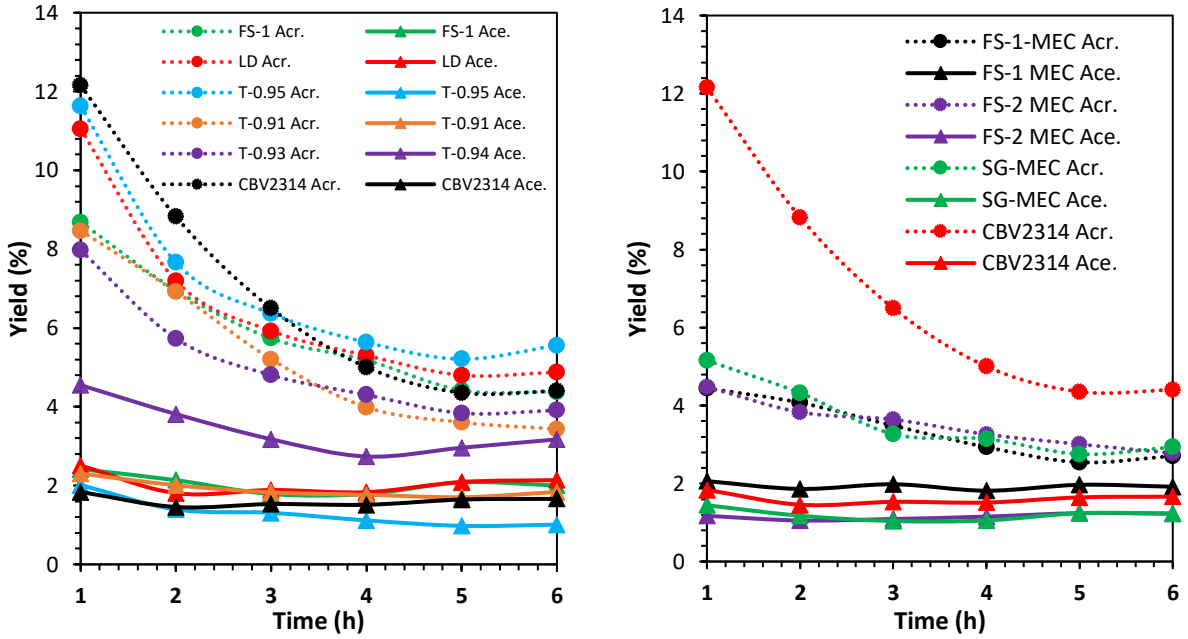

To analyze the effect of the Si/Al ratio on the catalytic properties, materials with Si/(Al+Si) ratio=0.91 and 0.95 were prepared with the TEOS precursor. The variation in the Si and Al content was verified by SEM-EDS analysis.

Regarding the effect of the Si/Al ratio on glycerol dehydration, it can be observed that the T-40 and T-60 materials present a similar behavior in terms of glycerol conversion over time, while the T- 26.6 presented a lower activity. Regarding yield to acrolein, concentration was higher when the silicon content in the materials increased. This was higher in the material with the highest Si concentration (T-0.95) than the material prepared with the same precursor (TEOS) but with a

Si/(Si+Al) =0.91 ratio. The acidity results (Table 3), where the T-0.95 material presents a higher concentration of Brønsted acid sites than the T-0.91 material, can explain this behavior. It has been reported in the literature that acrolein production in zeolitic materials is promoted by Brønsted acid sites, while Lewis acid sites increase acetol selectivity(Lago et al., 2018)(Decolatti et al., 2014)(de Oliveira et al., 2011); this statement coincides with the performance results reported for the materials T-0.95 and T-0.91. A higher concentration of Brønsted acid sites in the T-0.95 material generates a higher yield towards acrolein than the T-0.91 material.

4.5 Conclusion

The materials prepared through the free route of OSDA and by the commercial zeolite in the dehydration reaction of glycerol in the gas phase presented a similar activity. It was determined that, regardless of the silicon precursor used and the synthesis method, acrolein was the main product; such yield can be associated with the presence of Brønsted acid sites of major strength than Lewis acid sites. Finally, the materials synthesized through the solvent-free route and OSDA presented a lower catalytic activity than the one presented by the materials prepared through the Sol-Gel route and the commercial zeolite.

5. General conclusions

The results presented in the first part of this work allow us to conclude that the precursor TEOS offers a broader margin for obtaining zeolite ZSM-5 compared to the precursor's Ludox and Fumed Silica. Under the lowest alkalinity conditions, the ZSM-5 zeolite could be obtained with TEOS, even without the help of the seed zeolite, which was not possible with the other two silicon precursors. It was also shown that the seed zeolites can exert a directing effect on the structure of the synthesis mixture around them but that the composition of the said mixture was what determined the majority phase to be formed. Regarding the use of zeolite Y as seed, in this work, it was observed that it did not have a relevant or beneficial effect for obtaining zeolite ZSM-5 since the results without the presence of seed were the same or even better.

In addition, the concentration of NaOH in the synthesis was a crucial factor in obtaining zeolite ZSM-5. At the lowest concentration ($NaOH/SiO_2$=0.32), the presence of ZSM-5 seed was always necessary to obtain crystalline ZSM-5 zeolite with a high surface area, regardless of the silicon precursor. With the intermediate concentration ($NaOH/SiO_2$=0.42), it is possible to obtain zeolite ZSM-5 with the precursor TEOS and fumed Silica in the seedless system and with zeolite Y; however, the formation of the mordenite phase is also promoted. Finally, with the highest alkalinity ($NaOH/SiO_2$=0.58), the production of zeolite ZSM-5 is not favored, while the formation of the mordenite phase is promoted.

For the second part of this investigation, the size of the silicon particles in precursors only generated morphological changes when silica gel was used to synthesize zeolite ZSM-5 with the help of an organic structuring agent (OSDA). The crystals obtained using OSDA are much larger

than those obtained using seeds and have larger surface areas. It was found that a high concentration of Na favors the appearance of phases such as mordenite and larger silica gel particles. Finally, a comparison was made by varying the crystallization time between mechanochemical and sol-gel synthesis to study the differences and common aspects.

Finally, in the catalytic evaluation of the selected materials, it can be concluded that the materials prepared by the free method of OSDA and by the commercial zeolite in the glycerol dehydration reaction in the gas phase presented a similar activity. It was determined that, regardless of the silicon precursor used and the synthesis method, acrolein was the main product; such yield may be associated with the presence of Bronsted acid sites of greater strength than Lewis's acid sites. At last, the materials synthesized by the solvent-free route and OSDA presented a lower catalytic activity than that presented by the materials prepared by the Sol-Gel route and the commercial zeolite.

References

Alipour, S. M., Halladj, R., & Askari, S. (2014). Effects of the different synthetic parameters on the crystallinity and crystal size of nanosized ZSM-5 zeolite. In *Reviews in Chemical Engineering* (Vol. 30, Issue 3, pp. 289–322). https://doi.org/10.1515/revce-2014-0008

Asgar Pour, Z., & Sebakhy, K. O. (2022). A Review on the Effects of Organic Structure-Directing Agents on the Hydrothermal Synthesis and Physicochemical Properties of Zeolites. *Chemistry (Switzerland)*, *4*(2), 431–446. https://doi.org/10.3390/chemistry4020032

Asopa, R. P., Bhoi, R., & Saharan, V. K. (2022). Valorization of glycerol into value-added products: A comprehensive review on biochemical route. *Bioresource Technology Reports*, *20*(November). https://doi.org/10.1016/j.biteb.2022.101290

Bellussi, G., Perego, G., Carati, A., Cornaro, U., & Fattore, V. (1988). 5-1 SBU based zeolites from wholly inorganic systems. In *Studies in Surface Science and Catalysis* (Vol. 37, Issue C). Academic Press Inc. https://doi.org/10.1016/S0167-2991(09)60580-2

Caldeira, V. P. S., Santos, A. G. D., Pergher, S. B. C., Costa, M. J. F., & Araujo, A. S. (2016). Use of a low-cost template-free zsm-5 for atmospheric petroleum residue pyrolysis. *Quimica Nova*, *39*(3), 292–297. https://doi.org/10.5935/0100-4042.20160019

Corma, A., & Davis, M. E. (2004). Issues in the synthesis of crystalline molecular sieves: Towards the crystallization of low framework-density structures. *ChemPhysChem*, *5*(3), 304–313. https://doi.org/10.1002/cphc.200300997

Cundy, C. S., & Cox, P. A. (2003). The hydrothermal synthesis of zeolites: History and development from the earliest days to the present time. *Chemical Reviews*, *103*(3), 663–701. https://doi.org/10.1021/cr020060i

Cundy, C. S., & Cox, P. A. (2005). The hydrothermal synthesis of zeolites: Precursors, intermediates and reaction mechanism. *Microporous and Mesoporous Materials*, *82*(1–2), 1–78. https://doi.org/10.1016/j.micromeso.2005.02.016

De Oliveira, A. S., Vasconcelos, S. J. S., de Sousa, J. R., de Sousa, F. F., Filho, J. M., & Oliveira, A. C. (2011). Catalytic conversion of glycerol to acrolein over modified molecular sieves: Activity and deactivation studies. *Chemical Engineering Journal*, *168*(2), 765–774. https://doi.org/10.1016/j.cej.2010.09.029

Decolatti, H. P., Costa, B. O. D., & Querini, C. A. (2014). Dehydration of glycerol to acrolein using H-ZSM5 zeolite modified by alkali treatment with NaOH. *MICROPOROUS AND MESOPOROUS MATERIALS*. https://doi.org/10.1016/j.micromeso.2014.11.014

Dos Santos, M. B., Vianna, K. C., Pastore, H. O., Andrade, H. M. C., & Mascarenhas, A. J. S. (2020). Studies on the synthesis of ZSM-5 by interzeolite transformation from zeolite Y without using organic structure directing agents. *Microporous and Mesoporous Materials*, *306*(March), 110413. https://doi.org/10.1016/j.micromeso.2020.110413

Emeis, C. A. (1993). Determination of integrated molar extinction coefficients for infrared absorption bands of pyridine adsorbed on solid acid catalysts. In *Journal of Catalysis* (Vol. 141, Issue 2, pp. 347–354). https://doi.org/10.1006/jcat.1993.1145

Flanigen, E. M., Khatami, H., Szymanski, H. A., Coudurier, G., Naccache, C., Vedrine, J. C., Jansen, J. C., van der Gaag, F. J., van Bekkum, H., Sohn, J. R., DeCanio, S. J., Lunsford, J. H., O'Donnell, D. J., Trombetta, M., Armaroli, T., Alejandre, A. G., Solis, J. R., Busca,

G., Shukla, D. B., … Adnadjević, B. K. (1984). An FT-IR study of the internal and external surfaces of HZSM5 zeolite. *Applied Catalysis A: General*, *6*(1), 201–229. https://doi.org/10.1016/j.apcata.2009.03.009

Goel, S., Zones, S. I., & Iglesia, E. (2015). Synthesis of zeolites via interzeolite transformations without organic structure-directing agents. *Chemistry of Materials*, *27*(6), 2056–2066. https://doi.org/10.1021/cm504510f

Grand, J., Awala, H., & Mintova, S. (2016). Mechanism of zeolites crystal growth: New findings and open questions. *CrystEngComm*, *18*(5), 650–664. https://doi.org/10.1039/c5ce02286j

Heilig, M. L. (1994). United States Patent Office. *ACM SIGGRAPH Computer Graphics*, *28*(2), 131–134. https://doi.org/10.1145/178951.178972

Hoff, T. C., Thilakaratne, R., Gardner, D. W., Brown, R. C., & Tessonnier, J. P. (2016). Thermal Stability of Aluminum-Rich ZSM-5 Zeolites and Consequences on Aromatization Reactions. *Journal of Physical Chemistry C*, *120*(36), 20103–20113. https://doi.org/10.1021/acs.jpcc.6b04671

Huber, G. W., Iborra, S., & Corma, A. (2006). Synthesis of transportation fuels from biomass: Chemistry, catalysts, and engineering. *Chemical Reviews*, *106*(9), 4044–4098. https://doi.org/10.1021/cr068360d

Jones, C. W., Tsuji, K., Takewaki, T., Beck, L. W., & Davis, M. E. (2001). Tailoring molecular sieve properties during SDA removal via solvent extraction. *Microporous and Mesoporous Materials*, *48*(1–3), 57–64. https://doi.org/10.1016/S1387-1811(01)00330-4

Katryniok, B., Paul, S., Capron, M., & Dumeignil, F. (2009). Towards the sustainable production of acrolein by glycerol dehydration. *ChemSusChem*, *2*(8), 719–730. https://doi.org/10.1002/cssc.200900134

Kraleva, E., Palcheva, R., Dimitrov, L., Armbruster, U., Brückner, A., & Spojakina, A. (2011). Solid acid catalysts for dehydration of glycerol to acrolein in gas phase. *Journal of Materials Science*, *46*(22), 7160–7168. https://doi.org/10.1007/s10853-011-5379-x

Lago, C. D., Decolatti, H. P., Tonutti, L. G., Dalla Costa, B. O., & Querini, C. A. (2018). Gas phase glycerol dehydration over H-ZSM-5 zeolite modified by alkaline treatment with Na2CO3. In *Journal of Catalysis* (Vol. 366, pp. 16–27). https://doi.org/10.1016/j.jcat.2018.07.036

Lee, H., Zones, S. I., & Davis, M. E. (2003). A combustion-free methodology for synthesizing zeolites and zeolite-like materials. *Nature*, *425*(6956), 385–388. https://doi.org/10.1038/nature01980

Ma, Y., Wu, Q., Xie, Y., Zhang, L., Meng, X., & Xiao, F. S. (2020). Recent advances in organotemplate-free synthesis of zeolites. *Current Opinion in Green and Sustainable Chemistry*, *25*, 1–6. https://doi.org/10.1016/j.cogsc.2020.100363

Machado, F. J., López, C. M., Centeno, M. A., & Urbina, C. (1999). Template-free synthesis and catalytic behaviour of aluminium-rich MFI-type zeolites. *Applied Catalysis A: General*, *181*(1), 29–38. https://doi.org/10.1016/S0926-860X(98)00383-4

Majano, G., Borchardt, L., Mitchell, S., Valtchev, V., & Pérez-Ramírez, J. (2014). Rediscovering zeolite mechanochemistry-A pathway beyond current synthesis and modification boundaries. *Microporous and Mesoporous Materials*, *194*, 106–114. https://doi.org/10.1016/j.micromeso.2014.04.006

Nada, M. H., & Larsen, S. C. (2017). Insight into seed-assisted template free synthesis of ZSM-5 zeolites. *Microporous and Mesoporous Materials*, *239*, 444–452. https://doi.org/10.1016/j.micromeso.2016.10.040

Nimlos, M. R., Blanksby, S. J., Qian, X., Himmel, M. E., & Johnson, D. K. (2006). Mechanisms of glycerol dehydration. *Journal of Physical Chemistry A*, *110*(18), 6145–6156. https://doi.org/10.1021/jp060597q

Pan, F., Lu, X., Wang, T., & Yan, Y. (2017). Submicron ZSM-5 synthesized by green and fast route. *Materials Letters*, *196*, 245–247. https://doi.org/10.1016/j.matlet.2017.03.060

Pan, H., Pan, Q., Zhao, Y., Luo, Y., Shu, X., & He, M. (2010). A green and efficient synthesis of ZSM-5 using NaY as seed with mother liquid recycling and in the absence of organic template. *Industrial and Engineering Chemistry Research*, *49*(16), 7294–7302. https://doi.org/10.1021/ie100191a

Park, H., Yun, Y. S., Kim, T. Y., Lee, K. R., Baek, J., & Yi, J. (2015). Kinetics of the dehydration of glycerol over acid catalysts with an investigation of deactivation mechanism by coke. *Applied Catalysis B: Environmental*, *176–177*, 1–10. https://doi.org/10.1016/j.apcatb.2015.03.046

Pérez-Page, M., Makel, J., Guan, K., Zhang, S., Tringe, J., Castro, R. H. R., & Stroeve, P. (2016). Gas adsorption properties of ZSM-5 zeolites heated to extreme temperatures. *Ceramics International*, *42*(14), 15423–15431. https://doi.org/10.1016/j.ceramint.2016.06.193

Possato, L. G., Diniz, R. N., Garetto, T., Pulcinelli, S. H., Santilli, C. V., & Martins, L. (2013). A comparative study of glycerol dehydration catalyzed by micro/mesoporous MFI zeolites. *Journal of Catalysis*, *300*, 102–112. https://doi.org/10.1016/j.jcat.2013.01.003

Rao, G. S., Rajan, N. P., Sekhar, M. H., Ammaji, S., & Chary, K. V. R. (2014). Journal of Molecular Catalysis A : Chemical Porous zirconium phosphate supported tungsten oxide solid acid catalysts for the vapour phase dehydration of glycerol. *"Journal of Molecular Catalysis. A, Chemical," 395*, 486–493. https://doi.org/10.1016/j.molcata.2014.09.018

Razavian, M., Fatemi, S., & Komasi, M. (2015). Seed-assisted OSDA-free synthesis of ZSM-5 zeolite and its application in dehydrogenation of propane. *Materials Research Bulletin*, *65*, 253–259. https://doi.org/10.1016/j.materresbull.2015.01.062

Ren, L., Wu, Q., Yang, C., Zhu, L., Li, C., Zhang, P., Zhang, H., Meng, X., & Xiao, F. S. (2012). Solvent-free synthesis of zeolites from solid raw materials. *Journal of the American Chemical Society*, *134*(37), 15173–15176. https://doi.org/10.1021/ja3044954

Rieg, C., Li, Z., Kurtz, A., Schmidt, M., Dittmann, D., Benz, M., & Dyballa, M. (2021). A Method for the Selective Quantification of Brønsted Acid Sites on External Surfaces and in Mesopores of Hierarchical Zeolites. *Journal of Physical Chemistry C*, *125*(1), 515–525. https://doi.org/10.1021/acs.jpcc.0c09384

Sun, D., Yamada, Y., Sato, S., & Ueda, W. (2017). Glycerol as a potential renewable raw material for acrylic acid production. *Green Chemistry*, *19*(14), 3186–3213. https://doi.org/10.1039/c7gc00358g

Talebian-Kiakalaieh, A., Amin, N. A. S., & Hezaveh, H. (2014). Glycerol for renewable acrolein production by catalytic dehydration. *Renewable and Sustainable Energy Reviews*, *40*, 28–59. https://doi.org/10.1016/j.rser.2014.07.168

Tan, H. W., Abdul Aziz, A. R., & Aroua, M. K. (2013). Glycerol production and its applications as a raw material: A review. *Renewable and Sustainable Energy Reviews*, *27*, 118–127. https://doi.org/10.1016/j.rser.2013.06.035

García-Sánchez, J. T., Mora-Vergara, I. D., Molina-Velasco, D. R., Henao-Martínez, J.A., & Baldovino-Medrano, V. G. (2021). Key Factors During the Milling Stage of the Seed-assisted and Solvent-free Synthesis of MFI and Catalytic Behavior in the Alkylation of

Phenol with Tert-butyl Alcohol. *ChemCatChem*, *13*(16), 3713–3730. https://doi.org/10.1002/cctc.202100479

Vermeiren, W., & Gilson, J. P. (2009). Impact of zeolites on the petroleum and petrochemical industry. *Topics in Catalysis*, *52*(9), 1131–1161. https://doi.org/10.1007/s11244-009-9271-8

Wu, D., Yu, X., Chen, X., Yu, G., Zhang, K., Qiu, M., Xue, W., Yang, C., Liu, Z., Sun, Y., Wang, Y., Duan, H., Tan, Z., Meng, X., Xiao, F. S., Pan, T., Wu, Z., Yip, A. C. K., Mazonde, B., … Baldovino-medrano, V. G. (2019). Seed-Assisted, OSDA-Free, Solvent-Free Synthesis of ZSM-5 Zeolite from Iron Ore Tailings. *ChemSusChem*, *12*(16), 1–13. https://doi.org/10.1007/s12649-019-00752-4

Zhang, H., Hu, Z., Huang, L., Zhang, H., Song, K., Wang, L., Shi, Z., Zhuang, Y., Shen, W., Zhang, Y., Xu, H., & Tang, Y. (2015). *Dehydration of glycerol to acrolein over hierarchical ZSM-5 zeolites : Effects of mesoporosity and acidity*. https://doi.org/10.1021/cs5019953

Zholobenko, V., Freitas, C., Jendrlin, M., Bazin, P., Travert, A., & Thibault-Starzyk, F. (2020). Probing the acid sites of zeolites with pyridine: Quantitative AGIR measurements of the molar absorption coefficients. *Journal of Catalysis*, *385*, 52–60. https://doi.org/10.1016/j.jcat.2020.03.003

Zou, B., Ren, S., & Ye, X. P. (2016). *Glycerol Dehydration to Acrolein Catalyzed by ZSM-5 Zeolite in Supercritical Carbon Dioxide Medium*. 1–5. https://doi.org/10.1002/cssc.201601020

Appendixes

Appendix A. Suplementary information FIures S1

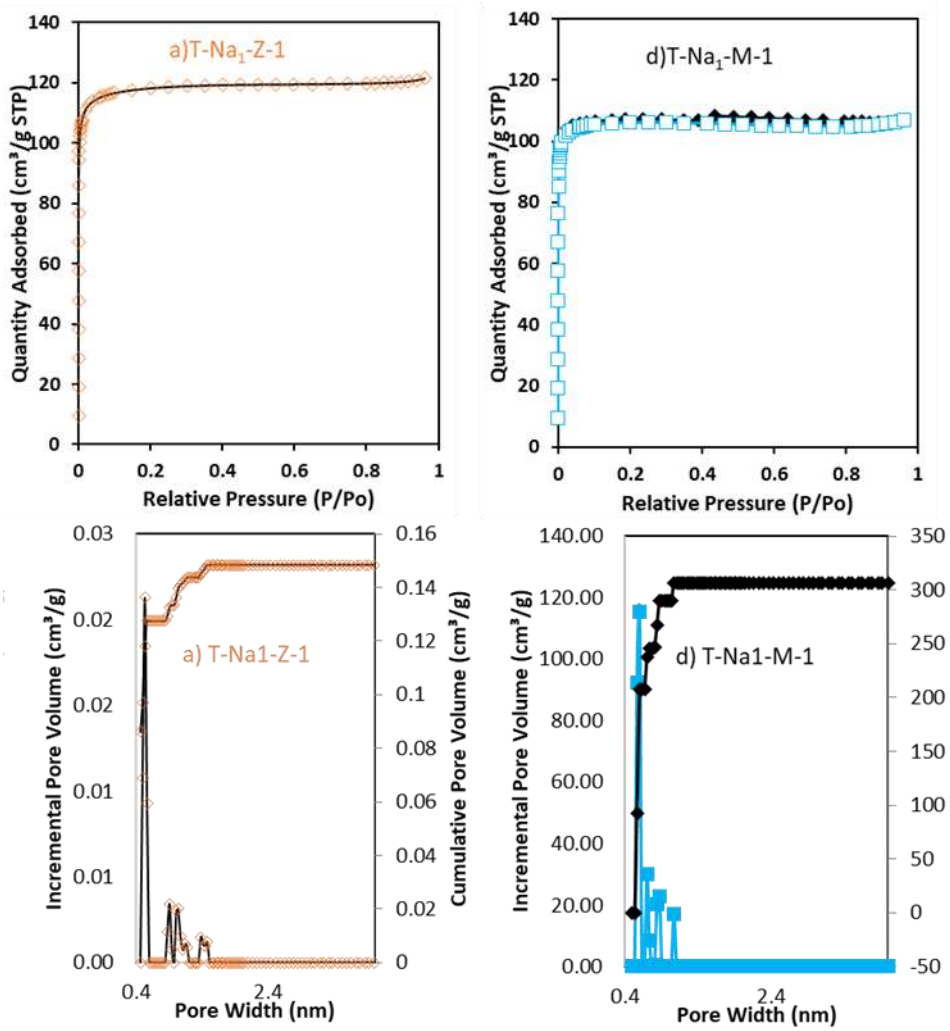

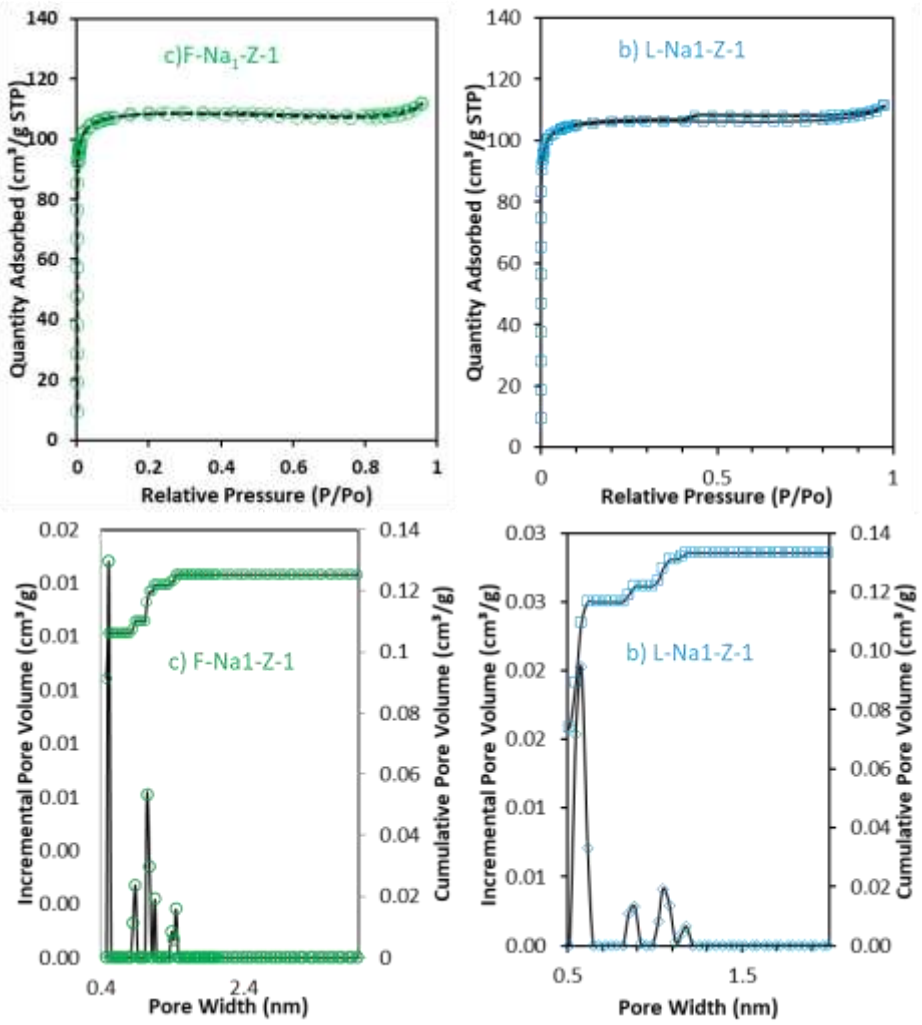
c)F-Na1-Z-1
Quantity Adsorbed (cm³/g STP)
Relative Pressure (P/Po)
b) L-Na1-Z-1
Quantity Adsorbed (cm³/g STP)
Relative Pressure (P/Po)
c) F-Na1-Z-1
Incremental Pore Volume (cm³/g)
Cumulative Pore Volume (cm³/g)
Pore Width (nm)
b) L-Na1-Z-1
Incremental Pore Volume (cm³/g)
Cumulative Pore Volume (cm³/g)
Pore Width (nm)

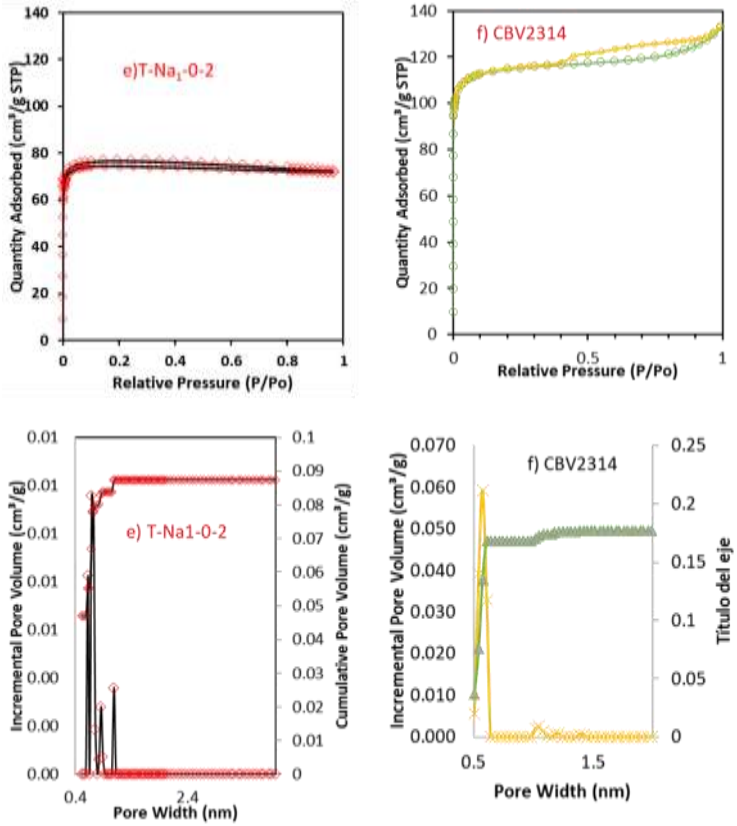
e)T-Na1-0-2
Quantity Adsorbed (cm³/g STP)
Relative Pressure (P/Po)
f) CBV2314
Quantity Adsorbed (cm³/g STP)
Relative Pressure (P/Po)
e) T-Na1-0-2
Incremental Pore Volume (cm³/g)
Cumulative Pore Volume (cm³/g)
Pore Width (nm)
f) CBV2314
Incremental Pore Volume (cm³/g)
Título del eje
Pore Width (nm)